AWARD NUMBER: **W81XWH-15-1-0559**

TITLE: **Neuroprotective Strategies for the Treatment of Blast-Induced Optic Neuropathy**

PRINCIPAL INVESTIGATOR: **Tonia S. Rex, Ph.D.**

CONTRACTING ORGANIZATION: **Vanderbilt University Medical Center**

REPORT DATE: December 2019

TYPE OF REPORT: Final

PREPARED FOR: U.S. Army Medical Research and Development Command
Fort Detrick, Maryland 21702-5012

REPORT DOCUMENTATION PAGE

Form Approved
OMB No. 0704-0188

1. REPORT DATE	2. REPORT TYPE	3. DATES COVERED
Dec 2019	Final	09/15/2015 - 09/14/2019

4. TITLE AND SUBTITLE

Neuroprotective Strategies for the Treatment of Blast-Induced Optic Neuropathy

5a. CONTRACT NUMBER

5b. GRANT NUMBER
W81XWH-15-1-0559

5c. PROGRAM ELEMENT NUMBER

6. AUTHOR(S)
Tonia S. Rex

E-Mail:

5d. PROJECT NUMBER

5e. TASK NUMBER

5f. WORK UNIT NUMBER

7. PERFORMING ORGANIZATION NAME(S) AND ADDRESS(ES)

Vanderbilt University Medical Center
Office of Sponsored Programs
3319 West End Ave, Nashville
TN 37203

8. PERFORMING ORGANIZATION REPORT NUMBER

9. SPONSORING / MONITORING AGENCY NAME(S) AND ADDRESS(ES)

U.S. Army Medical Research and Development Command
Fort Detrick, Maryland 21702-5012

10. SPONSOR/MONITOR'S ACRONYM(S)

11. SPONSOR/MONITOR'S REPORT NUMBER(S)

12. DISTRIBUTION / AVAILABILITY STATEMENT

Approved for Public Release; Distribution Unlimited

13. SUPPLEMENTARY NOTES

14. ABSTRACT

Background: Over 186,000 eye injuries were diagnosed in fixed (not deployed) U.S. Military medical facilities from 2000-2011. We have a mouse model of blast trauma that causes vision loss and optic nerve degeneration secondary to blast-induced oxidative stress and neuroinflammation. Importantly, all of these processes also occur in other models of CNS trauma. Therefore, **our study has implications for neurodegenerations from trauma extending beyond optic neuropathy. Objective:** To test the efficacy of targeted delivery of neuroprotective therapeutics in preventing degeneration of the retina and optic projection to the brain secondary to blast trauma. Galantamine was chosen because it preserves cholinergic signaling and is FDA approved for the treatment of Alzheimer's disease. Erythropoietin (EPO) was chosen because it decreases both oxidative stress and neuroinflammation. We will use a modified form of EPO (EPO-R76E) that has attenuated erythropoietic activity and therefore is safer for clinical use. We will also examine the mechanisms underlying blast-induced vision loss with the goal of identifying additional drug targets for therapeutic intervention. We **hypothesize** that the vision loss and optic nerve degeneration that occurs after blast is due to oxidative stress and neuroinflammation. **Military Benefit**: Currently there are no vision-preserving treatments available for trauma patients regardless of the mechanism of injury. Our study will determine the therapeutic efficacy of two FDA- approved neuroprotective agents.

15. SUBJECT TERMS

16. SECURITY CLASSIFICATION OF:			17. LIMITATION OF ABSTRACT	18. NUMBER OF PAGES	19a. NAME OF RESPONSIBLE PERSON
a. REPORT	b. ABSTRACT	c. THIS PAGE			USAMRMC
Unclassified	Unclassified	Unclassified	Unclassified		19b. TELEPHONE NUMBER *(include area code)*

TABLE OF CONTENTS

1. INTRODUCTION: *Narrative that briefly (one paragraph) describes the subject, purpose and scope of the research.*

A major limiting factor to the development of treatments for indirect traumatic optic neuropathy (ITON) has been the absence of a suitable animal model for: (1) mimicking the initial injury; and (2) tracking secondary degeneration. We will use our ocular blast injury system and assess the efficacy of two therapeutic agents. Our model causes early oxidative stress, neuroinflammation and inner retinal dysfunction followed by decreased vision and optic nerve degeneration, processes that also occur after TBI. Therefore, our study has implications for neurodegenerations from trauma extending beyond optic neuropathy.

2. KEYWORDS: *Provide a brief list of keywords (limit to 20 words).*

retinal ganglion cell (RGC), traumatic optic neuropathy, inflammasome, erythropoietin (EPO), electroretinogram (ERG), visual evoked potential (VEP), interleukin-1 (IL-1)

3. ACCOMPLISHMENTS: *The PI is reminded that the recipient organization is required to obtain prior written approval from the awarding agency grants official whenever there are significant changes in the project or its direction.*

What were the major goals of the project?

List the major goals of the project as stated in the approved SOW. If the application listed milestones/target dates for important activities or phases of the project, identify these dates and show actual completion dates or the percentage of completion.

Aim 1: Elucidate the cellular mechanisms underlying visual dysfunction after blast.
Major Task 1: Obtain approval for mouse studies.
Major Task 2: Assess if pyroptosis is activated after blast.
Major Task 3: Assess if signaling from starburst amacrine cells is altered by blast.
Major Task 4: Determine if the dendritic trees of the dsRGCs are altered by blast.
Aim 2: Assess the efficacy of galantamine in preventing neurodegeneration secondary to blast.
Major Task 1: Assess vision in treated and control blast mice.
Major Task 2: Assess histology of treated and control blast mice.
Major Task 3: Quantify neurochemical changes in the retina.
Aim 3: Assess if reduction in neuroinflammation and oxidative stress by EPO-R76E prevents neurodegeneration secondary to blast.
Major Task 1: Assess vision in treated and control blast mice.
Major Task 2: Assess histology of treated and control blast mice.
Major Task 3: Quantify EPO-R76E levels.

What was accomplished under these goals?

For this reporting period describe: 1) major activities; 2) specific objectives; 3) significant results or key outcomes, including major findings, developments, or conclusions (both positive and negative); and/or 4) other achievements. Include a discussion of stated goals not met. Description shall include pertinent data and graphs in sufficient detail to explain any significant results achieved. A succinct description of the methodology used shall be provided. As the project progresses to completion, the emphasis in reporting in this section should shift from reporting activities to reporting accomplishments.

1) Major Activities: We have published multiple manuscripts and have another paper in preparation for submission to another high impact journal.

A. Bricker-Anthony C, D'Surney L, Lunn B, Jo M, Bernardo-Colon A, Hines-Beard J, Rex TS. (2017) Erythropoietin either prevents or exacerbates retinal damage after eye trauma depending on treatment timing. *J Optom Vis Sci. (Trauma special issue)* 94:20-32.

B. Bernardo-Colon A, Vest V, Clark AF, Cooper M, Calkins DJ, Harrison FE, Rex TS. (2018) Antioxidants prevent inflammation and preserve the optic projection and visual function in experimental neurotrauma. *Cell Death & Dis.* 9:1097.

C. Vest V, Bernardo-Colon A, Watkins, D, Kim B, Rex TS. (2019) Rapid repeat exposure to sub-threshold trauma causes synergistic axonal damage and functional deficits in the visual pathway in a mouse model. *J. Neurotrauma*. 36:1646-1654.

D. Bernardo-Colon A, Vest V, Cooper M, Calkins DJ, Rex TS. (2019) Progression and pathology of blast-induced indirect traumatic optic neuropathy. *Frontiers Neurosci.* 13:719.

E. Naguib S, Bernardo-Colon A, Cencer C, Gandra N, Rex TS. (2019) Galantamine protects against synaptic, axonal, and vision deficits in experimental neurotrauma. *Neurobiology of Disease* 25:104695

We have also presented our findings at several research conferences including MHSRS and ARVO.

A. Bernardo-Colon A, Clark A, Rex TS. (2017) Ocular trauma induces sterile inflammation. *6th Military Vision Symposium on Ocular and Vision Injury*, Boston, MA.

B. Watkins D, Bernardo-Colon A, Rex TS. (2017) A blast device for inducing ocular trauma in mouse models. *6th Military Vision Symposium on Ocular and Vision Injury*, Boston, MA.

C. Clark A, Bernardo-Colon A, Rex TS. (2017) Ocular trauma induces sterile inflammation. *Invest Ophthalmol Vis Sci.* 57:1762.
D. Vest V, Bernardo-Colon A, Li Z, Clark A, Clifton J, Rex TS. (2017) Repeat lower magnitude trauma induces greater axon degeneration: treatment with antioxidants. *J Neurotrauma Suppl.* 10241
E. Rex TS, Bernardo-Colon A, Vest, Clark AL, Clifton JM, Kim B, Dahl R, Harrison F. (2018) The IL-1 pathway is a key mediator of axon degeneration and vision loss in a mouse model of indirect traumatic optic neuropathy. *Invest Ophthalmol Vis Sci.* 59:5514
F. Rex TS, Bernardo-Colon A, Vest V, Clark AL, Harrison F. (2018) Dietary interventions protect against blast-induced neurotrauma in an animal model. *Military Health Services Research Symposium*
G. Naguib S, Bernardo-Colon A, and Rex TS. (2018) Galantamine confers neuroprotection in a model of indirect traumatic optic neuropathy. *Southeast Vision Research Conference*
H. Bernardo-Colon A, Naguib S, Erwin MM, Kavanaugh T, Gupta M, Duvall CL, Rex TS. (2019) Post-trauma therapy with microparticle-mediated delivery of erythropoietin. *Invest Ophthalmol Vis Sci.* 60:4406
I. Naguib S, Bernardo-Colon A, and **Rex TS**. (2019) Galantamine confers neuroprotection in a model of indirect traumatic optic neuropathy. *Invest Ophthalmol Vis Sci.* 60:4407

2) Specific Objectives: To submit and publish the remaining manuscript.
Bernardo-Colón A, DeJulius CR, Backstrom JR, Collins T, Gupta M, Duvall C, Rex TS. (in preparation) Sustained delivery of erythropoietin-R76E via PPS microparticles is more protective than delivery via PLGA particles in a mouse model of indirect traumatic optic neuropathy. *Biomaterials*

3) Significant Results: A. Please find the most recent two manuscripts (Frontiers in Neuroscience and Neurobiology of Disease) attached. B. Please also find the current draft of the manuscript in preparation attached. C. Repeat low-level injury causes a different pathology than single high-level injury. D. Galantamine preserves vision and retina and optic nerve structure when given after the last of 3-days of injury. It does not mitigate all injury but does result in improved outcomes. E. Sustained intraocular delivery of EPO-R76E given one day after the last of 3-days of injury results in high levels of preservation of vision and optic nerve and retina structure.
Together these results suggest that there is a fairly large window of opportunity and that intraocular EPO-R76E should be pursued as a therapeutic.
4) Other achievements: We leveraged this data to obtain an NEI U24 Audacious Goals grant to move this model into the human-relevant tree shrew and optimize retinal ganglion cell replacement therapy.

What opportunities for training and professional development has the project provided?
If the project was not intended to provide training and professional development opportunities or there is nothing significant to report during this reporting period, state "Nothing to Report."

Describe opportunities for training and professional development provided to anyone who worked on the project or anyone who was involved in the activities supported by the project. "Training" activities are those in which individuals with advanced professional skills and experience assist others in attaining greater proficiency. Training activities may include, for example, courses or one-on-one work with a mentor. "Professional development" activities result in increased knowledge or skill in one's area of expertise and may include workshops, conferences, seminars, study groups, and individual study. Include participation in conferences, workshops, and seminars not listed under major activities.

Nothing to Report

How were the results disseminated to communities of interest?
If there is nothing significant to report during this reporting period, state "Nothing to Report."

Describe how the results were disseminated to communities of interest. Include any outreach activities that were undertaken to reach members of communities who are not usually aware of these project activities, for the purpose of enhancing public understanding and increasing interest in learning and careers in science, technology, and the humanities.

We presented the findings at the annual meeting for the Association for Research in Vision and Ophthalmology, National Neurotrauma Symposium, and the Military Health Services Research Symposium. We have also published 4 manuscripts with another underway.

What do you plan to do during the next reporting period to accomplish the goals?
If this is the final report, state "Nothing to Report."

Describe briefly what you plan to do during the next reporting period to accomplish the goals and objectives.

Nothing to Report.

4. IMPACT: D*escribe distinctive contributions, major accomplishments, innovations, successes, or any change in practice or behavior that has come about as a result of the project relative to:*

What was the impact on the development of the principal discipline(s) of the project?
If there is nothing significant to report during this reporting period, state "Nothing to Report."

Describe how findings, results, techniques that were developed or extended, or other products from the project made an impact or are likely to make an impact on the base of knowledge, theory, and research in the principal disciplinary field(s) of the project. Summarize using language that an intelligent lay audience can understand (Scientific American style).

We have identified a window of opportunity after injury during when therapeutic interventions are still effective. We have also identified the molecular pathways activated after injury that lead to ongoing degeneration and vision loss. Further, we have identified two therapeutics, galantamine and erythropoietin, that mitigate vision loss and cellular damage even when given 4 days after the first of 3-days of injuries (1-day after the last injury).

What was the impact on other disciplines?
If there is nothing significant to report during this reporting period, state "Nothing to Report."

Describe how the findings, results, or techniques that were developed or improved, or other products from the project made an impact or are likely to make an impact on other disciplines.

The effect of inter-injury interval occurs at the level of the CNS axon and is thus relevant to other CNS areas. In addition, the therapeutic interventions have a high likelihood of positively influencing other CNS systems as well.

What was the impact on technology transfer?
If there is nothing significant to report during this reporting period, state "Nothing to Report."

Describe ways in which the project made an impact, or is likely to make an impact, on commercial technology or public use, including:

- *transfer of results to entities in government or industry;*
- *instances where the research has led to the initiation of a start-up company; or*
- *adoption of new practices.*

We combined our patented EPO, EPO-R76E, with patented microparticle technology to result in a greater benefit and sustained release of EPO-R76E. This new technology could be licensed to a company.

What was the impact on society beyond science and technology?
If there is nothing significant to report during this reporting period, state "Nothing to Report."

Describe how results from the project made an impact, or are likely to make an impact, beyond the bounds of science, engineering, and the academic world on areas such as:

- *improving public knowledge, attitudes, skills, and abilities;*
- *changing behavior, practices, decision making, policies (including regulatory policies), or social actions; or*
- *improving social, economic, civic, or environmental conditions.*

Nothing to Report

5. CHANGES/PROBLEMS: *The PD/PI is reminded that the recipient organization is required to obtain prior written approval from the awarding agency grants official whenever there are significant changes in the project or its direction. If not previously reported in writing, provide the following additional information or state, "Nothing to Report," if applicable:*

Changes in approach and reasons for change

Describe any changes in approach during the reporting period and reasons for these changes. Remember that significant changes in objectives and scope require prior approval of the agency.

Nothing to Report

Actual or anticipated problems or delays and actions or plans to resolve them
Describe problems or delays encountered during the reporting period and actions or plans to resolve them.

Nothing to Report

Changes that had a significant impact on expenditures
Describe changes during the reporting period that may have had a significant impact on expenditures, for example, delays in hiring staff or favorable developments that enable meeting objectives at less cost than anticipated.

Nothing to Report

Significant changes in use or care of human subjects, vertebrate animals, biohazards, and/or select agents
Describe significant deviations, unexpected outcomes, or changes in approved protocols for the use or care of human subjects, vertebrate animals, biohazards, and/or select agents during the reporting period. If required, were these changes approved by the applicable institution committee (or equivalent) and reported to the agency? Also specify the applicable Institutional Review Board/Institutional Animal Care and Use Committee approval dates.

Significant changes in use or care of human subjects

Nothing to Report.

Significant changes in use or care of vertebrate animals

Nothing to Report.

Significant changes in use of biohazards and/or select agents

Nothing to Report.

6. PRODUCTS: *List any products resulting from the project during the reporting period. If there is nothing to report under a particular item, state "Nothing to Report."*

- **Publications, conference papers, and presentations**
  Report only the major publication(s) resulting from the work under this award.

  Journal publications. *List peer-reviewed articles or papers appearing in scientific, technical, or professional journals. Identify for each publication: Author(s); title; journal; volume: year; page numbers; status of publication (published; accepted, awaiting publication; submitted, under review; other); acknowledgement of federal support (yes/no).*

  Bernardo-Colon A, Vest V, Clark AF, Cooper M, Calkins DJ, Harrison FE, **Rex TS**. (2018) Antioxidants prevent inflammation and preserve the optic projection and visual function in experimental neurotrauma. *Cell Death & Dis.* 9:1097.

  Vest V, Bernardo-Colon A, Watkins, D, Kim B, **Rex TS**. (2019) Rapid repeat exposure to sub-threshold trauma causes synergistic axonal damage and functional deficits in the visual pathway in a mouse model. *J. Neurotrauma*. 36:1646-1654.

  Bernardo-Colon A, Vest V, Cooper M, Calkins DJ, **Rex TS**. (2019) Progression and pathology of blast-induced indirect traumatic optic neuropathy. *Frontiers Neurosci.* 13:719.

  Naguib S, Bernardo-Colon A, Cencer C, Gandra N, **Rex TS**. (2019) Galantamine protects against synaptic, axonal, and vision deficits in experimental neurotrauma. *Neurobiology of Disease* 25:104695

  Bernardo-Colón A, DeJulius CR, Backstrom JR, Collins T, Gupta M, Duvall C, **Rex TS**. (in preparation) Sustained delivery of erythropoietin-R76E via PPS microparticles is more protective than delivery via PLGA particles in a mouse model of indirect traumatic optic neuropathy. *Biomaterials*

Books or other non-periodical, one-time publications. *Report any book, monograph, dissertation, abstract, or the like published as or in a separate publication, rather than a periodical or series. Include any significant publication in the proceedings of a one-time conference or in the report of a one-time study, commission, or the like. Identify for each one-time publication: author(s); title; editor; title of collection, if applicable; bibliographic information; year; type of publication (e.g., book, thesis or dissertation); status of publication (published; accepted, awaiting publication; submitted, under review; other); acknowledgement of federal support (yes/no).*

Nothing to Report

Other publications, conference papers and presentations. *Identify any other publications, conference papers and/or presentations not reported above. Specify the status of the publication as noted above. List presentations made during the last year (international, national, local societies, military meetings, etc.). Use an asterisk (*) if presentation produced a manuscript.*

Bernardo-Colon A, Clark A, **Rex TS**. (2017) Ocular trauma induces sterile inflammation. *6th Military Vision Symposium on Ocular and Vision Injury.*

Watkins D, Bernardo-Colon A, **Rex TS**. (2017) A blast device for inducing ocular trauma in mouse models. *6th Military Vision Symposium on Ocular and Vision Injury*.

Clark A, Bernardo-Colon A, **Rex TS**. (2017) Ocular trauma induces sterile inflammation. *Invest Ophthalmol Vis Sci.* 57:1762.

Vest V, Bernardo-Colon A, Li Z, Clark A, Clifton J, **Rex TS**. (2017) Repeat lower magnitude trauma induces greater axon degeneration: treatment with antioxidants. *J Neurotrauma Suppl.* 10241

Rex TS, Bernardo-Colon A, Vest, Clark AL, Clifton JM, Kim B, Dahl R, Harrison F. (2018) The IL-1 pathway is a key mediator of axon degeneration and vision loss in a mouse model of indirect traumatic optic neuropathy. *Invest Ophthalmol Vis Sci.* 59:5514

Rex TS, Bernardo-Colon A, Vest V, Clark AL, Harrison F. (2018) Dietary interventions protect against blast-induced neurotrauma in an animal model. *Military Health Services Research Symposium*

Naguib S, Bernardo-Colon A, and **Rex TS**. (2018) Galantamine confers neuroprotection in a model of indirect traumatic optic neuropathy. *Southeast Vision Research Conference*

Bernardo-Colon A, Naguib S, Erwin MM, Kavanaugh T, Gupta M, Duvall CL, **Rex TS**. (2019) Post-trauma therapy with microparticle-mediated delivery of erythropoietin. *Invest Ophthalmol Vis Sci.* 60:4406

Naguib S, Bernardo-Colon A, and **Rex TS**. (2019) Galantamine confers neuroprotection in a model of indirect traumatic optic neuropathy. *Invest Ophthalmol Vis Sci.* 60:4407

- **Website(s) or other Internet site(s)**

List the URL for any Internet site(s) that disseminates the results of the research activities. A short description of each site should be provided. It is not necessary to include the publications already specified above in this section.

Nothing to Report.

- **Technologies or techniques**

Identify technologies or techniques that resulted from the research activities. Describe the technologies or techniques were shared.

Nothing to Report

- **Inventions, patent applications, and/or licenses**

Identify inventions, patent applications with date, and/or licenses that have resulted from the research. Submission of this information as part of an interim research performance progress report is not a substitute for any other invention reporting required under the terms and conditions of an award.

Nothing to report.

- **Other Products**

Identify any other reportable outcomes that were developed under this project. Reportable outcomes are defined as a research result that is or relates to a product, scientific advance, or research tool that makes a meaningful contribution toward the understanding, prevention, diagnosis, prognosis, treatment and /or rehabilitation of a disease, injury or condition, or to improve the quality of life. Examples include:

- *data or databases;*
- *physical collections;*
- *audio or video products;*
- *software;*
- *models;*
- *educational aids or curricula;*
- *instruments or equipment;*
- *research material (e.g., Germplasm; cell lines, DNA probes, animal models);*
- *clinical interventions;*
- *new business creation; and*
- *other.*

Nothing to Report

7. PARTICIPANTS & OTHER COLLABORATING ORGANIZATIONS

What individuals have worked on the project?

Provide the following information for: (1) PDs/PIs; and (2) each person who has worked at least one person month per year on the project during the reporting period, regardless of the source of compensation (a person month equals approximately 160 hours of effort). If information is unchanged from a previous submission, provide the name only and indicate "no change".

Example:

Name: *Mary Smith*
Project Role: *Graduate Student*
Researcher Identifier (e.g. ORCID ID): *1234567*
Nearest person month worked: *5*

Contribution to Project: *Ms. Smith has performed work in the area of combined error-control and constrained coding.*
Funding Support: *The Ford Foundation (Complete only if the funding support is provided from other than this award.)*

Tonia Rex: no change
Alexandra Bernardo-Colon: no change
Jon Backstrom: no change
Brian Carlson: no change
Jinsong Sheng: no change
Victoria Vest: removed in 2018

Has there been a change in the active other support of the PD/PI(s) or senior/key personnel since the last reporting period?
If there is nothing significant to report during this reporting period, state "Nothing to Report."

If the active support has changed for the PD/PI(s) or senior/key personnel, then describe what the change has been. Changes may occur, for example, if a previously active grant has closed and/or if a previously pending grant is now active. Annotate this information so it is clear what has changed from the previous submission. Submission of other support information is not necessary for pending changes or for changes in the level of effort for active support reported previously. The awarding agency may require prior written approval if a change in active other support significantly impacts the effort on the project that is the subject of the project report.

Nothing to Report

What other organizations were involved as partners?
If there is nothing significant to report during this reporting period, state "Nothing to Report."

Describe partner organizations – academic institutions, other nonprofits, industrial or commercial firms, state or local governments, schools or school systems, or other organizations (foreign or domestic) – that were involved with the project. Partner organizations may have provided financial or in-kind support, supplied facilities or equipment, collaborated in the research, exchanged personnel, or otherwise contributed.

Provide the following information for each partnership:
Organization Name:
Location of Organization: (if foreign location list country)
Partner's contribution to the project (identify one or more)

- *Financial support;*
- *In-kind support (e.g., partner makes software, computers, equipment, etc., available to project staff);*
- *Facilities (e.g., project staff use the partner's facilities for project activities);*
- *Collaboration (e.g., partner's staff work with project staff on the project);*
- *Personnel exchanges (e.g., project staff and/or partner's staff use each other's facilities, work at each other's site); and*
- *Other.*

None

8. SPECIAL REPORTING REQUIREMENTS

COLLABORATIVE AWARDS: *For collaborative awards, independent reports are required from BOTH the Initiating Principal Investigator (PI) and the Collaborating/Partnering PI. A duplicative report is acceptable; however, tasks shall be clearly marked with the responsible PI and research site. A report shall be submitted to* ***https://ers.amedd.army.mil*** *for each unique award.*

QUAD CHARTS: *If applicable, the Quad Chart (available on https://www.usamraa.army.mil) should be updated and submitted with attachments.*

9. APPENDICES: *Attach all appendices that contain information that supplements, clarifies or supports the text. Examples include original copies of journal articles, reprints of manuscripts and abstracts, a curriculum vitae, patent applications, study questionnaires, and surveys, etc.*

frontiers in Neuroscience

ORIGINAL RESEARCH
published: 11 July 2019
doi: 10.3389/fnins.2019.00719

Progression and Pathology of Traumatic Optic Neuropathy From Repeated Primary Blast Exposure

*Alexandra Bernardo-Colón[1], Victoria Vest[1], Melissa L. Cooper[2], Sarah A. Naguib[2], David J. Calkins[1,2] and Tonia S. Rex[1,2]**

[1] Vanderbilt Eye Institute, Vanderbilt University Medical Center, Nashville, TN, United States, [2] Department of Ophthalmology and Visual Sciences, Vanderbilt University School of Medicine, Nashville, TN, United States

Indirect traumatic optic neuropathy (ITON) is a condition that is often associated with traumatic brain injury and can result in significant vision loss due to degeneration of retinal ganglion cell (RGC) axons at the time of injury or within the ensuing weeks. We used a mouse model of eye-directed air-blast exposure to characterize the histopathology of blast-induced ITON. This injury caused a transient elevation of intraocular pressure with subsequent RGC death and axon degeneration that was similar throughout the length of the optic nerve (ON). Deficits in active anterograde axon transport to the superior colliculus accompanied axon degeneration and first appeared in peripheral representations of the retina. Glial area in the ON increased early after injury and involved a later period of additional expansion. The increase in area involved a transient change in astrocyte organization independent of axon degeneration. While levels of many cytokines and chemokines did not change, IL-1α and IL-1β increased in both the ON and retina. In contrast, glaucoma shows distal to proximal axon degeneration with astrocyte remodeling and increases in many cytokines and chemokines. Further, direct traumatic optic neuropathies have a clear site of injury with rapid, progressive axon degeneration and cell death. These data show that blast-induced ITON is a distinct neuropathology from other optic neuropathies.

Keywords: optic neuropathy, axon degeneration, axonopathy, blast, indirect traumatic optic neuropathy, repeat neurotrauma, intraocular pressure, retinal ganglion cells

OPEN ACCESS

Edited by:
Rafael Linden, Federal University of Rio de Janeiro, Brazil

Reviewed by:
Daniel Sun, Harvard Medical School, United States
Francisco M. Nadal-Nicolas, Retinal Neurophysiology Section (NEI), United States

****Correspondence:***
Tonia S. Rex
tonia.rex@vanderbilt.edu

Specialty section:
This article was submitted to Neurodegeneration, a section of the journal Frontiers in Neuroscience

Received: *01 March 2019*
Accepted: *26 June 2019*
Published: *11 July 2019*

Citation:
Bernardo-Colón A, Vest V, Cooper ML, Naguib SA, Calkins DJ and Rex TS (2019) Progression and Pathology of Traumatic Optic Neuropathy From Repeated Primary Blast Exposure. Front. Neurosci. 13:719. doi: 10.3389/fnins.2019.00719

INTRODUCTION

Indirect traumatic optic neuropathy (ITON) is a condition in which the optic nerve (ON) degenerates in the absence of a penetrating injury. It is a rare condition in the general U.S. population but occurs in 0.5–5.0% of patients with a traumatic brain injury (TBI) (Steinsapir and Goldberg, 1994; Sarkies, 2004). Approximately 50% of ITON patients present with immediate, severe vision loss even though the optic disk appears normal (Yu-Wai-Man, 2015). Four to six weeks after injury the optic disk typically develops pallor, indicative of atrophy (Agrawal et al., 2013). During this time approximately 10% of ITON patients exhibit further vision loss (Yu-Wai-Man, 2015). Interestingly, another subset of patients show some improvement over this time. The rarity and complexity of this condition has made clinical studies and trials challenging. Currently there are no therapies that have been shown to be more effective than observation alone.

We have developed a model of ITON in which an air-blast is directed at the eye to avoid causing a TBI and associated cortical visual system damage that could confound results (Hines-Beard et al., 2012; Bernardo-Colon et al., 2018). Repeated low level air blast exposure with our system damages the ON while avoiding damage to the photoreceptors unlike a single, greater magnitude blast or blunt force injury (Bernardo-Colon et al., 2018; Vest et al., 2019). This repeat injury paradigm is particularly relevant to the military population due to exposure to linked exposives (mines), large firearms, or improvised explosive devices, which result in multiple blast exposures in combination with blunt force injuries in a very short time scale. Our repeat blast paradigm induces 32% axon degeneration in the ON at 2 weeks after injury. The goal of this study was to examine the pathophysiology of axon degeneration after blast-induced ITON in order to better inform the development of treatment strategies. We assessed the intraocular pressure (IOP), progression of retinal ganglion cell (RGC) loss, axon degeneration, active anterograde transport capacity, and ON glial morphology and responses including levels of cytokines and chemokines.

MATERIALS AND METHODS

Mice

Three month old male C57Bl/6 mice were purchased from Jackson Laboratories (Bar Harbor, ME, United States). We previously detected no differences between male and female mice and most service members are male. All procedures were performed in accordance with AALAC and the Association for Research in Vision and Ophthalmology guidelines and the VUMC Institutional Animal Care and Use Committee approved protocol. Mice were perfused with PBS and 4% paraformaldehyde at collection.

Trauma Model

Injury was induced as previously described (Bernardo-Colon et al., 2018; Vest et al., 2019). Briefly, mice were anesthetized with 2.5% isofluorane and secured into a padded housing chamber. The housing chamber was placed inside of a PVC pipe. The left eye of the mouse was positioned against the hole in the pipe, which was aligned with the barrel of the paintball marker. All experiments were performed in the morning. Mice were exposed to two 15 psi blasts of air at a 0.5 sec interval per day for 3 days. Sham mice were anesthetized, placed into the housing chamber and exposed to the sound but not the air-blast due to obstruction of the air prior to it reaching the eye. Mice were provided gel recovery food (Clear H_2O, Portland, ME, United States) for the first 3 days post-injury.

IOP Measurement

Intraocular pressure was measured using the Icare TonoLab rebound tonometer (Colonial Medical Supply, Franconia, NH, United States). Mice were anesthetized using isoflurane, and 10 measurements were acquired from each eye within 2 min of induction of anesthesia. IOP was measured in mice immediately prior to the first blast exposure and then over time after the last blast exposure.

Anterograde Transport Tracing

Mice were anesthetized with isoflurane and injected intravitreally in the blast-exposed eye with 2 μL cholera toxin B subunit (CTB) conjugated to Alexa Fluor 594 (Thermo Fisher) using a 30 gauge Hamilton syringe. Seventy two hours following injection, mice were anesthetized via intraperitoneal injection of 2,2,2-tribromoethanol (Sigma-Aldrich, Saint Louis, MO, United States) and perfused with 4% paraformaldehyde in PBS. Brains were post-fixed in 4% paraformaldehyde in PBS for 2 days (2d), infiltrated 1 day each in 10, 20, and 30% sucrose for cryo-protection. Brains were then cryo-sectioned coronally at 50 μm thickness. Sections traversing the SC were mounted, and the SC was imaged via epifluorescence microscopy (Nikon Instruments, Melville, NY, United States). Fluorescence in the SC sections was quantified using ImagePro software (Media Cybernetics, Rockville, MD, United States) using an automated macro described earlier to quantify the fraction of the SC retinotopic representation containing intact anterograde transport (Bond et al., 2016). Briefly, fluorescence intensity was summed along the vertical dorsal-ventral columns through the SC sections, and a normalized fluorescence intensity score was generated along the medial-lateral length of the SC. A fluorescence intensity heat map was generated from fluorescence in all SC sections with red representing maximum fluorescence and blue representing no fluorescence. These values were normalized to sham to generate the percent intact transport values. Intact transport is defined as > 70% of maximum fluorescence. We used this data to generate a complete retinotopic map using our previously published protocol (Lambert et al., 2011; Ward et al., 2014). Briefly, the collicular intensity map was overlaid on a retino-collicular projection in Photoshop and manually stretched so that the collicular points directly overlaid the corresponding locations on the retinotopic projection, as established in Drager and Hubel (1976). Areas with transport deficits (less than 70% of maximum fluorescence) were represented with solid gray. The labels around the maps indicate eccentricity coordinates of the visual field. Abbreviations I, N, S, T indicate inferior, nasal, superior, and temporal quadrants of the retina, respectively.

Immunohistochemistry and Cell Counting

Eyes were preserved in 4% paraformaldehyde, cryoprotected in 30% sucrose overnight at 4°C and embedded in tissue freezing medium (Triangle Biomedical, Durham, NC, United States). Ten-micron thick sections were collected in round on a cryostat (Fisher, Pittsburgh, PA, United States). Each slide had representative sections from the entire eye when collected in round. Slides were then rinsed with PBS and incubated at room temperature in normal donkey serum (NDS; 0.05%) in 0.1M phosphate buffer with 0.5% bovine serum albumin and 0.1% Triton X-100 (phosphate buffer plus Triton X-100 [PBT]) for 2 h. The slides were incubated overnight at 4°C in anti-RBPMS

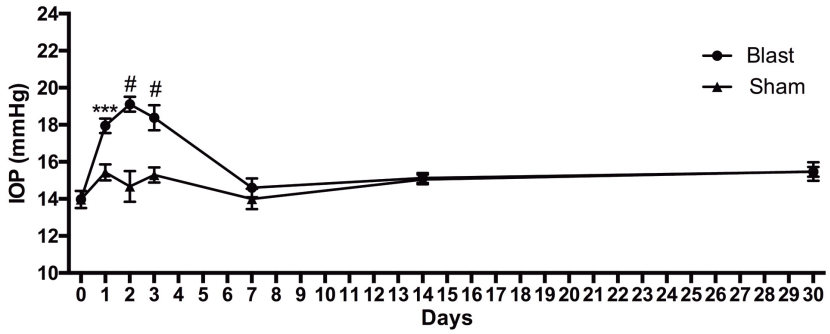

FIGURE 1 | IOP changes over time after blast injury. Student's *t*-test comparisons show elevations in IOP in the blast-exposed group as compared to shams at 1, 2, and 3 days after blast. ***$p < 0.001$; #$p < 0.0001$. Baseline, $n = 14$; 1 day sham, $n = 14$; 1 day blast, $n = 14$; 2 days sham, $n = 7$; 2 days blast, $n = 14$; 3 days sham, $n = 7$; 3 days blast, $n = 14$; 7 days sham, $n = 7$; 7 days blast, $n = 5$; 14 days sham, $n = 7$; 14 days blast, $n = 5$; 30 days sham, $n = 7$; 30 days blast, $n = 7$.

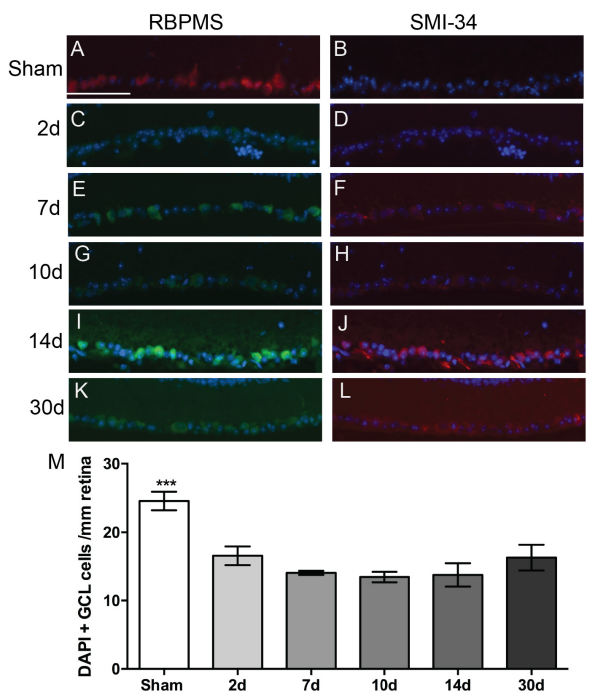

FIGURE 2 | Effect of blast on the RGCs. **(A–L)** Representative fluorescence micrographs of retina cross-sections labeled with anti-RPBMS (red in **A**; green in **C,E,G,I,K**), SMI-34 (red; **B,D,F,H,J,L**) and DAPI (blue) from: **(A,B)** sham, or **(C,D)** 2d, **(E,F)** 7d, **(G,H)** 10d, **(I,J)** 14d, and **(K,L)** 30 d post-blast mice. **(M)** Quantification of nuclei in the GCL over time after injury. Error bars represent s.d. Asterisks indicate that sham was different from all other groups at $p < 0.001$. Scale bar represents 50 μm and is applicable to all images in the figure. $N = 3$ for all groups.

(1:400; ABN1362; Millipore, Burlington, MA, United States) and anti-phosphorylated neurofilament H (SMI 34; 1:1000; 835503; Biolegend, San Diego, CA, United States) in PBT. Slides were then rinsed with PBS and incubated with their appropriate secondary antibody (donkey anti-rabbit 555 and donkey anti-mouse 594; Life Technologies, Carlsbad, CA, United States) for 2 h at room temperature. Finally, slides were rinsed in PBS, mounted in Vectashield Mounting medium with DAPI (Vector Laboratories, Burlingame, CA, United States) or Fluoromount-G (Southern Biotech, Birmingham, AL, United States). Slides were imaged on a Nikon Eclipse epifluorescence microscope (Nikon, Melville, NY, United States). All images were collected from sections through the ON at identical magnification, gain, and exposure settings. These same sections were used for quantification of DAPI-positive cells in the GCL. Nikon software was used to measure the length of the retina that was used for counting.

ON Histology and Axon Counting

The entire ON, from next to the globe to the optic chiasm, was collected, cut into three equal pieces, post-fixed in glutaraldehyde, and embedded in Resin 812 and Araldite 502 (cat 14900 and 10900, respectively; Electron Microscopy Sciences, Hatfield, PA, United States) according to previously published protocol (Bricker-Anthony et al., 2014, 2017; Bond et al., 2016; Hines-Beard et al., 2016). One-micron thick sections were collected on a Leica EM-UC7 microtome and stained with 1% paraphenylenediamine (ppd) and 1% toluidine blue. Proximal sections were collected from the end of the ON that was cut from the globe. Medial sections were collected from the end of the mid-section of the ON that faced the globe. Distal sections were collected from the distal piece of the ON and from the side that was cut away from the optic chiasm. Cross-sections were imaged on a Nikon Eclipse Ni-E microscope (Nikon Instruments Inc., Melville, NY, United States) using a 100x oil immersion objective. Total and degenerating axons were quantified using Image J. A grid was used to count 20% of the ON cross-sectional surface area to avoid bias.

Glial Analyses

Glial morphology and organization were analyzed as previously described (Cooper et al., 2016, 2018). Briefly, Matlab functions were used to quantify the fraction of total nerve area covered by glia, parallelism of astrocyte processes, and spatial distribution of astrocyte processes radially across the nerve. Higher parallelism values indicate a greater degree of alignment of the glial processes, while lower values indicate more disorder. Spatial distribution,

specifically bias toward the edge or center of the nerve, was quantified by defining a center of mass (CoM) based on division of the nerve into concentric rings. Values near 10 indicate an even distribution; values less than 10 indicate bias toward the edge of the nerve; and values greater than 10 indicate bias toward the center of the nerve. For each nerve, these metrics were plotted against each other, as well as against other disease indices (total axon count, axon density, nerve size, and time post-injury) to determine trends in disease progression. For each index pair, linear regression analysis was performed in SigmaPlot. A p-value less than 0.05 was considered to indicate significant correlation.

Multiplex ELISA

Retinas were sonicated and run in singlet on the Milliplex MAP Mouse Cytokine/Chemokine Magnetic Bead Panel I 25-plex assay per manufacturer's protocol (EMD Millipore, Billerica, MA, United States). Plates were read on a Luminex MAGPIX with xPONENT software (Thermo Fisher Scientific,

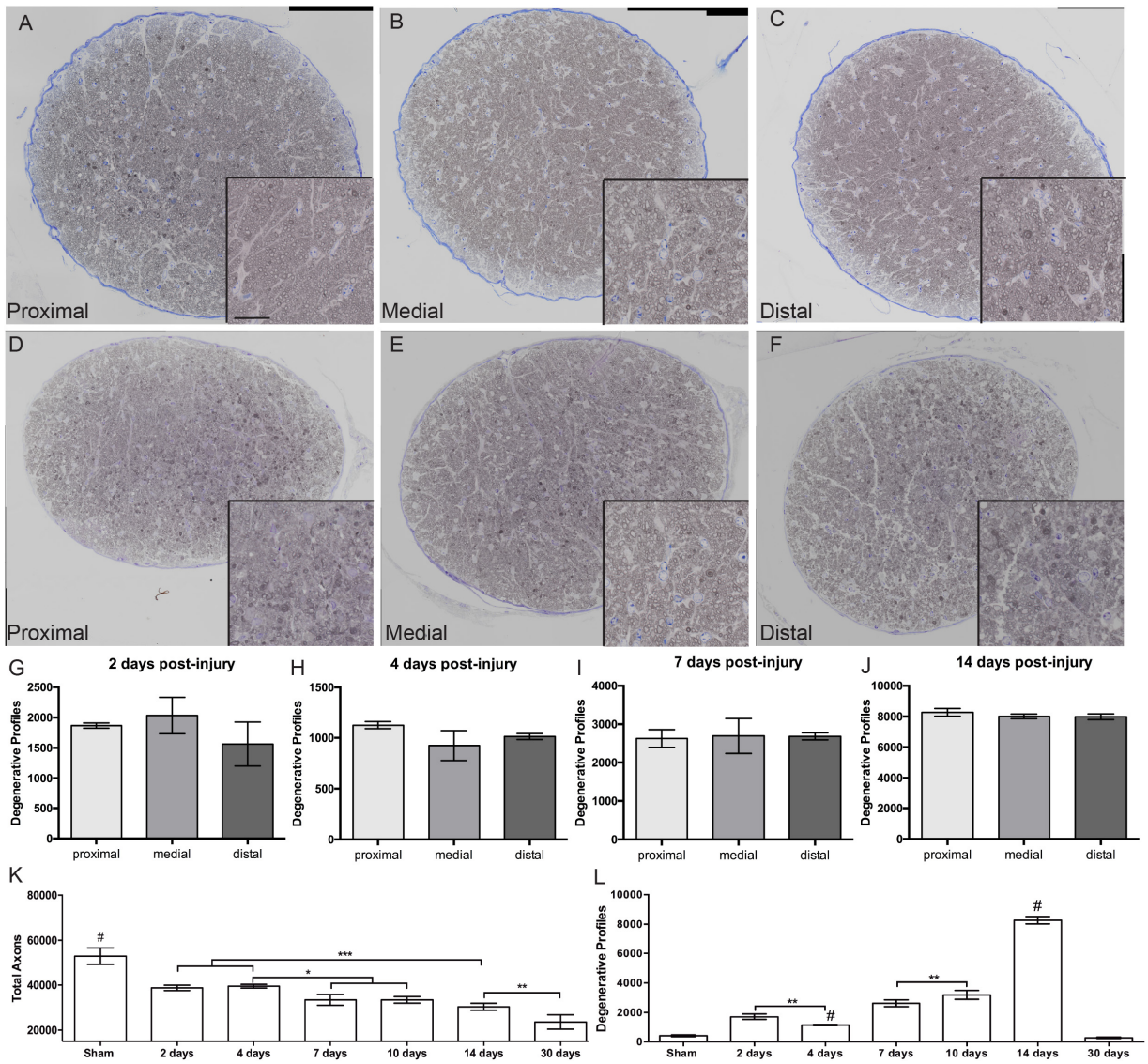

FIGURE 3 | Progression of ON degeneration after blast. **(A–F)** Representative bright-field micrographs of cross-sections from proximal **(A,D)**, medial **(B,E)**, and distal **(C,F)** regions of the ON at 7 days **(A–C)** and 14 days **(D–F)** post-blast. Insets are higher magnification images of the respective ONs. Scale bar for all insets = 20μm. **(G–J)** Quantification of degenerative axon profiles in each spatial location over-time post-injury; **(G)** 2 days, **(H)** 4 days, **(I)** 7 days, and **(J)** 14 days. There was no difference between spatial locations within any time-point. Data shown is mean ± s.d. **(K)** Quantification of total axons over time post-injury. The number of total axons was decreased at 2 days post-injury due to the primary event. Further decreases were detected at 7 and 10 days, 14 days, and 30 days post-blast. **(L)** Quantification of degenerative axon profiles over time post-injury. Degenerative axon profiles from the injury event were still present at 2 days after injury, but was decreased at 4 days. A slight increase was again detected at 7 and 10 days after injury. The peak of degeneration was at 14 days post-injury. Ongoing axon degeneration was completed by 30 days after blast. *$p < 0.05$, **$p < 0.01$, ***$p < 0.001$, #$p < 0.0001$. Sham, $n = 6$; 2 days, $n = 5$; 4 days, $n = 4$; 7 days, $n = 4$; 14 days, $n = 5$; 30 days, $n = 6$.

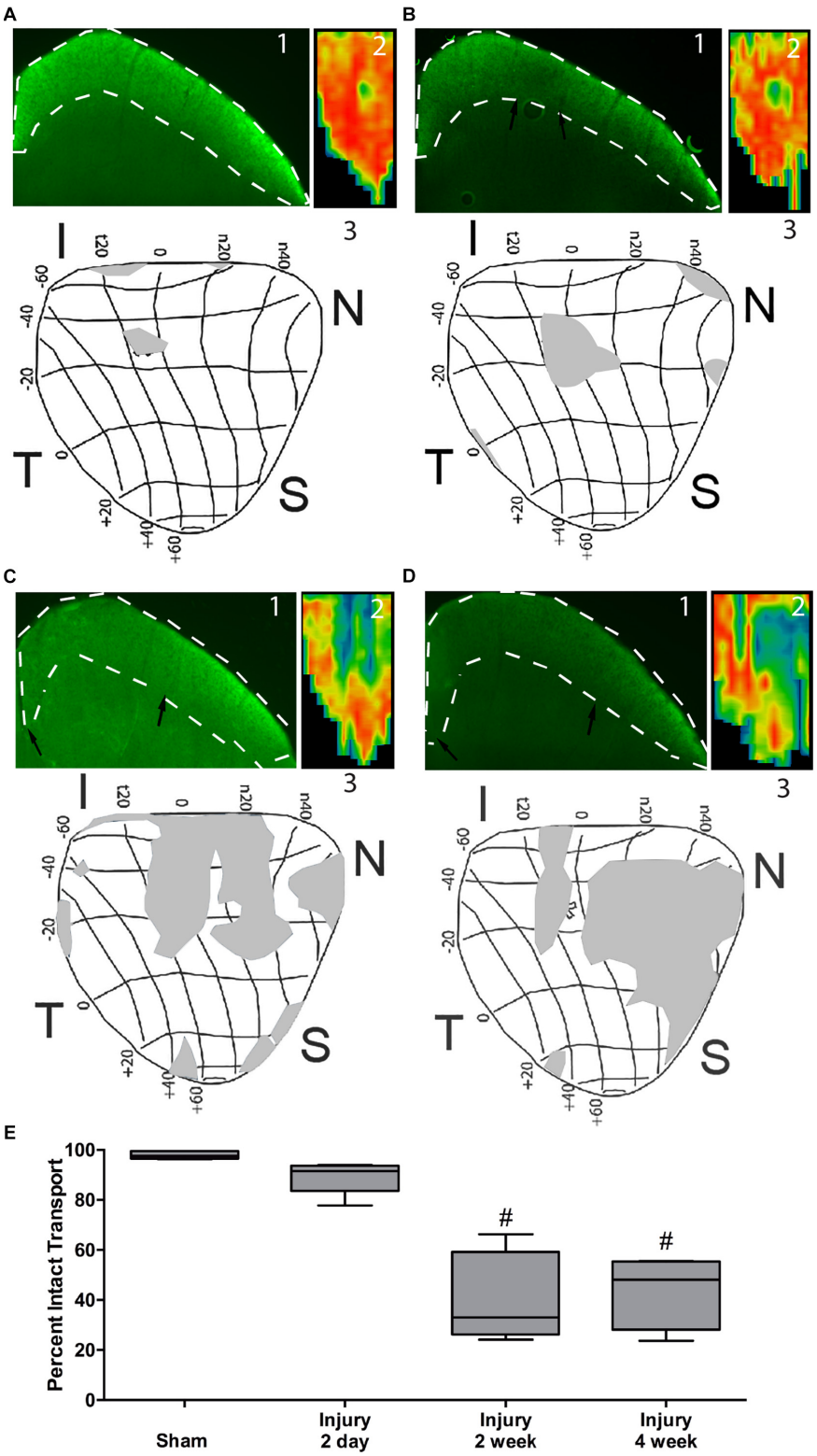

FIGURE 4 | Axon transport deficits after blast injury. A representative fluorescence micrograph of the superior colliculus (1), heat map of total superior colliculus fluorescence (2), and a retinotopic map of transport deficits (3) are shown for sham, $n = 7$, **(A)**, and 2 days, $n = 6$, **(B)**, 14 days, $n = 5$, **(C)**, and 30 days, $n = 5$, **(D)** post-blast animals. Black arrows indicate edges of transport loss in the superior colliculus. Asterisk indicates the location of the ON head in the retinotopic maps. The labels around the maps indicate eccentricity coordinates of the visual field. Abbreviations I, N, S, T indicate inferior, nasal, superior, and temporal quadrants of the retina, respectively. **(E)** Quantification of total axon transport over time post-blast. #$p < 0.0001$ compared to Sham.

Waltham, MA, United States) using settings stated in the manufacturer's protocol. Multiplex ELISA plates were read and analyzed through the use of the Vanderbilt Hormone Assay and Analytical Services Core.

Statistical Analysis

Graphpad Prism software was used to perform statistical analysis of all data. A minimum of four ONs was assessed per group for axon quantification. A one-way ANOVA and Tukey's *post hoc* test was performed. These numbers are based on our previous statistical analysis for these assays (Bond et al., 2016; Hines-Beard et al., 2016).

RESULTS

Blast-Exposure Causes a Short-Term Elevation in IOP

Normal sham, lightly anesthetized mice had IOPs ranging from 14 to 15.5 mmHg for the duration of the study (**Figure 1**). Blast-exposed mice had a baseline IOP of 14 ± 1.6 mmHg (avg ± sd). The IOP increased to 18 ± 1.4, 19 ± 1.4, and 18 ± 2.4 mmHg at 1, 2, and 3 days after blast, respectively. At 7 days post-injury and thereafter the IOP was similar to baseline levels.

Early, but Not Ongoing, RGC Death After Blast Injury

We immunolabeled retinas with anti-RBPMS, a marker for all RGCs, and anti-phosphorylated neurofilament-H, a marker for neuronal degeneration. We also labeled with the nuclear marker, DAPI. In sham mice, there was RPBMS immunolabeling of RGCs (red), but no SMI-34 labeling (red) (**Figures 2A,B**). At all time-points post-blast, RBPMS immunolabeling could be detected although the brightness of the labeling varied (**Figures 2C,E,G,I,K**; green). Labeling with SMI-34 was still absent at 2 days (**Figure 2D**). In contrast, labeling with SMI-34 was detectable at 7, 10, 14, and 30 days post-injury (**Figures 2F,H,J,L**; red). Phosphorylated neurofilament accumulates in neurons when the axons are degenerative, thus this data suggests that there is axon degeneration at 7 days and later after injury. Since labeling with RBPMS was not consistently present at high levels after injury, we were unable to accurately quantify RGCs using this immunohistochemical approach. Therefore, we instead quantified DAPI-positive cells

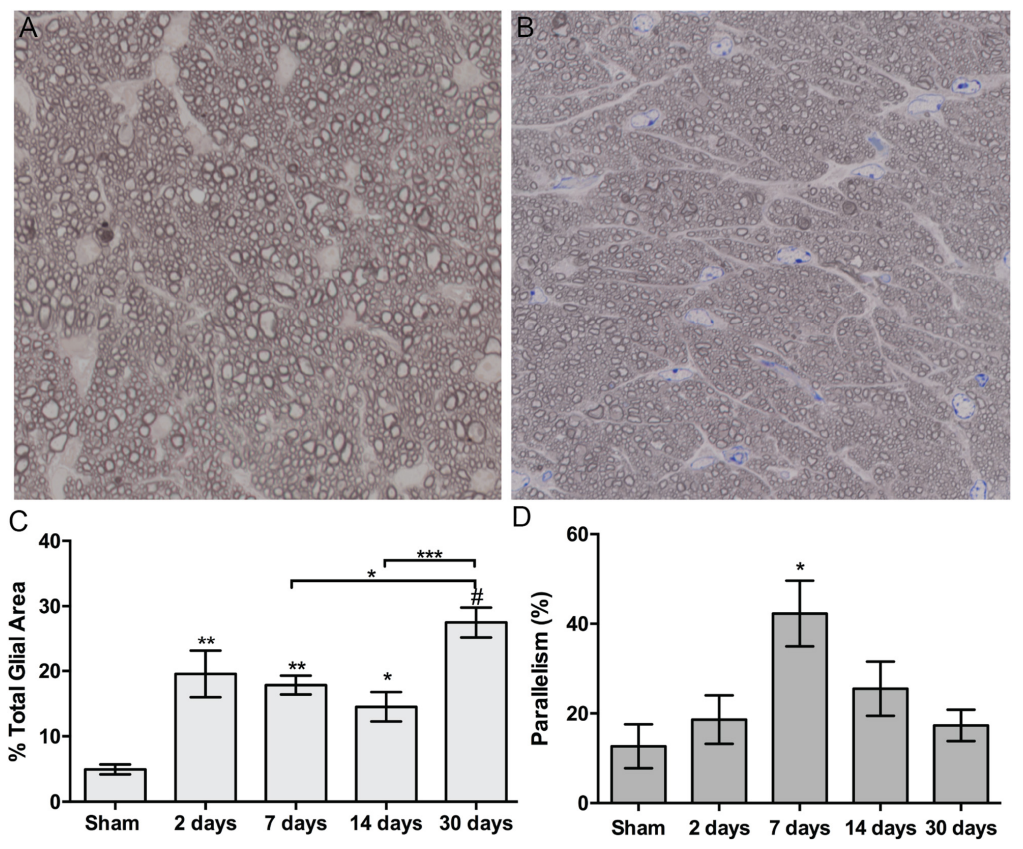

FIGURE 5 | Quantification of ON astrocyte responses to blast injury. **(A,B)** Brightfield micrographs of sham **(A)** and 7 days post-blast **(B)** ON showing glial changes after blast injury. **(C)** Quantification of percent glial area over time after injury. Asterisks above bars indicate differences compared to sham, $*p < 0.05$, $**p < 0.01$, $***p < 0.001$, $\#p < 0.0001$. **(D)** Quantification of percent parallelism over time after injury, $*p < 0.05$. Sham, $n = 7$; 2 days, $n = 6$; 7 days, $n = 7$; 14 days, $n = 12$; 30 days, $n = 11$.

in the ganglion cell layer (GCL) of the retina, recognizing that displaced amacrine cells, astrocytes, and microglial cells would be included in the total numbers. Using this approach we detected fewer cells in the GCL at all post-blast time-points as compared to shams (**Figure 2M**). There was no statistically significant difference between post-blast groups.

Blast-Exposure Does Not Cause Distal Axonopathy

To investigate if blast-induced axon degeneration occurs in a particular region of the ON or progresses in a particular direction over time we assessed cross-sections from proximal, medial, and distal regions of the ON over time (**Figure 3**). Within each time point the histology looked similar at each location along the nerve (**Figures 3A–F**). Quantification of degenerative axon profiles confirmed a lack of difference between the proximal, medial, or distal regions of the ON at all time points examined (**Figures 3G–J**).

Two days after injury, there was a significant increase in degenerative profiles and loss of total axons as compared to shams (**Figures 3K,L**). At 4 days after injury there were fewer degenerative profiles and the total axon number was unchanged.

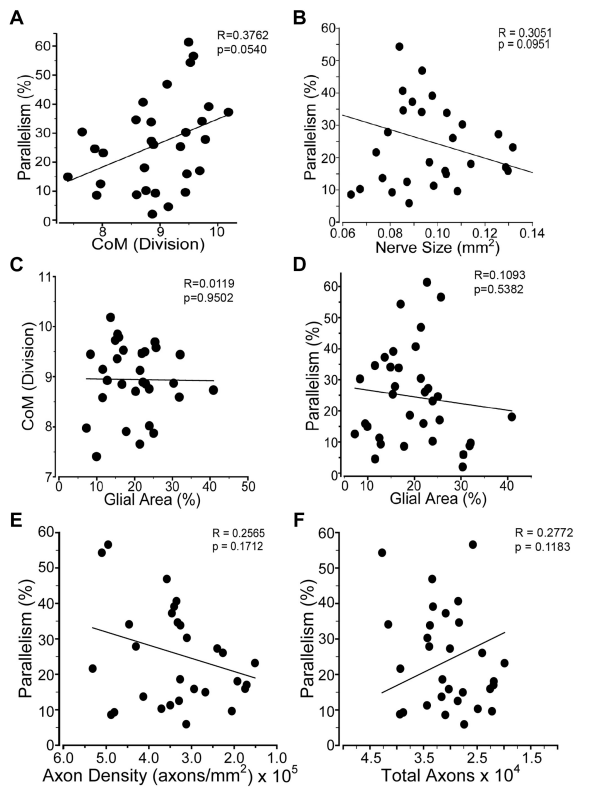

FIGURE 6 | Glial distribution in the ON after injury. Graphs comparing: **(A)** percent glial parallelism and glial center of mass (CoM); **(B)** percent glial parallelism and ON cross-sectional size; **(C)** CoM and percent glial area; **(D)** percent parallelism and percent glial area; **(E)** percent parallelism and axon density; and **(F)** percent parallelism and total axons. Sham, $n = 7$; 2 days, $n = 6$; 7 days, $n = 7$; 14 days, $n = 12$; 30 days, $n = 11$.

At 7 and 10 days post-blast there was a slight but statistically significant decrease in total axons and a correlative increase in degenerative profiles. There was a strikingly large increase in degenerative profiles at 14 days after injury (**Figure 3L**), in agreement with our previous studies (Bernardo-Colon et al., 2018). At 30 days after blast there was a 55% reduction in the total number of axons as compared to sham, but the number of degenerative profiles was no longer significantly different from sham (**Figures 3K,L**). This suggests that ongoing degeneration had ceased.

Localization and Timing of Blast-Induced Axon Transport Deficits

In sham animals, the RGC axons actively transport labeled CTB to throughout the superior colliculus as shown by bright fluorescence and red heat map (**Figures 4A1,2**). The retina representation of transport to the superior colliculus shows complete transport with the exception of the representation of the ON head (**Figure 4A3**). At 2 days after blast there were small regions with decreased fluorescence indicative of a loss of transport (**Figures 4B1,2**). These regions were in areas representative of far peripheral retina (**Figure 4B3**). Transport deficits were similar at 14 and 30 days after blast (**Figures 4C,D**). There appeared to be a progression of deficits from the periphery to the center of the retina representation of the superior colliculus (**Figures 4C,D**). Quantification of fluorescence in the superior colliculus showed a trend toward a decrease in transport at 2 days post-blast that did not reach statistical significance (**Figure 4E**). Transport continued to decline such that at the peak of axon degeneration (14 days after injury) only 41% $\pm$ 18 (avg $\pm$ sd) axon transport was detected. The percent transport was similar at 30 days after injury. Thus there was a close correlation in timing and level of axon degeneration and transport deficits.

Astrocytes Are Reactive but Do Not Change Their Overall Pattern or Orientation After Trauma

Astrocyte size and process distribution appears altered at 7 days post-blast (**Figures 5A,B**). Astrocyte processes aligned along a more common axis at 7 days after blast, while sham processes appeared to orient at random. We previously published that blast injury causes an increase in glial area in the ON at 2- and 4- weeks after injury, concordant with increased axonal degeneration (Bernardo-Colon et al., 2018). Here we have added additional time points post-blast to better describe injury pathogenesis. We detect an increase in glial area at 2 days after blast as a result of the primary injury (**Figure 5C**). The percent glial area trended down at 7 and 14 days after injury when compared to the levels at 2 days after injury, but were still higher than shams. Intriguingly, glial coverage increased at 30 days after blast, suggesting a response to the peak of axon degeneration at 14 days. No statistically significant change in glial center of mass was detected at any time after injury (data not shown). The percent of glial parallelism, a measure of process orientation along a common axis, was increased transiently at 7 days after blast (**Figure 5D**). To further assess the glial response to blast, we compared glial

parallelism and center of mass to nerve size, percent glial area, axon density, or total number of axons (**Figures 6A–F**). No statistically significant changes were detected. Thus, blast injury induces: (1) an increase in glial area following the two peaks of axon degeneration, and (2) a transient increase in glial parallelism in between the two peaks of axon degeneration.

Blast-Induced Trauma Increases Levels of IL-1 Related Proteins Only

We performed a multiplex cytokine ELISA on retinas and ONs from sham and blast-injured animals. The majority of cytokines and chemokines detected in the ELISA did not change at any time after blast examined (**Table 1**). In the retina, we detected elevated IL-1α at both 14 and 30 days post-blast (**Figure 7A**). We also detected elevated IL-1β at 30 days post-blast (**Figure 7B**), consistent with our previously published results (Bernardo-Colon et al., 2018). In addition we detected an increase in IL-2 at 30 days post-blast (**Figure 7C**), and a statistically significant decrease in the chemokine KC/CXCL1 at 14 days, but not 30 days after blast (**Figure 7D**). In the ON, the only cytokine altered after blast was IL-1α, which was statistically significantly elevated at 10 and 14 days after blast, and trended high at 30 days after blast (**Figure 7E**).

DISCUSSION

In explosive blasts, propagation of the over-pressure blast wave through the body can cause axon shearing and stress to which long axons appear to be most vulnerable (Garman et al., 2011; Koliatsos et al., 2011). Computer modeling of blast exposure to the eye shows elevated IOP, but these models typically only assess changes that occur during or immediately after blast (Rossi et al., 2012; Bhardwaj et al., 2014; Esposito et al., 2015; Karimi et al., 2016; Notghi et al., 2017). Surprisingly, we detected a 20% elevation in IOP that lasted for 3 days after the last blast exposure. Sustained elevation in IOP is typically associated with glaucoma, a progressive optic neuropathy. In addition to chronic models of elevated IOP, there are acute models that induce a short time course of IOP elevation, similar in duration to what we detected in our trauma model, which also induces ON damage (Valiente-Soriano et al., 2015; Ou et al., 2016). However, the magnitude of the IOP increase is greater in these acute models of ocular hypertension than what we detected after blast. Yet, the amount of axon degeneration detected in our animals was much higher at the same time-point. It is feasible that transient corneal edema that was not visible upon gross exam was responsible for the transient elevation in IOP that we detected. Together this suggests that axon degeneration in our model is not due primarily to post-injury elevated IOP.

We detected a rapid decrease in nuclei present in the GCL at 2 days after blast, without further loss over time. This is comparable to the time course of RGC loss recently reported after ON crush or transection (Sánchez-Migallón et al., 2018).

However, in the absence of a reliably detectable RGC-specific marker after blast injury, it leaves the possibility that some of the cell loss may have been due to death of displaced amacrine cells

TABLE 1 | Quantification of cytokines and chemokines in the retina and ON after injury.

	14d retina	30d retina	10d ON	14d ON	30d ON
G-CSF	ND	89.7±18.0(2)	101.6±8.7(2)	89.8±5.0(3)	75.0±22.2(4)
GM-CSF	108.3±18.3(3)	77.0±39.2(3)	68.4±21.4(4)	98.2±17.8(5)	52.1±18.3(3)
IFNγ	243.4 (1)	94.3±17.7(2)	ND	97.8 (1)	149.3±76.1(7)
IL-1α	421.6±58.1(8)*	396.5±299.4(8)*	222.0±21.7(4)*	266.1±32.4(5)*	132.5±58.6(8)
IL-1β	81.4±43.7(8)	278.0±134.7(8)*	84.2±10.5(4)	103.1±11.9(5)	91.2±3.5(3)
IL-2	100.7±38.3(8)	142.0±42.3(8)*	82.6±24.9(3)	85.0±13.4(5)	107.9±31.6(8)
IL-4	ND	50.0±36.3(7)	ND	ND	88.1±9.1(4)
IL-5	ND	101.5±0(2)	ND	ND	67.7±14.9(3)
IL-6	ND	64.5±11.2(3)	ND	ND	84.5±24.2(4)
IL-7	ND	98.1±1.8(2)	ND	88.6±5.1(3)	93.6±18.6(4)
IL-9	83.5±28.4(8)	74.1±26.6(4)	77.8±52.9(4)	95.4±15.6(5)	119.4±63.6(8)
IL-10	65.2±49.6(7)	63.6±41.1(4)	68.9±19.4(4)	88.4±11.6(5)	69.3±29.3(6)
IL-12(p40)	ND	ND	ND	79.6±3.7(3)	96.2±32.6(3)
IL-12(p70)	68.4±18.9(5)	73.1±18.2(3)	ND	90.6 (1)	107.3±17.6(4)
IL-15	ND	82.4 (1)	ND	ND	105.0±55.5(4)
IL-17	ND	104.7±33.4(5)	59.2±25.9(4)	88.1±11.4(5)	97.8±16.4(4)
IP-10	93.8±20.6(6)	103.6±7.6(2)	ND	ND	127.6±130.0(8)
KC	64.9±16.9(6)	77.4±20.7(4)	81.3±56.9(3)	58.9±19.0(5)	92.3±21.0(4)
MCP-1	ND	85.0±23.3(4)	85.1±7.7(3)	94.8±15.9(5)	89.6±30.9(7)
MIP-1α	106.7±27.3(8)	72.0±13.2(4)	79.9±15.1(3)	89.1±17.7(5)	129.7±137.6(8)
MIP-1β	ND	ND	78.1±44.3(4)	111.0±13.1(5)	99.4±4.0(4)
MIP-2	135.1±95.8(8)	75.4±31.6(4)	62.3±3.6(3)	78.8±11.4(4)	64.4±26.1(4)

Indicates statistically significant difference, see **Figure 6. Values are average ± s.d. (n).*

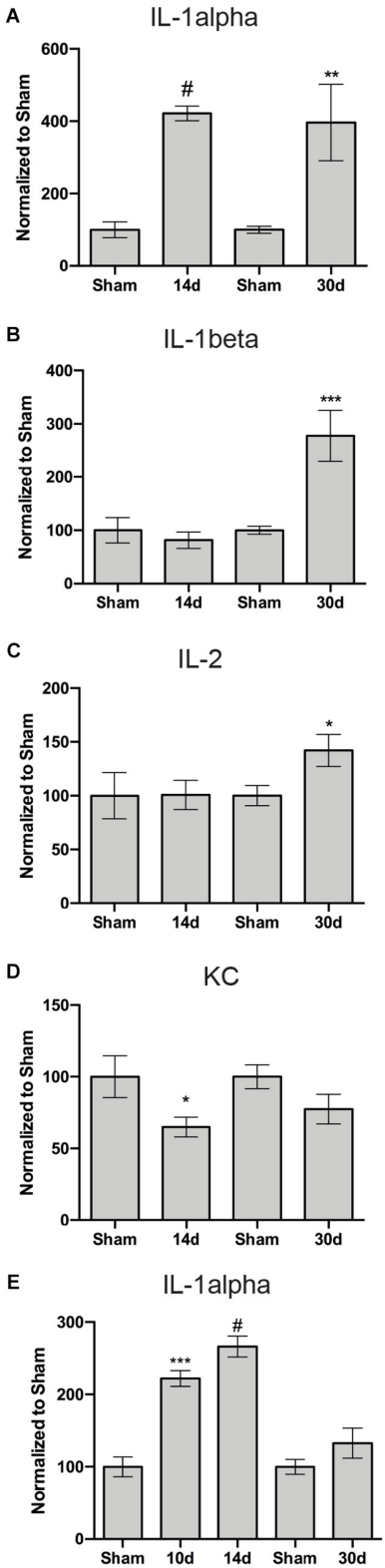

FIGURE 7 | Inflammation-associated proteins with altered levels in the retina **(A–D)** or ON **(E)** after blast. Graphs show: **(A,E)** IL-1α; **(B)** IL-1β; **(C)** IL-2; and **(D)** KC. *$p < 0.05$, **$p < 0.01$, ***$p < 0.001$, #$p < 0.0001$. All analytes are presented in **Table 1**. The n for each is provided in **Table 1**.

or astrocytes, or migration of microglial cells out of this layer, potentially into the ON. We also detected an accumulation of phosphorylated neurofilament in the cell bodies of the remaining RGCs that was first evident at 7 days and was greatest at 14 days after injury, suggesting that secondary axon dysfunction begins at 7 days post-injury. The decrease in GCL nuclei at 2 days correlates with the presence of fewer axons at this time-point and suggest that loss of these cells and their axons was due to the initial injury event. It is interesting that no secondary loss of GCL nuclei was detected despite a delayed peak of axon degeneration at 14 days post-injury and loss of axons at 30 days post-injury. This could, in part, be due to infiltration of microglia into the GCL, which would counteract decreases in RGC nuclei since DAPI detects all nuclei in a cell-type independent manner. This should be explored in future studies. Altogether these data demonstrate that RGC loss does not precede axon degeneration. It is feasible that there is additional RGC loss at later time-points, after the loss of axons at 14–30 days. It is interesting to note that the presence of phosphorylated neurofilament in the RGCs at 30 days post-blast suggests that the remaining axons are not entirely healthy. Future studies should explore the long-term effects of repeat blast exposure on the RGCs and axons.

Our model showed comparable axon degeneration at multiple locations along the length of the ON. This suggests that there is not a particular region of the ON that is susceptible to injury from blast wave forces. This is in contrast both to glaucoma, which shows a distal to proximal pattern of axon degeneration progression, and direct TON, which obviously has a specific area of injury in the ON. Further, our data suggests two stages of axon degeneration. The first appears to occur prior to 2 days after blast since there was already a significant loss of total axons and cells in the GCL at this time. This was likely a direct result of the initial injury. The second stage was first detectable at 7—10 days post-injury and peaked at 14 days post-injury and did not correlate with additional loss of cells in the GCL. This stage was likely due to the activity of molecular pathways initiated by the injury event (Bernardo-Colon et al., 2018; **Figure 7**). The staging of axon degeneration and GCL cell loss we detect here is different from the progressive degeneration that occurs in glaucoma or the rapid, acute degeneration that occurs in models of direct traumatic optic neuropathy (Calkins, 2012).

We detected axon transport deficits that appeared to correlate with axon degeneration, rather than preceding frank axon degeneration or cell death as in models of glaucoma (Crish et al., 2010; Calkins, 2012; Valiente-Soriano et al., 2015). However, we may have missed subtle decreases at intermediate time points or in individual axons. Deficits in axon transport machinery have been detected at the level of the individual axon in blast-induced TBI models by measuring levels of phosphorylated neurofilament in different regions of the neuron (Saljo et al., 2000). Further, the spatial location of axon transport deficits was different between our model and the microbead occlusion model of glaucoma. In the microbead occlusion model, transport deficits were first detected in the inferior nasal quadrant and progressed toward the superior nasal quadrant before then spreading temporally (Lambert et al., 2011). In our model of ITON, axon transport

loss after the primary insult is detected centrally and in the far periphery. The secondary degeneration causes transport deficits to increase, moving from the periphery to the center of the retinotopic map. The reason for this is unclear and should be an area of active investigation.

An important role for inflammation has been suggested for both traumatic and glaucomatous optic neuropathies, thus we also explored alterations in the astrocytes and cytokine/chemokine levels. Unlike in the DBA/2J model of glaucoma, we did not detect decreased parallelism or CoM of the ON astrocytes (Cooper et al., 2016, 2018). In fact we detected a trend toward elevated parallelism as CoM increases, which is the opposite to what we have detected in the DBA/2J model of glaucoma. Further, although increases in TNFa, and IL6 have been shown to contribute to glaucoma pathogenesis (Agarwal and Agarwal, 2012; Echevarria et al., 2017), we do not detect increases in either in our model, in fact, TNFa was below the detection limit in our assay. However, we did detect increases in IL-1α and IL-1β, which are also elevated in glaucoma (Adornetto et al., 2019). Increases in IL-1 family proteins is indicative of activation of the inflammasome pathway, which has received increasing attention in both the fields of glaucoma and TBI (Mortezaee et al., 2018; Adornetto et al., 2019). The early increase in IL-1α in both the retina and ON suggests that it is a driver of pathology. Interestingly, a recent paper suggests that IL-1α induces cortical astrocytes to convert to a neurotoxic, reactive, A1, phenotype (Liddelow et al., 2017). Future studies are needed to determine if this is the case in our model. The continued elevation of IL-1α levels at 30 days in the retina, but not the ON may suggest that pathogenesis may continue longer-term in the retina. Further, differences in cytokine levels between ON and retina could also be due to the higher concentration of astrocytes and oligodendrocytes in the ON, while the retina is enriched for neurons. Finally, we recognize that microglia may play an important role in ON pathology due to glaucoma or trauma. We intend to explore any role of these cells in our model of ITON in future studies.

CONCLUSION

This study shows that ITON has a neuropathology distinct from direct TON or glaucoma. Finally, the increases in IL-1 related proteins and oxidative stress in our model and models of glaucomatous optic neuropathies suggests that therapies that target these pathways might be effective in both conditions.

DATA AVAILABILITY

The raw data supporting the conclusions of this manuscript will be made available by the authors, without undue reservation, to any qualified researcher.

ETHICS STATEMENT

All procedures were performed in accordance with the AALAC and the Association for Research in Vision and Ophthalmology guidelines and the VUMC Institutional Animal Care and Use Committee approved protocol.

AUTHOR CONTRIBUTIONS

TR conceived and designed the study, supervised implementation, performed the data analysis, and wrote the manuscript. AB-C performed the blast-exposure experiments, axon quantifications and ELISA, and edited the manuscript. VV performed the microscopy, digital quantitative analysis of fluorescence and histology, astrocyte analysis, and edited the manuscript. SN performed ELISAs and edited the manuscript. MC assisted in astrocyte analysis and edited the manuscript. DC supervised the data analysis and edited the manuscript.

FUNDING

Support for TR was provided by DoD W81XWH-15-1-0096 and W81XWH-17-2-0055, NEI R01 EY022349, NIA R01 NS094595, Potocsnak Discovery Grant in Regenerative Medicine, Ayers Foundation Regenerative Visual Neuroscience Pilot Grant, and Jones Gift. Support for DC was provided by NIH R01EY024997, the Glaucoma Research Foundation, and the Stanley Cohen Innovation Fund. Support for MC and SN was provided by T32 EY021833. All investigators were supported by the Vanderbilt University Medical Center Cell Imaging Shared Resource core facility (Clinical and Translational Science Award Grant UL1 RR024975 from the National Center for Research Resources), NEI P30EY008126, and the Research Prevent Blindness, Inc.

ACKNOWLEDGMENTS

The authors thank Purnima Ghose for histological processing.

REFERENCES

Adornetto, A., Russo, R., and Parisi, V. (2019). Neuroinflammation as a target for glaucoma therapy. *Neural Regen. Res.* 14, 391–394. doi: 10.4103/1673-5374.245465

Agarwal, R., and Agarwal, P. (2012). Glaucomatous neurodegeneration: an eye on tumor necrosis factor-alpha. *Indian J. Ophthalmol.* 60, 255–261. doi: 10.4103/0301-4738.98700

Agrawal, R., Shah, M., Mireskandari, K., and Yong, G. (2013). Controversies in ocular trauma classification and management: review. *Int. Ophthalmol.* 33, 435–445. doi: 10.1007/s10792-012-9698-y

Bernardo-Colon, A., Vest, V., Clark, A., Cooper, M., Calkins, D. J., Harrison, F. E., et al. (2018). Antioxidants prevent inflammation and preserve the optic projection and visual function in experimental neurotrauma. *Cell Death Dis.* 9:1097. doi: 10.1038/s41419-018-1061-4

Bhardwaj, R., Ziegler, K., Seo, J., Ramesh, K., and Nguyen, T. (2014). A computational model of blast loading on the human eye. *Biomech. Model. Mechanobiol.* 13, 123–140. doi: 10.1007/s10237-013-0490-3

Bond, W., Hines-Beard, J., GoldenMerry, Y., Davis, M., Farooque, A., Sappington, R., et al. (2016). Virus-mediated EpoR76E therapy slows optic nerve axonopathy in experimental glaucoma. *Mol. Ther.* 24, 230–239. doi: 10.1038/mt.2015.198

Bricker-Anthony, C., D'Surney, L., Lunn, B., Hines-Beard, J., Jo, M., Bernardo-Colon, A., et al. (2017). Erythropoietin either prevents or exacerbates retinal damage from eye trauma depending on treatment timing. *Optom. Vis. Sci.* 94, 20–32. doi: 10.1097/OPX.0000000000000898

Bricker-Anthony, C., Hines-Beard, J., and Rex, T. S. (2014). Molecular changes and vision loss in a mouse model of closed-globe blast trauma. *Invest. Ophthalmol. Vis. Sci.* 55, 4853–4862.

Calkins, D. J. (2012). Critical pathogenic events underlying progression of neurodegeneration in glaucoma. *Progr. Ret. Eye Res.* 31, 702–719. doi: 10.1016/j.preteyeres.2012.07.001

Cooper, M., Collyer, J., and Calkins, D. J. (2018). Astrocyte remodeling without gliosis precedes optic nerve axonopathy. *Acta Neuropathol. Commun.* 6:38. doi: 10.1186/s40478-018-0542-0

Cooper, M., Crish, S., Inman, D., Horner, P., and Calkins, D. J. (2016). Early astrocyte redistribution in the optic nerve precedes axonopathy in the DBA/2J mouse model of glaucoma. *Exp. Eye Res.* 150, 22–33. doi: 10.1016/j.exer.2015.11.016

Crish, S., Sappington, R. M., Inman, D., Horner, P., and Calkins, D. J. (2010). Distal axonopathy with structural persistence in glaucomatous neurodegeneration. *Proc. Natl. Acad. Sci. U.S.A.* 107, 5196–5201. doi: 10.1073/pnas.0913141107

Drager, U. C., and Hubel, D. H. (1976). Topography of visual and somatosensory projections to mouse superior colliculus. *J. Neurophysiol.* 39, 91–101. doi: 10.1152/jn.1976.39.1.91

Echevarria, F., Formichella, C., and Sappington, R. M. (2017). Interleukin-6 deficiency attenuates retinal ganglion cell axonopathy and glaucoma-related vision loss. *Front. Neurosci.* 11:318. doi: 10.3389/fnins.2017.00318

Esposito, L., Clemente, C., Bonora, N., and Rossi, T. (2015). Modelling human eye under blast loading. *Comput. Methods Biomech. Biomed. Eng.* 18, 107–115. doi: 10.1080/10255842.2013.779684

Garman, R., Jenkins, L., Switzer, R. R., Bauman, R., Tong, L., Swauger, P., et al. (2011). Blast exposure in rats with body shielding is characterized primarily by diffuse axonal injury. *J. Neurotrauma* 28, 947–959. doi: 10.1089/neu.2010.1540

Hines-Beard, J., Bond, W., Backstrom, J., and Rex, T. S. (2016). Virus-mediated EpoR76E gene therapy preserves vision in a glaucoma model by modulating neuroinflammation and decreasing oxidative stress. *J. Neuroinflamm.* 13:39. doi: 10.1186/s12974-016-0499-5

Hines-Beard, J., Marchetta, J., Gordon, S., Chaum, E., Geisert, E., and Rex, T. S. (2012). A mouse model of ocular blast injury that induces closed globe anterior and posterior pole damage. *Exp. Eye Res.* 99, 63–70. doi: 10.1016/j.exer.2012.03.013

Karimi, A., Razaghi, R., Navidbakhsh, M., Sera, T., and Kudo, S. (2016). Computing the stresses and deformations of the human eye components due to a high explosive detonation using fluid-structure interaction model. *Injury* 47, 1042–1050. doi: 10.1016/j.injury.2016.01.030

Koliatsos, V., Cernak, I., Xu, L., Song, Y., Savonenko, A., Crain, B., et al. (2011). A mouse model of blast injury to brain: initial pathological, neuropathological, and behavioral characterization. *J. Neuropathol. Exp. Neurol.* 70, 399–416. doi: 10.1097/NEN.0b013e3182189f06

Lambert, W., Ruiz, L., Crish, S., Wheeler, L., and Calkins, D. J. (2011). Brimonidine prevents axonal and somatic degeneration of retinal ganglion cell neurons. *Mol. Neurodegen.* 6:4. doi: 10.1186/1750-1326-6-4

Liddelow, S. A., Guttenplan, K. A., Clarke, L. E., Bennett, F. C., Bohlen, C. J., Schirmer, L., et al. (2017). Neurotoxic reactive astrocytes are induced by activated microglia. *Nature* 541, 481–487. doi: 10.1038/nature21029

Mortezaee, K., Khanlarkhani, N., Beyer, C., and Zendedel, A. (2018). Inflammasome: Its role in traumatic brain and spinal cord injury. *J. Cell Physiol.* 233, 5160–5169. doi: 10.1002/jcp.26287

Notghi, B., Bhardwaj, R., Bailoor, S., Thompson, K., Weaver, A., Stitzel, J., et al. (2017). Biomechanical evaluations of ocular injury risk for blast loading. *J. Biomech. Eng.* 139:081010. doi: 10.1115/1.4037072

Ou, Y., Jo, R., Ullian, E., Wong, R., and Della Santina, L. (2016). Selective vulnerability of specific retinal ganglion cell types and synapses after transient ocular hypertension. *J. Neurosci.* 36, 9240–9252. doi: 10.1523/JNEUROSCI.0940-16.2016

Rossi, T., Boccassini, B., Esposito, L., Clemente, C., Iossa, M., Placentino, L., et al. (2012). Primary blast injury to the eye and orbit: finite element modeling. *Invest. Ophthalmol. Vis. Sci.* 53, 8057–8066. doi: 10.1167/iovs.12-10591

Saljo, A., Bao, F., Haglid, K., and Hansson, H. (2000). Blast exposure causes redistribution of phosphorylated neurofilament subunits in neurons of adult rat brain. *J. Neurotrauma* 17, 719–726. doi: 10.1089/089771500415454

Sánchez-Migallón, M. C., Valiente-Soriano, F. J., Salinas-Navarro, M., Nadal-Nicolás, F. M., Jiménez-López, M., Vidal-Sanz, M., et al. (2018). Nerve fibre layer degeneration and retinal ganglion cell loss long term after optic nerve crush or transection in adult mice. *Exp. Eye Res.* 170, 40–50. doi: 10.1016/j.exer.2018.02.010

Sarkies, N. (2004). Traumatic optic neuropathy. *Eye* 18, 1122–1125.

Steinsapir, K., and Goldberg, R. (1994). Traumatic optic neuropathyi. *Surv. Ophthalmol.* 38, 487–518.

Valiente-Soriano, F. J., Salinas-Navarro, M., Jimenez-Lopez, M., Alarcon-Martinez, L., Ortin-Martinez, A., Bernal-Garro, J. M., et al. (2015). Effects of ocular hypertension in the visual system of pigmented mice. *PLoS One* 10:e0121134. doi: 10.1371/journal.pone.0121134

Vest, V., Bernardo-Colon, A., Watkins, D., Kim, B., and Rex, T. (2019). Rapid repeat exposure to sub-threshold trauma causes synergistic axonal damage and functional deficits in the visual pathway in a mouse model. *J. Neurotrauma* 36, 1646–1654. doi: 10.1089/neu.2018.6046

Ward, N., Ho, K., Lambert, W., Weitlauf, C., and Calkins, D. J. (2014). Absence of transient receptor potential vanilloid-1 accelerates stress-induced axonopathy in the optic projection. *J. Neurosci.* 34, 3161–3170. doi: 10.1523/JNEUROSCI.4089-13.2014

Yu-Wai-Man, P. (2015). Traumatic optic neuropathy - clinical features and management issues. *Taiwan J. Ophthalmol.* 5, 3–8. doi: 10.1016/j.tjo.2015.01.003

Conflict of Interest Statement: The authors declare that the research was conducted in the absence of any commercial or financial relationships that could be construed as a potential conflict of interest.

Journal Pre-proof

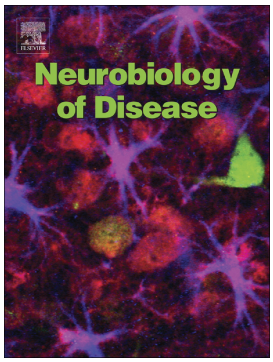

Galantamine protects against synaptic, axonal, and vision deficits in experimental neurotrauma

Sarah Naguib, Alexandra Bernardo-Colón, Caroline Cencer, Neha Gandra, Tonia S. Rex

PII: S0969-9961(19)30370-5

DOI: https://doi.org/10.1016/j.nbd.2019.104695

Reference: YNBDI 104695

To appear in: *Neurobiology of Disease*

Received date: 30 July 2019

Revised date: 22 October 2019

Accepted date: 24 November 2019

Please cite this article as: S. Naguib, A. Bernardo-Colón, C. Cencer, et al., Galantamine protects against synaptic, axonal, and vision deficits in experimental neurotrauma, *Neurobiology of Disease*(2019), https://doi.org/10.1016/j.nbd.2019.104695

Galantamine protects against synaptic, axonal, and vision deficits in experimental neurotrauma

Sarah Naguib[1], Alexandra Bernardo-Colón[2], Caroline Cencer[3], Neha Gandra[1] and Tonia S. Rex[1,2,*]

[1]Department of Ophthalmology and Visual Sciences, 11435 MRB IV, 2213 Garland Ave, Vanderbilt University School of Medicine, Nashville, TN, 37232, USA
[2]Vanderbilt Eye Institute, 2311 Pierce Ave, Vanderbilt University Medical Center, Nashville, TN, 37232, USA
3Department of Cell and Developmental Biology, PMB 407935 U-3218 Medical Research Building III Nashville, TN 37240-7935
*Corresponding Author

Sarah Naguib:
Sarah.naguib@vanderbilt.edu

Alexandra Bernardo-Colón:
Alexandra.bernardo@vumc.org

Caroline Cencer:
Caroline.s.cencer@vanderbilt.edu

Neha Gandra:
Neha.gandra@vanderbilt.edu

Tonia S. Rex:
Tonia.rex@vanderbilt.edu

Keywords: blast injury, galantamine, optic nerve, electroretinogram, visual evoked potential, oxidative stress, inflammation, neurotrauma, indirect traumatic optic neuropathy

ABSTRACT

Our goal was to investigate the neuroprotective effects of galantamine in a mouse model of blast-induced indirect traumatic optic neuropathy (bITON). Galantamine is an FDA-approved acetylcholinesterase inhibitor used to treat mild-moderate Alzheimer's disease. We exposed one eye of an anesthetized mouse to repeat bursts of over-pressurized air to induce traumatic optic neuropathy. Mice were given regular or galantamine-containing water (120mg/L) ad libitum, beginning immediately after blast and continuing for one month. Electroretinograms and visual evoked potentials were performed just prior to endpoint collection. Histological and biochemical assessments were performed to assess activation of sterile inflammation, axon degeneration, and synaptic changes. Galantamine treatment mitigated visual function deficits induced by our bITON model via preservation of the b-wave of the electroretinogram and the N1 of the visual evoked potential. We also observed a reduction in axon degeneration in the optic nerve as well as decreased rod bipolar cell dendritic retraction. Galantamine also showed anti-inflammatory and antioxidant effects. Galantamine may be a promising treatment for blast-induced indirect traumatic optic neuropathy as well as other optic neuropathies.

INTRODUCTION

Eye injuries affect approximately 2.4 million people every year.[1] Between 2000 and 2010, 186,555 eye injuries occurred worldwide in military hospitals.[2] Further, up to 40% of monocular blindness is due to ocular trauma. [3] Damage to the optic nerve and retina, resulting in permanent visual deficits, occurred in more than 60,000 Veterans with blast-induced traumatic brain injury (TBI) between the years of 2000-2011.[4] Additionally, up to 5% of patients experiencing head trauma will also develop traumatic optic neuropathy (TON).[5,6] Some of the most common ocular blast injuries include, but are not limited to, hyphema, retinal detachments, retinal edema, TON, and loss of visual field. [7] In cases of direct TON, anatomical disruption of the optic nerve occurs from a projectile penetrating the optic nerve or avulsion. Indirect TON (ITON) results from force transmission to the optic nerve from a distant site without overt damage to the surrounding tissue.[8,9] Patients with ITON can experience severe vision loss, and while some experience limited recovery, they never return to baseline.[9,10] Corticosteroids or observation alone are the current standards of treatment for patients with ITON.[11]

Our lab has developed a model of blast-induced ITON (bITON), utilizing a repeat blast paradigm in order to simulate repeat injuries most often seen in military populations.[12,13] This model induces extensive axon degeneration in the optic nerve at two weeks after injury, as well as a decrease in the amplitude and an increase in the latency of the visual evoked potential (VEP).[14] It causes an increase in reactive oxygen species (ROS), and secondary activation of the IL-1 pathway, both of which contribute to axon degeneration and vision loss.[12,13] Finally, we detected rapid loss of cells in the ganglion cell layer at two days after injury without further progression out to 30 days after injury.[15]

Altered levels of neurotransmitters, such as acetylcholine and GABA, occur in several neurodegenerations.[16] For example, in Alzheimer's Disease, decreased levels of acetylcholine correlates with disease progression.[17,18] Notably, we detected caspase-1 immunolabeling in the cholinergic amacrine cells after single blast injury.[12] One of the treatments for mild to moderate Alzheimer's disease, as well as other myopathies and peripheral neuropathies, is the FDA-approved compound, galantamine.[19,20] Galantamine has multiple modes of actions: it increases acetylcholine via mild inhibition of acetylcholinesterase, it increases GABA release via allosteric modulation of the nicotinic acetylcholine receptor (α7nAChR), and it has been shown to protect neurons against glutamate-induced neurotoxicity.[21] Previous studies have also shown that galantamine can have antioxidant properties; galantamine treatment reduced ROS and increased cell viability after exposure to hydrogen peroxide[22,23] and protected rat cortical neurons against oxidative stress after exposure to synthetic amyloid β [24] It also has been shown to decrease inflammation in a stroke model of rats, by preventing an increase IL-1β levels.[25] Additional studies have shown that galantamine can protect retinal ganglion cells in a rat model of glaucoma.[26,27]

We hypothesized that galantamine would be protective in our model of bITON. Here, we show that oral galantamine, given after bITON, mitigates visual function deficits and axon degeneration in the optic nerve, and that it does so while modulating acetylcholine, glutamate, ROS, and IL-1 levels.

METHODS

Mice: Anesthetized C57Bl/6J mice (Jackson Labs, Bar Harbor, ME) were exposed to two repeat bursts (0.5 seconds apart) of 15 psi air directed at the left eye once a day for three days in a row.

Sham mice were exposed to everything except the air pressure due to a barrier placed between the eye and the barrel of the paintball marker, as previously described.[13-15] Galantamine sham and blast mice were given 120 mg/L of galantamine in their water, which was changed every 72 hours (TCI America, Boston, MA). Control mice were given normal water ad libitum for one month, while galantamine-treated mice drank galantamine-containing water for one-month post-injury. Average daily water intake for a laboratory mouse is 4ml, thus we estimate that the mice consumed 480 micrograms galantamine per day for 30 days. This equates to an average dose of 15.3 mg/kg, based on the average weight of a C57Bl/6 male mouse of 31.4 grams. While previous studies administered galantamine intraperitoneally at 1-5 mg/kg,[28–30] it is important to note that because galantamine is delivered orally, the dose is higher. Experimental procedures were performed in accordance with the Use of Animals in Vision and Ophthalmic research and an approved Vanderbilt University Institutional Animal Care and Use Committee protocol.

Electroretinograms (ERG) and VEPs: Mice were dark-adapted overnight, dilated with 1% tropicamide for 10 minutes, and anesthetized with 20/8/0.8 mg/kg ketamine/xylaxine/urethane according to previously published methodology.[14] Mice were placed on the heated surface of the ERG system to maintain body temperature. Corneal electrodes with integrated stimulators were placed on eyes lubricated with Genteel drops using the Celeris system (Diagnosys LLC, Lowell, MA). Subdermal platinum needle electrodes were placed in the snout and back of the head at the location of the visual cortex. A ground electrode was placed in the back of the mouse. For VEPs, mice were exposed to 50 flashes of 1Hz, 0.5 cd.s/m^2 white light. To collect ERGs, electrodes were placed on lubricated corneas were placed. Mice were then exposed to 15 flashes of 1Hz, 1 cd.s/m^2.

Western Blot: Single retinas were homogenized and sonicated in lysis buffer and centrifuged. Sample buffer was added to the supernatant just prior to use. Known amounts of protein (10 to 20 µg) or protein ladder were loaded into each well of an SDS-polyacrylamide gel. The Bio-Rad mini-trans blot cell system and mini protean pre-cast gels at 4-20% were used (Hercules, CA). Loading control was GAPDH (rabbit; 1:1000; ab9485, Abcam, Cambridge, MA). The protein was transferred onto nitrocellulose using the Bio-Rad trans blot turbo transfer system (Hercules, CA), probed with anti-SOD2 (rabbit; 1:1000; ab13533; Abcam), probed with secondary antibody (alkaline phosphatase-conjugated AffiniPure Goat Anti-Rabbit IgG; 1:1000; cat #133466; Jackson ImmunoResearch Laboratories) and alkaline phosphatase was used for band detection. Band density was quantified by scanning the blot using an EPSON scanner and Adobe Photoshop to convert to grayscale and invert the image. Each band was selected with the same frame and set measurements were used to obtain the grey mean value for each.[14]

High-performance liquid chromatography (HPLC):

Tissue Extraction

The brain sections were homogenized, using a tissue disruptor, in 100-750 ul of 0.1M TCA, which contained 10^{-2} M sodium acetate, 10^{-4} M EDTA, and 10.5% methanol (pH 3.8). Ten microliters of homogenate was used. Then samples were spun in a microcentrifuge at 10,000g for 20 minutes. The supernatant was removed for biogenic monoamines analysis.

Biogenic Amine Analysis using HPLC-ECD

Biogenic amine concentrations were determined in the Vanderbilt University Medical Center Hormone Assay & Analytical Core utilizing an Antec Decade II (oxidation: 0.65) electrochemical detector operated at 33°C. Twenty microliter samples of the supernatant were injected using a Water 2707 autosampler onto a Phenomenex Kintex C18 HPLC column (100 x

4.60 mm, 2.6um). Biogenic amines were eluted with a mobile phase consisting of 89.5% 0.1M TCA, 10^{-2} M sodium acetate, 10^{-4} M EDTA and 10.5% methanol (pH 3.8). Solvent was delivered at 0.6 ml/min using a Waters 515 HPLC pump. HPLC control and data acquisition were managed by Empower software. Isoproterenol (5ng/mL) was included in the homogenization buffer for use as a standard to quantify the biogenic amines.

Biogenic Amine Analysis using LC/MS

Biogenic amines were determined in the Vanderbilt University Medical Center Hormone Assay & Analytical Core by a highly sensitive and specific liquid chromatography/mass spectrometry (LC/MS) methodology following derivatization of analytes with benzoyl chloride (BZC). Five microlitersμ of either tissue extract or microdialysis fluid was added to a 1.5mL microcentrifuge tube containing 20 µL acetonitrile. Ten microliters each of 500mM $NaCO_3$ (aqueous) and 2% BZC in acetonitrile was added to each tube. After 2 min, the reaction was stopped by the addition of 20 µL internal standard solution (in 20% acetonitrile containing 3% sulfuric acid) and 40 µL water. The samples were then ready for LC/MS analysis. LC was performed on a 2.0 x 50mm, 1.7 µm particle Acquity BEH C18 column (Waters Corporation, Milford, MA, USA) using a Waters Acquity UPLC. Mobile phase A was 15% aqueous formic acid and mobile phase B was acetonitrile. Samples were separated by a gradient of 98–5% of mobile phase A over 11 min at a flow rate of 600 µL /min prior to delivery to a SCIEX 6500+ QTrap mass spectrometer.

Protein assay

Protein concentration was determined by BCA Protein Assay Kit (Thermo Scientific). Ten microliters of tissue homogenate was distributed into 96-well plate and 200 µl of mixed BCA reagent (25ml of Protein Reagent A is mixed with 500µl of Protein Reagent B) was added. The plate was incubated at room temperature for two hours for the color development. A BSA

standard curve was run at the same time. Absorbance was measured by the plate reader (POLARstar Omega), purchased from BMG Labtech Company.

Multiplex Cytokine ELISA: We performed a mouse multiplex mouse cytokine/chemokine magnetic bead panel for IL-1α and IL-1β, loading 25 µl of sample per well. Samples were tested in duplicates and results were averaged. We performed the ELISA according to manufacturer directions (cat #: MCYTOMAG-70K, Millipore, Burlington, MA).

Immunohistochemistry: Eyes (n=40) were preserved in 4% paraformaldehyde, cryoprotected in 30% sucrose overnight at 4ºC and embedded in tissue freezing medium (Triangle Biomedical, Durham, NC). Ten-micron thick sections were collected in round on a cryostat (Fisher, Pittsburgh, PA). Each slide had representative sections from the entire eye. Slides were rinsed with PBS and incubated at room temperature in normal donkey serum (NDS; 0.05%) in 0.1 M phosphate buffer with 0.5% bovine serum albumin and 0.1% Triton X-100 (phosphate buffer plus Triton X-100 [PBT]) for 2 hours. The slides were incubated overnight at 4ºC in primary antibody (see table below) in PBT, then rinsed with PBS and incubated with their appropriate secondary antibody (donkey anti-rabbit, donkey anti-mouse or donkey anti-goat 488 or 594; Life Technologies, Carlsbad, CA) for 2 hours at room temperature. Then, slides were rinsed in PBS, mounted in Vectashield Mounting medium with DAPI (DAPI; Vector Laboratories, Burlingame, CA) or Fluoromount-G (Southern Biotech, Birmingham, AL). Slides were imaged on a Nikon Eclipse epifluorescence microscope (Nikon, Melville, NY) or an Olympus FV-1000 confocal microscope. All images were collected from the same retinal region with identical magnification, gain and exposure settings. Fluorescence intensity was quantified via ImageJ. A rectangle was selected around the region of interest, channels were split for multiple antibodies, threshold was

adjusted, noise was de-speckled and fluorescence intensity was measured. Fluorescence intensity was normalized to sham mice. Each experimental group included 5 eyes.

Table 1. Antibodies Used for Immunohistochemistry

Antibody	**Concentration**	**Animal**	**Catalog Number**	**Company**
Anti-calbindin D	1:200	Mouse	126M4810V	Sigma-Aldrich, St. Louis, MO
Anti-synaptophysin	1:500	Rabbit	GR30790220	Abcam, Cambridge, MA
Anti-nitrotyrosine	1:500	Rabbit	2459610	Millipore, Burlington, MA
Anti-PKCα	1:40	Mouse	GR3164443	Abcam, Cambridge, MA
Anti-NeuN	1:200	Rabbit	MAB377	Millipore, Burlington, MA

Optic Nerves: Optic nerves were post-fixed in glutaraldehyde followed by embedding in Resin 812 and Araldite 502 (cat # 14900 and 10900, Electron Microscopy sciences, Hatfield, PA) according to previous published protocols[13,14,28,29]. Leica EM-UC7 microtome was used to collect 1 µm-thick sections. Sections were then stained with 1% paraphenylenediamine and 1% toluidine blue and were imaged on a Nikon Eclipse Ni-E microscope using a 100x oil immersion objective (Nikon Instruments Inc., Melville, NY). The optic nerves were montaged into a 5x5 image using the Nikon Elements software. We used the Counting Array and Better Cell Counter plugins to ImageJ, which creates a grid of nine squares overtop the montaged optic nerve. We manually counted healthy and degenerating axons, which are color-coded by the plugins. The grid accounts for 20% of the optic nerve cross-sectional area to avoid bias, and we multiplied these numbers by 5 to estimate total and degenerating axons within the nerve.

Acetylcholinesterase Activity Assay: Activity of AChE in the retina was measured using Acetylcholinesterase Colorimetric Assay Kit according to manufacturer's directions (ab138871, Abcam, Cambridge, MA).

Experimental Design and Statistical Analysis: Western blot data was normalized to loading controls. Data were analyzed using GraphPad Prism (La Jolla, CA). All experimental groups

were compared to each other using a one-way ANOVA and the Tukey post-hoc test. All groups are shown (mean ± SEM).

RESULTS

Oral galantamine reached bioactive levels in the mouse retina

To determine if galantamine entered the retina and was active, we quantified acetylcholinesterase activity (Figure 1A) and acetylcholine levels (Figure 1B). Interestingly, control bITON retinas had a slight, but statistically significant increase in acetylcholinesterase activity in comparison to control shams, 0.48 ± 0.03 U/mg (mean ± SEM) and 0.42 ± 0.01 U/mg, respectively ($p<0.05$; Figure 1A). Acetylcholinesterase activity was decreased in both galantamine sham (0.28 ± 0.01 U/mg) and galantamine bITON (0.34 ± 0.08 U/mg) groups, as compared to its control, $p < 0.001$ for both galantamine groups (Figure 1A). Interestingly, there is also a statistically significant increase in acetylcholinesterase activity between galantamine-sham and galantamine-bITON mice, $p<0.05$.

The levels of retinal acetylcholine in mice treated with galantamine was greater than controls (Figure 1B). Acetylcholine levels were 11.0 ± 1.2, 13.0 ± 3.6; 23.8 ± 10.0, and 30.0 ± 17.2 ng/mg respectively for sham, bITON, galantamine sham, and galantamine-bITON groups (Figure 1B). Total choline levels remained unchanged in all four experimental groups (Figure 1C).

Previous studies have elucidated that galantamine can modulate glutamate levels. We detected a 2.07-fold increase in glutamate levels in retinas from bITON mice as compared to those from control sham mice ($p<0.0001$; Figure 1D). In contrast, levels of glutamate in galantamine-treated mice were similar to control sham levels. To determine if galantamine

modulated glutamate levels by affecting glutamate production or recycling, we performed immunohistochemistry and quantification of fluorescence for a marker of glutamine synthetase (GLAST) and a marker for glutamate transporter 1 (EAAT). No differences in the total fluorescence of either of these markers in the retina were detected (data not shown).

Galantamine treatment mitigates bITON-induced reduction in the ERG

We assessed retinal function by ERG, and observed no difference in the amplitude or latency of the a-wave, indicating that our model of bITON does not affect the photoreceptors (Figure 2A,B). However, the amplitude of the b-wave (b_{max}) of the ERG was decreased after bITON (Figure 2A,C). Control shams had a mean b_{max} of 203.3 ± 7.4 µV, while control bITON had a mean b_{max} of 100.6 ± 11.6µV, p<0.001. Additionally, bITON mice had a longer b-wave latency than the control sham mice: 41.3 ± 12.1ms as compared to 54.6 ± 9.3ms, p<0.0001 (Figure 2A, D). The b-wave is generated primarily by the rod bipolar cells, thus these data suggest that these cells are affected by bITON. Galantamine treatment after bITON partially protected the b_{max} and the b-wave latency (Figure 2C, D). The mean b_{max} in galantamine sham and galantamine-treated bITON mice was 190.8 ± 37.7µV and 158.8 ± 48.0µV, respectively, with p<0.05 between the galantamine-treated groups (Figure 2C). The latencies of the b-wave in galantamine sham and bITON mice were 40.5 ± 8.2ms and 45.2 ± 10.2ms, respectively, with no statistically significant difference between them (Figure 2D). Importantly, there was a statistically significant difference between the control bITON group and the galantamine-treated bITON groups for both b wave amplitude and latency (p<0.0001 and p<0.00001, respectively).

Galantamine treated mice retain synaptic overlap in the OPL after bITON

We performed immunohistochemical analysis to explore the morphological basis for the ERG b-wave changes. We co-labeled retina cross-sections with anti-PKCα, a marker for rod bipolar cells, and anti-synaptophysin, a marker for the photoreceptor ribbon synapse. In control sham mice, the rod bipolar cells extend dendrites up to the photoreceptor terminals (Figure 2E). In contrast, in control bITON mice, the rod bipolar cell dendrites were retracted toward their cell bodies (Figure 2E). The rod bipolar cell dendrites of both sham and bITON mice treated with galantamine looked similar to normal sham mouse retinas (Figure 2E). In an effort to quantify changes in dendritic overlap with the photoreceptor synaptic terminals, we quantified the extent of double-labeling of the two antibodies. Importantly, galantamine-treated bITON mice had a mean overlap that was comparable to the two sham groups: the mean overlap was 54 ± 2% for galantamine-bITON, sham mice, mean overlap for control-sham was 62 ± 3%, and mean overlap for galantamine-sham mice was 59 ± 3%. There was no statistically significant difference between any of the groups (Figure 2F). In contrast, after bITON, mean overlap of anti-PKCα and anti-synaptophysin decreased to 41 ± 5% ($p<0.05$, in comparison to either sham group or galanamine-bITON group).

In order to check the other major synapse at the outer plexiform, we also co-immunolabeled with anti-synaptophysin and anti-calbindin-D, a marker for horizontal cells (Figure 2G). There was a marked decrease in calbindin-D immunolabeling after bITON, which prevented visualization of changes in horizontal cell morphology. bITON mice that were treated with galantamine had preserved calbindin labeling. As expected, we quantified a significant difference in overlap in calbindin-D and synaptophysin between sham and bITON mice: sham mean overlap was 59 ± 2% and bITON mean overlap was 42 ± 4%, $p<0.05$ (Figure 2H). Galantamine preserved the horizontal cell and ribbon synapse double labeling: galantamine sham

mean overlap was 59 ± 2%, and galantamine bITON mean overlap was 53 ± 5% (Figure 2H). There was no statistical difference between the either of the galantamine groups.

Galantamine treatment mitigated axon degeneration after bITON

Representative micrographs of optic nerve cross-sections from control sham, control bITON, and galantamine-treated bITON mice are shown. Control sham and galantamine-treated bITON nerves exhibit more axons than the control bITON nerve (Figure 3A-C). Similar to our previous studies, bITON mice had an average of 23,609 ± 1302 axons in the optic nerve with $p < 0.0001$ in comparison to control shams (52464 ± 4075 axons).[13,14] Galantamine-treated shams had 52014 ± 2673 axons, and galantamine-treated bITON mice had 48,693 ± 1160 axons (Figure 3D), both of which were comparable to the control sham mice.

Galantamine treatment mitigated bITON induced changes in the VEP

In order to assess transmission of the visual signal to the visual cortex, we performed flash VEPs (Figure 3E). Similar to our previously reported findings, the control sham mice had an average VEP N1 amplitude of 42.56 ± 6.78 μV while control bITON mice had an average amplitude of 21.85 ± 11.26 μV, a nearly 2-fold reduction in amplitude ($p< 0.0001$; Figure 3F).[14] The control bITON mice also had a longer VEP N1 latency than the control sham mice: 49.34 ± 11.19 ms for bITON as compared to 36.17 ± 7.30 ms ($p< 0.0001$; Figure 3G). Regarding the right-shifted latencies of the bITON group, these are due to a deficit in axon conductance, possibly due to changes in energetics or in myelination of the optic nerve.

Galantamine treatment after bITON resulted in partial retention of both the amplitudes and the latencies of the VEP N1 ($p<0.001$ for amplitudes and $p<0.0001$ for latencies as compared

to control bITON mice) (Figures 3E-G). Galantamine sham and galantamine-treated bITON mice had mean VEP N1 amplitudes of 41.98 ± 7.64 µV and 34.47 ± 8.19 µV, respectively, with no statistically significant difference between them (Figure 3F). Galantamine sham and bITON mean N1 latencies were 40.38 ± 5.50 ms and 45.75 ± 2.11 ms respectively, with no statistically significant difference between them (Figure 3G).

Galantamine mitigated bITON-induced oxidative stress and inflammation

We performed nitrotyrosine immunolabeling and quantified levels of immunofluorescence in order to assess the effect of galantamine on oxidative stress in the retina after bITON (Figure 4A-F). Nitrotyrosine immunolabeling was nearly absent in control sham retinas (Figure 4A). In the control bITON mice, nitrotyrosine immunolabeling was present specifically in the retinal ganglion cell layer (Figure 4B). The immunolabeling was significantly reduced in the galantamine-treated bITON retinas (Figure 4B, D). To determine which cell type labeled for nitrotyrosine, we co-labeled bITON retinas with the neuronal marker, anti-NeuN. We found that the anti-nitrotyrosine labeling overlapped with the anti-NeuN labeling in the ganglion cell layer (Figure 4E). We quantified fluorescence in the retinal ganglion cell layer of all groups (Figure 4F). Control bITON mice contained 174 ± 2% more fluorescence than control sham mice, $p<0.0001$, and 151 ± 5% more fluorescence than galantamine-bITON mice, $p<0.0001$ (Figure 4F). There was no statistically significant difference in fluorescence levels between galantamine sham mice and galantamine-treated bITON mice (Figure 4F).

Mitochondrial superoxide dismutase (SOD2) converts the superoxide that is formed as a metabolic by-product of oxidative phosphorylation into oxygen and thus is a critical enzyme in regulating intracellular ROS levels. Similar to our previously studies, we detected a 59 ± 4%

decrease in SOD2 levels at one month after control bITON as compared to control shams (Figure 4G).[14] In contrast, SOD2 levels in galantamine-treated sham and bITON mice were comparable to control shams. We detected a statistically significant difference ($p<0.001$) between either galantamine-treated group and the control bITON group (Figure 4G).

We detected an increase in the pro-inflammatory cytokines, IL-1α and IL-1β in the control bITON retinas, in agreement with our previous findings (Figure 4H).[14] bITON retinas had IL-1α mean levels of 17.77 ± 6.41pg/ml in comparison to shams with mean levels of 2.26 ± 0.98pg/ml, $p<0.00001$. Average galantamine sham levels for IL-1α were 6.30 pg/ml ± 3.37 and mean galantamine bITON levels were 5.43 pg/ml ± 2.26. There was no statistically significant difference between control sham retinas, galantamine-treated sham retinas, and galantamine-treated bITON retinas. Similarly, bITON resulted in an elevation of IL-1β levels to 9.18 ± 2.4 pg/ml, compared to 4.1 ± 1.9 pg/ml detected in control sham retinas ($p<0.001$) (Figure 4I). In contrast, galantamine-treated sham retinas and galantamine-treated bITON retinas contained similar levels of IL-1β: 2.7 ± 1.7 pg/ml and 2.8 ± 1.4 pg/ml, respectively and were not significantly different from control sham retinas.

DISCUSSION

In this study, we initiated treatment of galantamine after the last of a 3-day series of blast exposures. We previously demonstrated that our bITON model induces axon degeneration after only three blasts, which suggests that injury responses started prior to the last day of the blasts and the start of galantamine treatment.[15] We show that oral galantamine given ad libitum reached the retina, where it increased acetylcholine levels and decreased acetylcholinesterase activity. This treatment paradigm mitigated bITON-induced visual function deficits, axon degeneration in

the optic nerve and rod bipolar cell dendritic retraction. Further, it moderated oxidative stress, inflammation, and glutamate levels.

After bITON, rod bipolar cells were present, but their dendrites were retracted toward their cell bodies (Figure 2E). This correlates with the decrease in the b-wave amplitude (Figure 2A, C) and increase in the b-wave latency detected after bITON (Figure 2A, D). Co-immunolabeling of nitrotyrosine and NeuN in the ganglion cell layer demonstrates that the cells primarily affected by bITON-induced oxidative stress are retinal ganglion cells and possibly displaced amacrine cells (Figure 4E). This is consistent with our previously study showing loss of cells in the ganglion cell layer.[15] We have performed TUNEL and do not detect active cell death in the retina at the post-bITON time-points we have examined (data not shown). In contrast, based on the ERG, OCT thickness (data not shown), and immunolabeling results, bITON does not cause significant loss of bipolar or amacrine cells. We do not detect a difference in overall retinal thickness or in the thickness of any particular layer of the retina by OCT (data not shown). In addition, the a-wave and the oscillatory potentials of the ERG are unaltered in our bITON model suggesting that the photoreceptors and AII amacrine cells are unaffected (data not shown). Thus, while we cannot discount some loss of other retinal neurons, it is likely minimal. In contrast, the right-shifted latencies of the VEP of the bITON group (Figure 3G) suggest a deficit in axon conductance, possibly due to changes in axon energetics or myelination in the optic nerve, which again points to dysfunction of the RGCs and matches the optic nerve histological findings reported here and elsewhere.[14,15]

In most cases, galantamine treatment resulted in partial protection of the retina. Treating earlier after injury may be more effective. There also may be injury pathways activated by bITON that are unaffected by galantamine. Further studies are needed to determine how long

after injury galantamine treatment can be initiated and still be effective. Additionally, the decreases in oxidative stress and inflammation in galantamine-treated retinas may be an indirect result of galantamine action that prevents secondary axon degeneration and cell injury as opposed to a direct action on these pathways.

Detection of elevated glutamate in post-bITON retinas is consistent with reports in other models of TBI or blast injury. In a rat TBI study, there was a nine-fold increase in extracellular glutamate levels in the brain as compared to control animals.[32] In a model of rat blast injury, glutamate was significantly increased in the retina.[33] Additionally, many preclinical and clinical studies have demonstrated altered glutamate production, clearance, and buffering after TBI that results in an excess of glutamate.[32,34] It possible that glutamate may play a large role in determining the state of the post-injury CNS. Glutamate is the most abundant excitatory neurotransmitter within the CNS and excess glutamate can lead to a massive increase in neuronal activity, increased intracellular calcium, and even cell death, i.e. excitotoxicity. Retinal astrocytes and Müller glia play an important role in glutamate buffering and clearance. Knockout of the glial protein, EAAT1, in mice exposed to TBI exhibit excitotoxic levels of glutamate in comparison to controls.[35] Additionally, TBI in rats results in excess glutamate followed by a downregulation in expression of GLAST and EAAT1 in glial cells.[36] However, in this study, we did not find a difference in the immunohistochemical labeling of GLAST or EAAT1 between any of our groups, despite the observed increases in retinal glutamate following bITON. Galantamine has been shown to act as a modulator of glutamate-induced excitotoxicity by preventing increases in cell death following exposure to NMDA.[21] It is feasible that galantamine acted upstream to the mechanism that caused an increase in glutamate. This should be explored in future studies.

The positive effect of galantamine on oxidative stress and inflammation in our bITON model are in agreement with other reports showing that galantamine has antioxidant and anti-inflammatory effects on cells both in culture and *in vivo*.[23,24] Galantamine treatment reduced IL-1β levels in the brain of a hypoxia-ischemic rat model, and protected cortical neurons following injury.[36] Additionally, galantamine decreased oxidative stress and apoptosis in cortical neurons exposed to amyloid-beta peptides and in neuroblastoma cells that were treated with hydrogen peroxide.[22,24]

Galantamine has been utilized in a variety of neurodegenerative disease models other than Alzheimer's, and has demonstrated protection. Galantamine treatment, via modulation of the muscarinic acetylcholine receptors in the retina, has shown to be protective in multiple models of glaucoma by promoting retinal ganglion cell survival.[27,38] Additionally, through its inhibition of acetylcholinesterase, galantamine treatment was protective in another model of glaucoma via increasing blood flow.[26] Outside the retina, efferent vagus nerve activity, via the cholinergic anti-inflammatory pathway, is responsible for regulation of cytokine production via α7nAChR-dependent signaling.[39] Galantamine is a positive allosteric modulator of α7nAChRs, so it is feasible that the protection we detected was due to activation of this anti-inflammatory pathway.[21,40,41] Overall, our results are comparable with previous studies showing that galantamine has antioxidant and anti-inflammatory effects and is neuroprotective.

In conclusion, galantamine treatment given after three days of blasts partially protected against visual function deficits, oxidative stress, inflammation and axon degeneration in a model of bITON. Future studies are needed to elucidate galantamine's therapeutic window for partial protection following bITON. Additionally, future studies should determine the exact mechanism by which galantamine exerts antioxidant and anti-inflammatory effects in our model of bITON.

Since it is already FDA-approved, it has good pharmacokinetics and is safe to use, galantamine should be further studied as a potential treatment for optic neuropathies.

ACKNOWLEDGEMENTS

We would like to acknowledge the Vanderbilt University Medical Center Cell Imaging Shared Resource core facility, Vanderbilt University Neurochemistry Core, and the Vanderbilt University Medical Center Hormone Assay and Analytical Core for their help with confocal microscopy, ELISAs, and HPLC, respectively.

FUNDING

DoD W81XWH-15-1-0096, W81XWH-17-2-0055, NEI R01 EY022349, NEI P30 EY008126, NIA R01 NS094595, Research to Prevent Blindness Unrestricted Funds, Ret. Maj. General Stephen L. Jones, MD Fund, Mark Pigott Fund,Potoscnak Family-CSC Research Fund, Ayers Research Fund in Regenerative Visual Neuroscience, NIH T32 Training Grant in Vision Research (S. Naguib), U24EY22893

DoD NON-ENDORSEMENT DISCLAIMER

The views, opinions and/or findings contained in this research presentation are those of the authors and do not necessarily reflect the views of the Department of Defense and should not be construed as an official DoD/Army position, policy or decision unless so designated by other documentation. No official endorsement should be made.

FIGURE LEGENDS

Figure 1. Oral galantamine inhibited retinal acetylcholinesterase activity, increased acetylcholine, and decreased glutamate. A) Acetylcholinesterase activity assay. B) Acetylcholine levels quantified with HPLC. C) Choline levels quantified with HPLC. D) Glutamate levels quantified with HPLC. *N* =5 retinas for all groups. *p<0.05, **p<0.001, ****p<0.00001.

Figure 2. Galantamine mitigated bITON-induced the ERG b-wave deficits and rod bipolar cell dendritic retraction. A) Representative ERG waveforms. B) Graphed a-wave amplitudes. C) Graphed b-wave amplitudes. D) Graphed b-wave latencies. E) Representative fluorescent micrographs of anti-PKC-α (red) and anti-synaptophysin (blue) co-labeling in the outer plexiform layer (OPL) of retina sections. F) Quantification of co-localization of anti-PKC-α and anti-synaptophysin markers using ImageJ. G) Representative fluorescent micrographs of anti-calbindin-D (red) and anti-synaptophysin (blue) co-labeling in the OPL. H) Quantification of co-localization of anti-calbindin-D and anti-synaptophysin markers using ImageJ. For all ERG data shown, *N*=31 for control sham, 28 for control bITON, and 15 for both galantamine sham and galantamine bITON groups. For all immunohistochemistry shown, *N*=5 retinas per group and 2 sections per retina. *p<0.05, **p<0.001, ****p<0.00001. Scale bar indicates 100um.

Figure 3. Galantamine mitigated the VEP deficits and axon degeneration. A-C) Representative brightfield micrograph of optic nerves. Scale bar represents 20µm and applies to all micrographs. D) Quantification of total axon counts. *N*=5 for all groups. *p<0.05. ****p<0.00001 E) Representative VEP waveforms. F) Graphed VEP N1 amplitudes. For all VEP data, *N* =15 for control sham, 14 for control bITON, galantamine sham and galantamine bITON groups. G) Graphed VEP N1 latencies.

Figure 4. Galantamine has antioxidant and anti-inflammatory effects. A-D) Representative fluorescent micrographs of anti-nitrotyrosine labeling. Scale bar represents 50µm and applies to all images. E) Representative fluorescent micrographs of anti-nitrotyrosine labeling (green), anti-NeuN labeling (red), and DAPI (blue). Co-localization of these markers indicated with white arrows. F) Quantification of anti-nitrotyrosine fluorescence in the ganglion cell layer using ImageJ and compared as a percent of control sham mouse. G) Representative western blot of SOD2. H) Quantification of retinal SOD2 levels. *N*=5 retinas per group for all biochemical analyses. I) Quantification of retinal IL-1α levels. J) Quantification of retinal IL-1β levels. *N*=5 retinas per group and 2 sections per retina. *p<0.05, **p<0.001, ***p<0.0001, ****p<0.00001. Scale bar indicates 100um

REFERENCES

1. Feist, R. M. & Farber, M. D. Ocular Trauma Epidemiology. *Arch. Ophthalmol.* **107**, 503–504 (1989).

2. Andreotti, G., Lange, J. L. & Brundage, J. F. The nature, incidence, and impact of eye

injuries among US military personnel: Implications for Prevention. *Arch. Ophthalmol.* **119**, 1693–1697 (2001).

3. Aghadoost, D. A Brief Overview of Occular Trauma. *Arch. Trauma Res.* **3**, (2014).
4. Weichel, E. D., Colyer, M., Bautista, C., *et al.* Traumatic brain injury associated with combat ocular trauma. *J. Head Trauma Rehabil.* **24**, 41–50
5. Steinsapir, K. D. & Goldberg, R. A. Traumatic optic neuropathy: an evolving understanding. *Am. J. Ophthalmol.* **151**, 928-933.e2 (2011).
6. Kumaran, A., Sundar, G. & Chye, L. Traumatic Optic Neuropathy: A Review. *Craniomaxillofacial Trauma Reconstr.* **08**, 031–041 (2014).
7. WHO | Priority eye diseases. *WHO* (2018).
8. Warner, N. & Eggenberger, E. Traumatic optic neuropathy: a review of the current literature. *Curr. Opin. Ophthalmol.* **21**, 459–62 (2010).
9. Singman, E. L., Daphalapurkar, N., White, H., *et al.* Indirect traumatic optic neuropathy. *Military Medical Research* **3**, (2016).
10. Burke, E. G., Cansler, S. M. & Evanson, N. K. Indirect traumatic optic neuropathy: Modeling optic nerve injury in the context of closed head trauma. *Neural Regeneration Research* **14**, 593–594 (2019).
11. Eye Health Statistics - American Academy of Ophthalmology. Available at: https://www.aao.org/newsroom/eye-health-statistics. (Accessed: 30th September 2019)
12. Bricker-Anthony, C., Hines-Beard, J. & Rex, T. S. Molecular changes and vision loss in a mouse model of closed-globe blast trauma. *Investig. Ophthalmol. Vis. Sci.* **55**, 4853–4862 (2014).
13. Hines-Beard, J., Marchetta, J., Gordon, S., *et al.* A mouse model of ocular blast injury that

induces closed globe anterior and posterior pole damage. *Exp. Eye Res.* **99**, 63–70 (2012).

14. Bernardo-Colon, A., Vest, V., Clark, A., *et al.* Antioxidants prevent inflammation and preserve the optic projection and visual function in experimental neurotrauma. *Cell Death Dis.* **9**, (2018).
15. Bernardo-Colón, A., Vest, V., Cooper, M.L., *et al.* Progression and Pathology of Traumatic Optic Neuropathy From Repeated Primary Blast Exposure. *Front. Neurosci.* **13**, 719 (2019).
16. McKee, A. C. & Robinson, M. E. Military-related traumatic brain injury and neurodegeneration. *Alzheimer's Dement.* **10**, (2014).
17. Francis, P. T. The interplay of neurotransmitters in Alzheimer's disease. *CNS Spectr.* **10**, 6–9 (2005).
18. Giacobini, E., DeSarno, P., Clark, E., *et al*. The cholinergic receptor system of the human brain: Neurochemical and pharmacological aspects in aging and Alzheimer. *Prog. Brain Res.* **79**, 335–343 (1989).
19. Lilienfeld, S. Galantamine--a novel cholinergic drug with a unique dual mode of action for the treatment of patients with Alzheimer's disease. *CNS Drug Rev.* **8**, 159–76 (2002).
20. Durães, F., Pinto, M. & Sousa, E. Old Drugs as New Treatments for Neurodegenerative Diseases. *Pharmaceuticals (Basel).* **11**, (2018).
21. Lopes, J., Tarozzo, G., Reggiani, A., *et al.* Galantamine potentiates the neuroprotective effect of memantine against NMDA-induced excitotoxicity. *Brain Behav.* **3**(2): 67-74 (2013).
22. Ezoulin, M. J., Ombetta, J., Dutertre-Catella, H., *et al.* Antioxidative properties of galantamine on neuronal damage induced by hydrogen peroxide in SK-N-SH cells.

Neurotoxicology **29**, 270–277 (2008).

23. Romero, A., Egea, J., Garcia, A., *et al*. Synergistic neuroprotective effect of combined low concentrations of galantamine and melatonin against oxidative stress in SH-SY5Y neuroblastoma cells. *J. Pineal Res.* **49**, 141–148 (2010).

24. Melo, J. B., Sousa, C., Garcao, P., *et al*. Galantamine protects against oxidative stress induced by amyloid-beta peptide in cortical neurons. *Eur. J. Neurosci.* **29**, 455–64 (2009).

25. Furukawa, S., Yang, L. & Sameshima, H. Galantamine, an acetylcholinesterase inhibitor, reduces brain damage induced by hypoxia-ischemia in newborn rats. *Int. J. Dev. Neurosci.* **37**, 52–7 (2014).

26. Almasieh, M., MacIntyre, J., Pouliot, M., *et al.* Acetylcholinesterase inhibition promotes retinal vasoprotection and increases ocular blood flow in experimental glaucoma. *Investig. Ophthalmol. Vis. Sci.* **54**, 3171–3183 (2013).

27. Almasieh, M., Zhou, Y., Kelly, M., *et al*. Structural and functional neuroprotection in glaucoma: role of galantamine-mediated activation of muscarinic acetylcholine receptors. *Cell Death Dis.* **1**, e27 (2010).

28. Shimizu, S., Mizuguchi, Y., Sobue, A., *et al.* Interaction between anti-Alzheimer and antipsychotic drugs in modulating extrapyramidal motor disorders in mice. *J. Pharmacol. Sci.* **127**, 439–445 (2015).

29. Kita, Y., Ago, Y., Higashino, K., *et al.* Galantamine promotes adult hippocampal neurogenesis via muscarinic and α7 nicotinic receptors in mice. *Int. J. Neuropsychopharmacol.* **17**, 1957–1968 (2014).

30. Noda, Y., Mouri, A., Ando, Y., *et al.* Galantamine ameliorates the impairment of recognition memory in mice repeatedly treated with methamphetamine: Involvement of

allosteric potentiation of nicotinic acetylcholine receptors and dopaminergic-ERK1/2 systems. *Int. J. Neuropsychopharmacol.* **13**, 1343–1354 (2010).

31. Hines-Beard, J., Bond, W., Backstrom, J., *et al*. Virus-mediated EpoR76E gene therapy preserves vision in a glaucoma model by modulating neuroinflammation and decreasing oxidative stress. *J. Neuroinflammation* (2016). doi:10.1186/s12974-016-0499-5
32. Guerriero, R. M., Giza, C. C. & Rotenberg, A. Glutamate and GABA imbalance following traumatic brain injury. *Curr. Neurol. Neurosci. Rep.* **15**, 27 (2015).
33. Mammadova, N., Ghaisas, S., Zenitsky, G., *et al.* Lasting Retinal Injury in a Mouse Model of Blast-Induced Trauma. *Am. J. Pathol.* **187**, 1459–1472 (2017).
34. Tehse, J. & Taghibiglou, C. The overlooked aspect of excitotoxicity: Glutamate-independent excitotoxicity in traumatic brain injuries. *Eur. J. Neurosci.* **49**, 1157–1170 (2019).
35. Dorsett, C. R., McGuire, L., DePasquale, E., *et al.* Glutamate Neurotransmission in Rodent Models of Traumatic Brain Injury. *J. Neurotrauma* **34**, 263–272 (2017).
36. Rao, V., Baskaya, M., Dogan, A., *et al.* Traumatic Brain Injury Down-Regulates Glial Glutamate Transporter (GLT-1 and GLAST) Proteins in Rat Brain. *J. Neurochem.***70,** 2020-2027 (2002).
37. Satapathy, S. K., Ochani, M., Dancho, M., *et al.* Galantamine alleviates inflammation and other obesity-associated complications in high-fat diet-fed mice. *Mol. Med.* **17**, 599–606 (2011).
38. Di Polo, A., Almasieh, M., & Zhou, Y. Galantamine: A Novel Neuroprotective Strategy For Injured Retinal Ganglion Cells In Glaucoma. *Invest. Opthalmol. Vis. Sci.* **47**, (2006).
39. Borovikova, L. V., Ivanova, S., Zhang, M., *et al.* Vagus nerve stimulation attenuates the

systemic inflammatory response to endotoxin. *Nature* **405**, 458–462 (2000).

40. Texidó, L. *et al.* Effect of galantamine on the human α7 neuronal nicotinic acetylcholine receptor, the Torpedo nicotinic acetylcholine receptor and spontaneous cholinergic synaptic activity. *Br. J. Pharmacol.* **145**, 672–678 (2005).

41. Faghih, R., Gfesser, G. A. & Gopalakrishnan, M. Advances in the discovery of novel positive allosteric modulators of the alpha7 nicotinic acetylcholine receptor. *Recent Pat. CNS Drug Discov.* **2**, 99–106 (2007).

Highlights

- Galantamine is an FDA approved acetylcholinesterase inhibitor used for the treatment of mild Alzheimer's disease.
- Exposure to repeated over-pressure air blasts causes a decrease in the ERG b-wave amplitude, an increase in the ERG b-wave latency, and rod bipolar cell dendrite retraction. This was mitigated by post-injury treatment with galantamine.
- Repeat blast exposure induced an indirect traumatic optic neuropathy (ITON). Post-injury treatment with galantamine mitigated optic nerve damage and partially preserved the visual evoked potential.
- Post-injury treatment with galantamine mitigated blast-induced changes in levels of IL-1α, IL-1β, glutamate, nitrotyrosine, and SOD2.

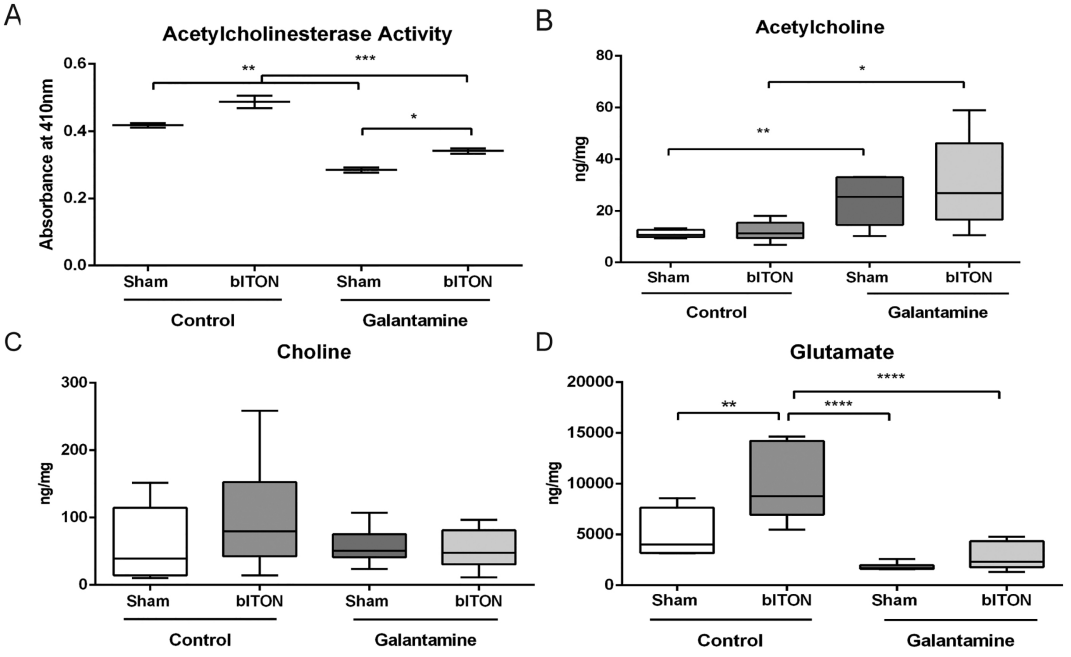
A
Acetylcholinesterase Activity
Absorbance at 410nm
0.6
0.4
0.2
0.0
**
***
*
Sham
bITON
Sham
bITON
Control
Galantamine
B
Acetylcholine
ng/mg
80
60
40
20
0
*
**
Sham
bITON
Sham
bITON
Control
Galantamine
C
Choline
ng/mg
300
200
100
0
Sham
bITON
Sham
bITON
Control
Galantamine
D
Glutamate
ng/mg
20000
15000
10000
5000
0
**
****
****
Sham
bITON
Sham
bITON
Control
Galantamine

Figure 1

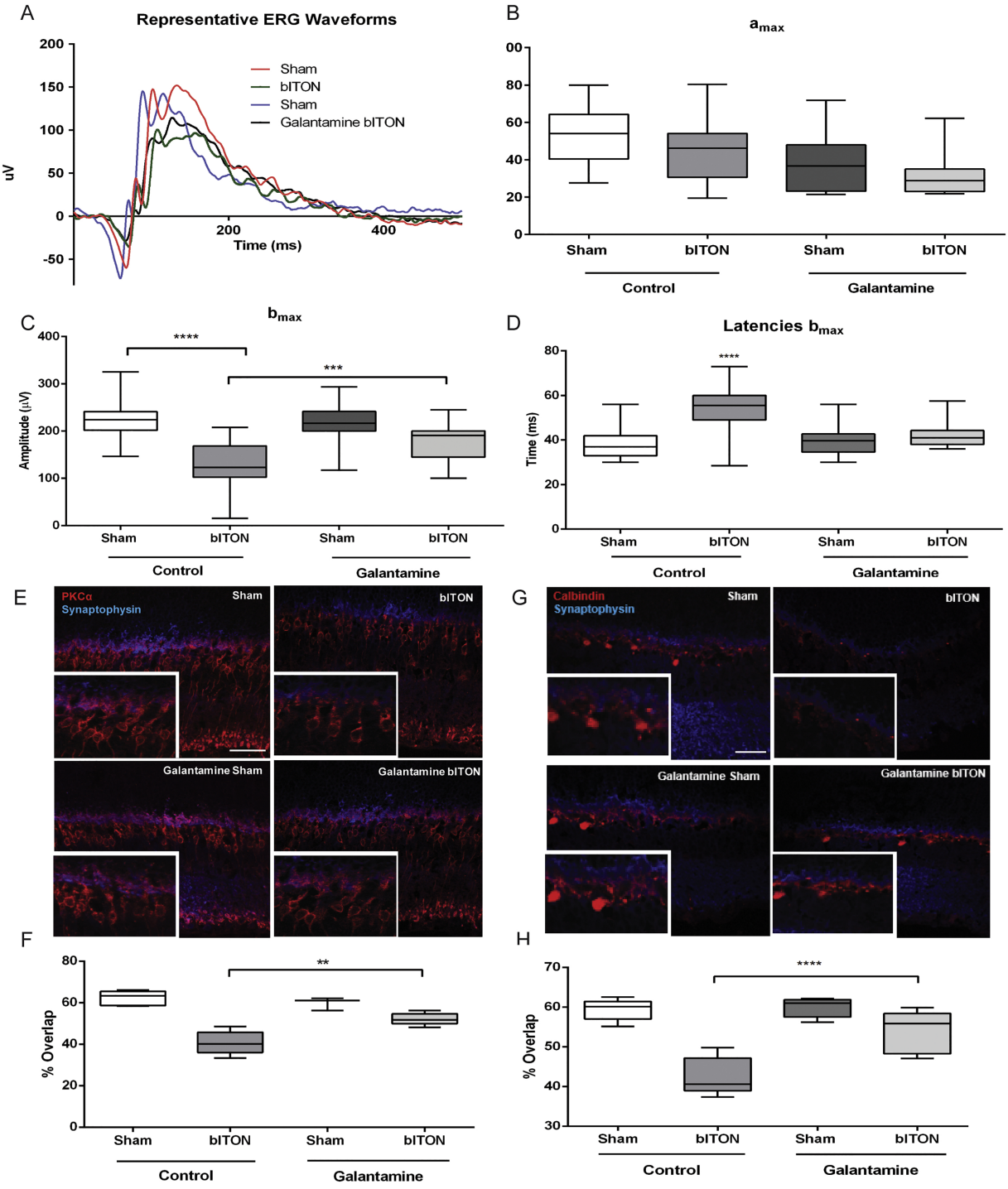
A
Representative ERG Waveforms
Sham
bITON
Sham
Galantamine bITON
uV
Time (ms)
B
amax
Sham
bITON
Sham
bITON
Control
Galantamine
C
bmax
Amplitude (μV)
****
***
Sham
bITON
Sham
bITON
Control
Galantamine
D
Latencies bmax
Time (ms)
****
Sham
bITON
Sham
bITON
Control
Galantamine
E
PKCα
Synaptophysin
Sham
bITON
Galantamine Sham
Galantamine bITON
G
Calbindin
Synaptophysin
Sham
bITON
Galantamine Sham
Galantamine bITON
F
% Overlap
**
Sham
bITON
Sham
bITON
Control
Galantamine
H
% Overlap
****
Sham
bITON
Sham
bITON
Control
Galantamine

Figure 2

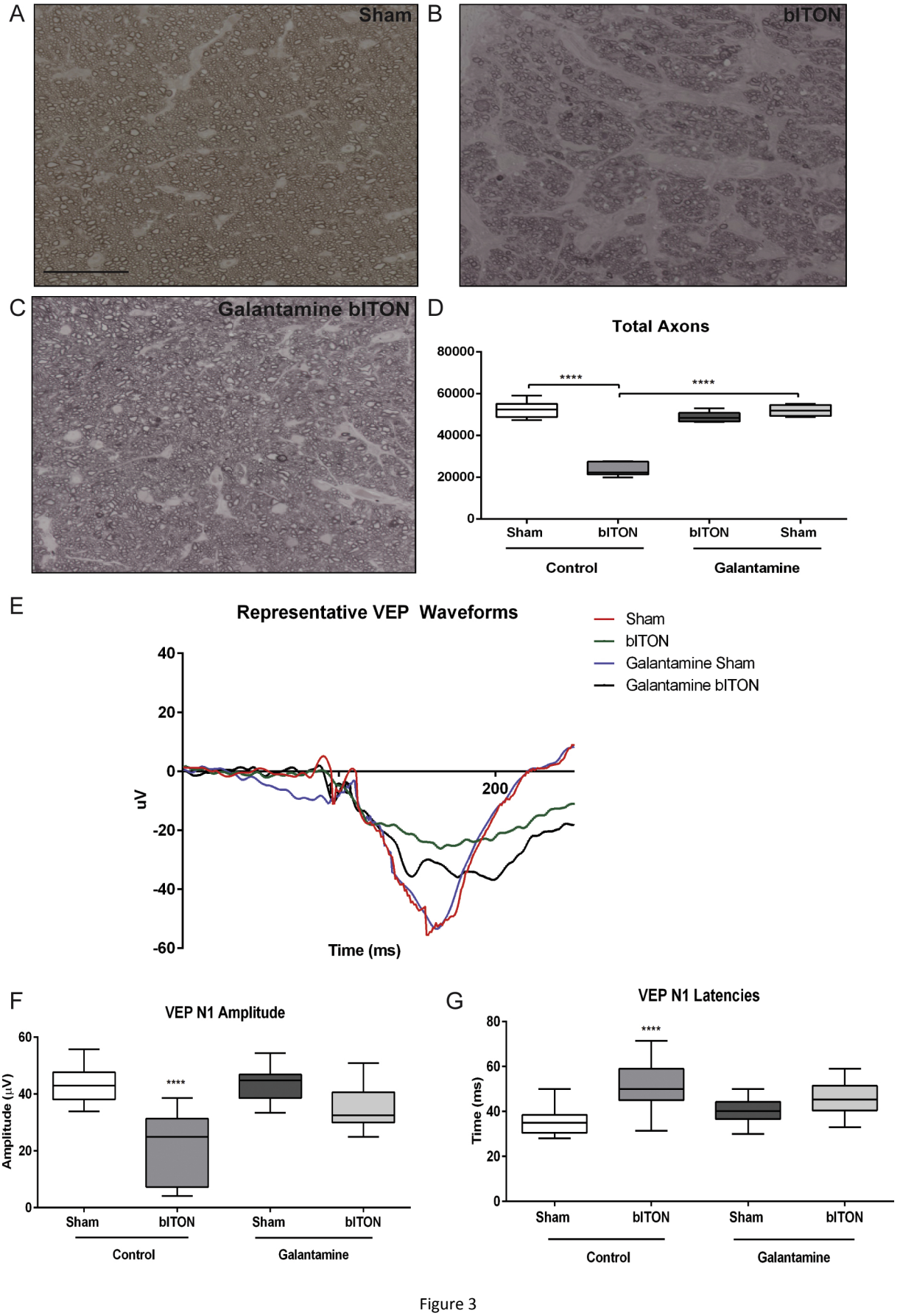
A
Sham
B
bITON
C
Galantamine bITON
D
Total Axons
80000
60000
40000
20000
0
****
****
Sham
bITON
bITON
Sham
Control
Galantamine
E
Representative VEP Waveforms
Sham
bITON
Galantamine Sham
Galantamine bITON
40
20
0
-20
-40
-60
uV
200
Time (ms)
F
VEP N1 Amplitude
60
40
20
0
Amplitude (μV)
****
Sham
bITON
Sham
bITON
Control
Galantamine
G
VEP N1 Latencies
80
60
40
20
0
Time (ms)
****
Sham
bITON
Sham
bITON
Control
Galantamine

Figure 3

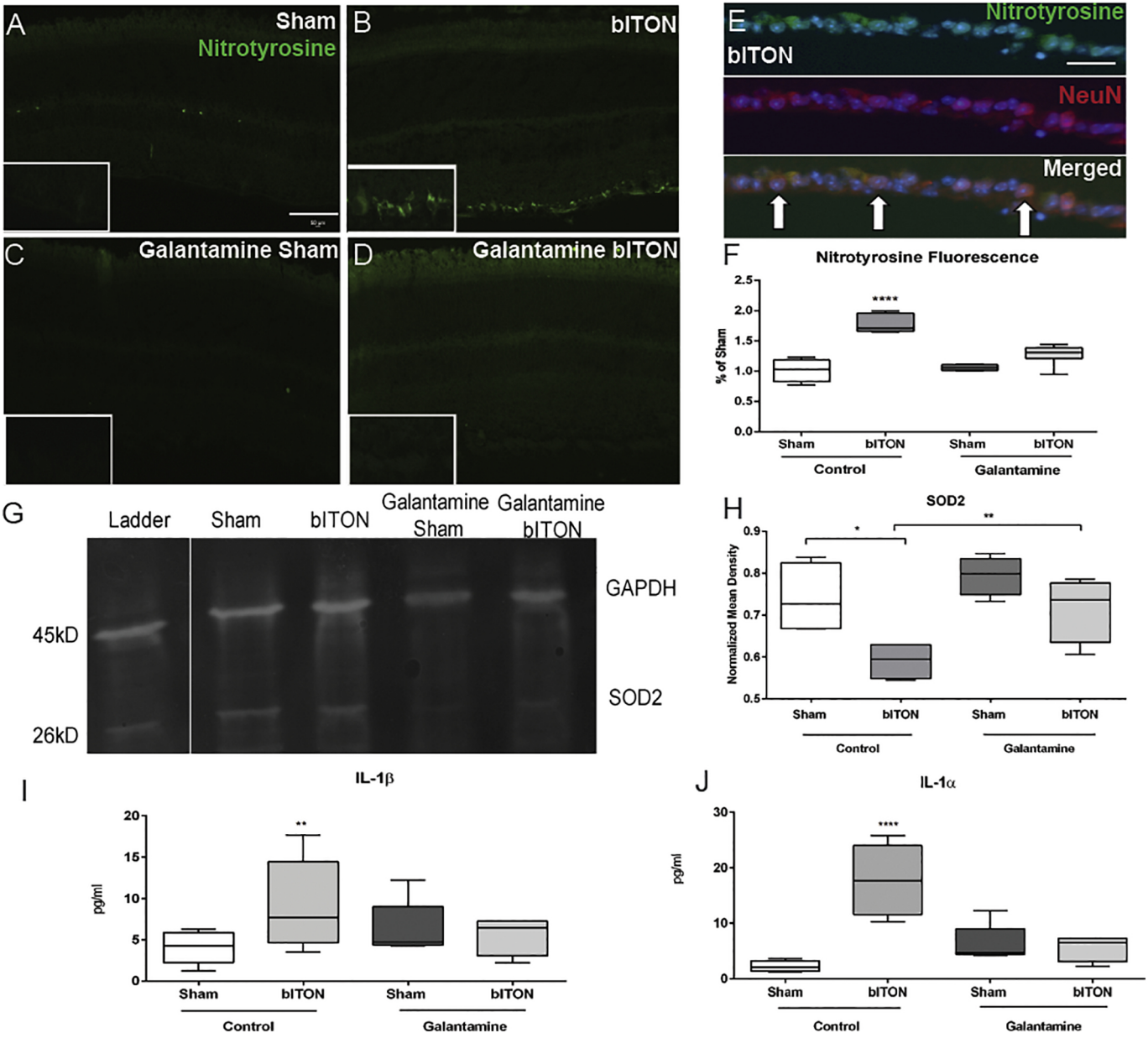
A
Sham
Nitrotyrosine
B
bITON
C
Galantamine Sham
D
Galantamine bITON
E
Nitrotyrosine
bITON
NeuN
Merged
F
Nitrotyrosine Fluorescence
% of Sham
2.5
2.0
1.5
1.0
0.5
0.0
****
Sham
bITON
Sham
bITON
Control
Galantamine
G
Ladder
Sham
bITON
Galantamine Sham
Galantamine bITON
45kD
26kD
GAPDH
SOD2
H
SOD2
Normalized Mean Density
0.9
0.8
0.7
0.6
0.5
*
**
Sham
bITON
Sham
bITON
Control
Galantamine
I
IL-1β
pg/ml
20
15
10
5
0
**
Sham
bITON
Sham
bITON
Control
Galantamine
J
IL-1α
pg/ml
30
20
10
0
****
Sham
bITON
Sham
bITON
Control
Galantamine

Figure 4

Neuroprotective strategies for the treatment of blast-induced optic neuropathy

MR141315
W81XWH-15-1-0559

PI: Tonia S. Rex **Org:** Vanderbilt University Medical Center **Award Amount:** $1.5 million

Study/Product Aim(s)

- We hypothesize that blast-induced optic nerve degeneration and vision loss is due to oxidative stress and neuroinflammation, which causes cholinergic neuron dysfunction.
- Aim 1: We will test the working hypothesis that blast activates inflammation-mediated cell death in the cholinergic amacrine cells and leads to decreased signaling to the direction-selective retinal ganglion cells and degeneration of their axons.
- Aim 2: We will test the working hypothesis that restoration of signaling to the retinal ganglion cells by treatment with galantamine will preserve the optic nerve and vision after blast.

Aim 3: We will test the working hypothesis that a non-erythropoietic form of erythropoietin (EPO-R76E) will block oxidative stress and neuroinflammation and preserve the optic nerve and vision after blast.

Approach

We will use our model of blast induced optic neuropathy to assess the efficacy of galantamine and erythropoietin. We will quantify relevant neurotransmitters, oxidative stress, neuroinflammation, axon transport, histology, and vision.

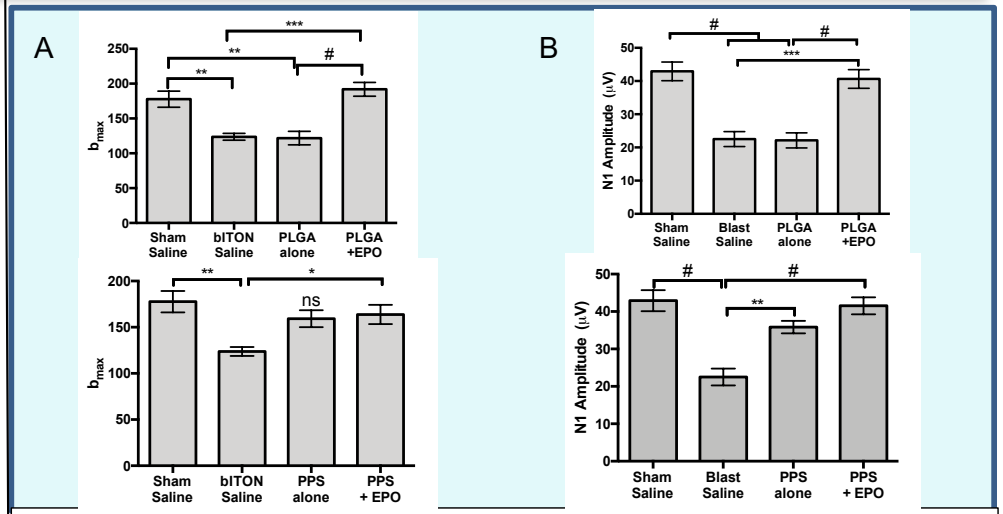

Epo-R76E-containing microparticles given 1-day after the last day of a 3-day series of blast exposures significantly preserve vision. A) ERG amplitudes, B) VEP amplitudes. Top: EPO-R76E delivered in PLGA particles. Bottom: EPO-R76E delivered in PPS particles, which are inherently antioxidant.

Timeline and Cost

Activities CY	15	16	17	18
Specific Aim 1				
Specific Aim 2				
Specific Aim 3				
Apprx. Budget ($K)	**$350**	**$500**	**$500**	**$150**

Updated: 12/12/19

Goals/Milestones

CY16 Goals – Completed.
CY17 Goal – Completed.
CY 18 Goal - Completed
CY19 Goal – Publish the EPO-R76E study.

Budget Expenditure to Date

Projected Expenditure: $1.5M
Actual Expenditure: $1.5M

Microsphere Antioxidant and Sustained Erythropoietin-R76E Release Functions Cooperate to Reduce Traumatic Optic Neuropathy

Bernardo-Colón A[1,#], DeJulius CR[2,#], Naguib S[3], Backstrom JR[1], Kavanaugh T[2], Gupta M[2], Duvall CL[2,*], Rex TS[1,3,*].

[1]Vanderbilt Eye Institute, Vanderbilt University Medical Center; [2]Department of Biomedical Engineering, Vanderbilt University, [3]Department of Ophthalmology & Visual Science, Vanderbilt University School of Medicine

#These authors contributed equally
*Corresponding Authors

ABSTRACT

Wild-type erythropoietin (EPO) is promising for neuroprotection, but its therapeutic use is limited because it causes a dangerous rise in hematocrit. We have developed an EPO-R76E derivative that maintains neuroprotective function without effects on hematocrit, but this protein is limited for therapeutic use by its short half-life *in vivo*. Here, we compare the safety and efficacy of two polymeric microparticle EPO-R76E sustained release formulations based on conventional hydrolytically degradable poly(lactic-co-glycolic acid) (PLGA) or reactive oxygen species (ROS)-degradable poly(propylene sulfide) (PPS). Both particle types effectively loaded EPO-R76E and achieved sustained release, providing detectable levels of EPO-R76E at the injection site in the eye *in vivo* for at least 28 days. Testing in an *in vitro* oxidative stress assay and a mouse model of blast-induced indirect traumatic optic neuropathy (bITON) showed that PLGA-mediated delivery of EPO-R76E provided partial therapeutic protection. However, the therapeutic protein must overcome the effects of the blank PLGA particles, which inherently increase levels of pro-inflammatory cytokines and exacerbate the injury response in the bITON model. In contrast, drug-free PPS particles have inherent antioxidant properties that, as opposed to PLGA, provide partial therapeutic protection both *in vitro* and *in vivo*. Finally, EPO-R76E-loaded PPS particles

provide the highest overall therapeutic benefit both *in vitro* and *in vivo*, at least in part due to EPO-R76E-driven production of antioxidant proteins such as SOD2. Our data demonstrate that PPS particles are safer than PLGA particles for intraocular use and that PPS and EPO-R76E work through complementary pathways that provide neuroprotection following traumatic eye injury.

KEYWORDS
Antioxidant, intraocular, neurotrauma, neuroprotection, sustained delivery, erythropoietin

INTRODUCTION

Neuroprotective therapeutics are especially attractive for the treatment of complex neurodegenerative processes lacking a defined genetic target, such as neurotrauma. Traumatic brain injuries occur in 2.8 million civilians each year [1], and indirect traumatic optic neuropathy (ITON) is estimated to occur in 0.5% to 2% of these individuals [2]. Notably, current interventions for ITON are no more effective than observation alone [3]. Unlike treatment of inherited conditions, it may not be advantageous, or even safe, to provide permanent and irreversible treatment (e.g., with a viral gene therapy) with a neuroprotective agent, as these agents are often pleiotropic. At the same time, short-lasting treatment (e.g., weekly) into the back of the eye is not practical and may further mechanically damage the tissue.

The natural history of ITON is not well understood due to the low incidence of the condition and the high variability of its course in patients [4,5]. Animal studies and case reports suggest that the neurodegeneration and loss of vision stabilizes about 1-month after injury [6,7,8]. Thus, it is desirable to provide sustained, but not permanent, treatment with tight dose control, which we seek herein using sustained-release

polymeric microparticles. The intravitreal space represents a local environment with multiple clearance mechanisms including conjunctival, choroidal, and lymphatic circulation [9], motivating use of micron-sized particles large enough (~1-100 μm) to provide size-based retention [10] and that respond to environmental cues to trigger particle degradation and cargo release [11].

We and others have previously demonstrated that erythropoietin (EPO) can preserve retinal neurons and optic nerve axons in a variety of models of neuronal cell death including our model of blast-induced ITON (bITON) [7,8,12]. Recently, microparticle-mediated delivery of EPO for nerve regeneration has gained interest. Rong and colleagues formulated a dextran-EPO poly(lactic-co-glycolic acid)/poly(lactic acid) (PLGA/PLA) microparticle system and demonstrated its efficacy in a rat model of optic nerve crush. A single injection of their microparticle system rescued a similar number of retinal ganglion cells (RGCs) 4- and 8-weeks post-optic nerve crush as injections of free EPO every 2 weeks, with no effect of empty PLGA/PLA microparticles [13]. Similarly, Zhang and colleagues showed that a single local injection of PLGA-EPO but not unloaded PLGA microparticles significantly increased nerve conduction velocity, muscle action potentials, axon counts, and myelin thickness in a rat sciatic nerve defect model 8 weeks post-surgery [14]. PLGA has improved EPO efficacy by providing slow release of the drug; however, the major drawback of PLGA is its breakdown into lactic acid and glycolic acid which may exacerbate inflammation [15].

In this study, we compare the therapeutic efficacy of a mutant EPO (EPO-R76E) delivered intraocularly by two different polymeric microparticle systems in our bITON model. EPO-R76E carries a mutation converting the arginine at position 76 to a

glutamate. This mutation prevents the significant increase in hematocrit caused by systemic administration of wild-type EPO in non-anemic animals, while preserving equal neuroprotective efficacy [16,17]. We compare EPO-R76E formulated into microparticles comprising the commonly used PLGA versus poly(propylene sulfide) (PPS), which we recently innovated for application in peripheral arterial disease [18,19]. PPS is an attractive delivery system for neurodegenerative diseases because this polymer reacts with and thus scavenges certain reactive oxygen species (ROS), including hydrogen peroxide (H_2O_2) [20], that in excess exacerbate inflammation [18,19,21]. Oxidation by H_2O_2 causes a transition of PPS from a hydrophobic to hydrophilic state, resulting in breakdown of the particle over time and providing sustained, ROS-triggered drug cargo release. By contrast, PLGA degrades via nonspecific hydrolysis into acidic byproducts which lower the local pH and can worsen inflammation [15,22]. Notably, oxidative stress is a hallmark of our bITON model, causing secondary axon degeneration [7]. Thus, we hypothesized that: 1) the PPS particles should degrade in the eye after ITON due to the presence of ROS resulting in release of EPO-R76E, 2) combined treatment with PPS and EPO-R76E would be more effective than either alone due to different antioxidant mechanisms, and 3) the PPS particles would be better tolerated than PLGA particles for intraocular delivery.

METHODS

EPO-R76E Purification: Human epithelial kidney (HEK) cells grown to confluence in 10 cm plates were transfected with 5 μg of pcDNA plasmids that express either wild-type EPO or EPO-R76E with carboxyl-terminal His-tags. A 19-amino acid linker containing a Tobacco Etch Virus (TEV) protease recognition site was inserted after the carboxyl-

terminus of EPO-R76E to increase the accessibility of the His-tag to the metal ion matrix used for purification. The next day, plates were washed and replaced with serum-free DMEM. After an additional three days, the media was collected and centrifuged to pellet cells. Supernatant was applied to a TALON cobalt resin column (Takara BIO, Mountain View, CA) and washed with 20 bed volumes of PBS. Protein was eluted from the matrix with 50 mM potassium acetate, pH 5.0 buffer containing 100 mM NaCl. The pH of the solution was neutralized with a 1:40 volume (2.5 μl:100 μl eluate) of 0.8 M Tris, pH 9.3. Protein was judged to be at least 90% pure based on gels stained with SimplyBlue SafeStain (Invitrogen, Carlsbad, CA). His-tagged EPO or EPO-R76E was detected on blots with mouse anti-His tag (Cell Signaling, Danvers MA; #2366 diluted 1:1000) or rabbit anti-hEPO (R&D Systems Inc., Minneapolis MN; #AB286 at 1 μg/ml).

Synthesis of PPS: PPS was prepared by anionic polymerization of propylene sulfide (Sigma-Aldrich, St. Louis, MO) using 1,8-diazabicyclo[5.4.0]undec-7-ene (DBU)/1-butane thiol as an initiator [23,24,25]. Briefly, DBU (4.5 mmol, 0.673ml) and anhydrous THF (10 ml) were transferred to a dried 25 ml round bottom (RB) flask and degassed for 30 min. In another 50 ml RB flask, 1-butane thiol (1.5 mmol, 0.161 ml) in THF (20 ml) was degassed for 30 min and the reaction mixture temperature was lowered to 0°C. To this solution, the previously degassed solution of DBU in THF was added dropwise. The flask was brought to room temperature and allowed to stir for 30 min. Next, freshly distilled and degassed propylene sulfide (120 mmol, 9.39 ml) monomer was added dropwise to the reaction mixture at 0°C and maintained for 30 min. After 2 hr stirring at room temperature, the polymerization reaction was quenched by addition of 2-iodoethanol (2 mmol, 0.40 g) and stirred overnight at room temperature. The next day,

the polymer solution was filtered to remove precipitated salt and further purified by three precipitations into cold methanol before vacuum-drying to yield a colorless viscous polymer. ^{1}H NMR (400 MHz; $CDCl_3$, δ): 1.3-1.4 (s, CH_3), 2.5-2.8 (s, CH), 2.8-3.1 (s, CH_2), 3.72 (t, CH_2-OH). (poly(PPS), Mn = 6,700 g/mol, PDI = 1.3).

Characterization of PPS: PPS was characterized for structure, molecular weight (Mn), and polydispersity (PDI) as described previously [18,19,23-25]. PPS chemical structure was confirmed *via* ^{1}H NMR recorded in $CDCl_3$ with a Brüker 400 MHz spectrometer. Gel permeation chromatography (GPC, Agilent Technologies, Santa Clara, CA, USA) was used to assess Mn and PDI of the polymer. PPS was dissolved in dimethylformamide (DMF) + 0.1 M LiBr and run through three serial Tosoh Biosciences TSKGel Alpha columns (Tokyo, Japan) at 60°C. Offline injections into the Agilent refractive index (RI) detector determined dn/dc values experimentally. The dn/dc value was used to calculate absolute Mn using the RI detector and a Wyatt miniDAWN TREOS light scattering (LS) detector (Wyatt Technology Corp., Santa Barbara, CA).

EPO-R76E microparticle formulation: PPS or PLGA (10 kDa, 50:50 lactide:glycolide, Sigma) was dissolved in dichloromethane (DCM) at 50 mg/ml (100 mg polymer in 2 ml DCM). For EPO-R76E-loaded particles, EPO-R76E (470 μg/ml, 500 μl) was added dropwise, and the mixture was homogenized at 20,000 rpm for 30 sec. The resulting polymer solution was added dropwise to 1.5% polyvinyl alcohol (PVA, 10 ml), and this mixture was homogenized at 10,000 rpm for 30 sec. To remove DCM, the particle suspension underwent rotary evaporation for 1 hr. The particles were washed once with deionized (DI) water to remove excess PVA and resuspended in DI water. The

suspension was frozen at -80°C and lyophilized until further use. Unloaded microparticles were formulated similarly without the addition of EPO-R76E.

Quantification of EPO-R76E loading: EPO-R76E was labeled with N-hydroxysuccinimide-cyanine7 (NHS-Cy7) dye to quantify protein loading into PPS and PLGA microparticles. Briefly, 500 μl sodium bicarbonate buffer (0.3 M, pH 8.3) was added to 1 ml EPO-R76E (250 μg/ml). NHS-Cy7 was dissolved in dimethyl sulfoxide (DMSO) at 589 μM, and 100 μl was added to the EPO-R76E solution (final concentration 36.8 μM). The mixture was reacted at room temperature for 4 hrs on a shaker. The EPO-R76E-Cy7 protein was purified via a desalting column. The fluorescently-labeled protein was lyophilized to yield a dry powder. The protein yield was measured by bicinchoninic acid (BCA) assay. EPO-R76E-Cy7-loaded particles were formulated as above. The particles were fully dissolved in DMSO, and the fluorescence of the released EPO-R76E was measured on a plate reader at excitation/emission 750/773 nm. EPO-R76E concentration was calculated from a standard curve of EPO-R76E-Cy7 in DMSO.

Quantification of Microparticle Size: PLGA-blank, PLGA+EPO-R76E, PPS-blank, and PPS+EPO-R76E microparticles were resuspended in DI water. A 50μl droplet was placed on a coverslip and allowed to settle for 30 minutes. Five images per sample were acquired on a Nikon Eclipse Ti inverted microscope. Particle size was measured using Nikon Ts software. One hundred particles per image were measured.

***In Vitro* Release of EPO-R76E**: PLGA+EPO-R76E or PPS+EPO-R76E microparticles were resuspended in phosphate buffered saline (PBS) at 4 mg/ml. 250 μl of suspension was added to a 12-well plate transwell submerged in 1 ml PBS, 50 mM hydrogen

peroxide (H_2O_2) or 500 mM H_2O_2. The releasate was collected over the course of 28 days and replaced with fresh PBS or H_2O_2 solution and frozen at -80°C until EPO-R76E quantification.

EPO-R76E ELISA: EPO-R76E concentration in the releasate was measured by sandwich ELISA using Quantikine Human EPO ELISA kit (R&D Systems, Minneapolis, MN) according to manufacturer directions. Samples were loaded at 10 µl per well and tested in duplicate, and the results were averaged.

Cell Culture: The human retinal pigment epithelial ARPE-19 cell lines obtained from the American Type Culture Collection (ATCC, Manassas, VA; #CRL-2302) was grown in DMEM/F12 Medium (Gibco #10565–018) with 10% Fetal Bovine serum (FBS; Gibco # 26140-079), 15 mM HEPES buffer (Gibco #15630-080) and incubated in a standard incubator containing 5% CO_2.

Microparticle Cytotoxicity Assay: ARPE-19 cells were seeded in 96-well plates in serum-free medium and allowed to adhere for 24 hrs. The media was replaced with 100 µl media containing particle suspensions at varying concentrations. The doses were calculated to deliver 10, 20, 40, or 80 ng EPO-R76E, or a corresponding dose of unloaded particles (0.08, 0.16, 0.32, or 0.64 mg/ml PLGA microparticles; 0.1, 0.2, 0.4, or 0.8 mg/ml PPS microparticles). After 24 hrs, cell viability was measured using the Cell TiterGlo kit according to the manufacturer's protocol: 100 µl Cell TiterGlo reagent was added to each well, and the luminescence was measured on an *In Vivo* Imaging System (IVIS).

Protection from H_2O_2 *In Vitro*: Cytoprotection of the microparticles from H_2O_2-induced death was measured *via* trypan blue stain. ARPE-19 cells were treated with 300 µM

H_2O_2 alone or with PLGA-blank, PLGA+EPO-R76E, PPS-blank, or PPS+EPO-R76E (50 ng EPO-R76E). After 24 hours, cells were collected and stained with trypan blue, and cell death was quantified using a hemocytometer.

Quantification Intracellular of ROS: Intracellular ROS was measured using dihydroethidium (DHE; ThermoFisher Scientific, Waltham, MA). ARPE-19 cells were treated with 100 μM H_2O_2 alone or with PLGA-blank, PLGA+EPO-R76E, PPS-blank, or PPS+EPO-R76E (50 ng EPO-R76E). After 6 hrs, cells were washed twice with HBSS and loaded with 10 μM DHE. After cells were incubated for 30 min, dye was removed and cells were washed and analyzed on a fluorescence plate reader (POLARstar Omega, BMG Labtech Company) at 581 nm emission, 608 nm emission.

bITON model: Eye injury was induced as previously described [7,12]. Briefly, C57Bl/6J mice (Jackson Labs, Bar Harbor, ME) were anesthetized with 1.5% isofluorane and secured into a padded housing chamber. The housing chamber was placed inside of a pipe. The left eye of the mouse was positioned against a hole in the pipe, which was aligned with the barrel of a paintball marker. All experiments were performed in the morning. Mice were exposed to two 15 psi air-blasts at a 0.5 sec interval per day for three days. Sham mice were anesthetized and placed in the trauma system, but the air was blocked from reaching the eye. Mice were provided gel recovery food (Clear H_2O, Portland, ME) for the first 3-days post-injury. At 1-day after the last blast exposure, mice were anesthetized with isofluorane and injected with a single 1 μl intravitreal injection using a 30 gauge Hamilton syringe. Mice were injected with PBS, PPS with or without EPO-R76E (at 10 μg particle/μl PBS), or PLGA with or without EPO-R76E (at 10 μg particle/μl PBS). EPO-R76E levels in the eye were quantified *via* ELISA as described

above after sonicating the tissue in 2 ml PBS + Halt 100X protease inhibitor cocktail (25 µl) and 10% Triton X-100 (50 µl). All experiments were conducted in compliance with the ARVO Statement for the Use of Animals in Ophthalmic and Vision Research. This study was carried out under an animal protocol approved by the Vanderbilt University Medical Center Institutional Animal Care and Use Committee.

***In vivo* ROS Imaging**: Mice were anesthetized with isofluorane and intravitreally injected with 1 µl of DHE in PBS using a 30 gauge Hamilton syringe. Just prior to imaging, mice were anesthetized with 20/8/0.8mg/kg ketamine/xylazine/urethane and eyes were dilated with tropicamide. 30 min after DHE injection, fluorescence was imaged on a Micron IV retinal imaging microscope (Phoenix Research Labs, Pleasanton, CA) using an FF02-475/50nm excitation filter (Semrock, Inc. Rochester, NY) and ET620/60X emission filter (Chroma Technology Corp., Bellows Falls, VT). Using ImageJ, the average intensity of the fluorescence throughout the retina was quantified. Data was analyzed in Graphpad Prism. Mice collected 4 wks after injury were imaged just prior to collection.

SOD2 Western Blot: Single retinas were homogenized and sonicated in lysis buffer and centrifuged. Sample buffer was added to the supernatant just prior to use. Known amounts of superoxide dismutase 2 (SOD2) protein (10 to 20 µg) or protein ladder were loaded into each well of an SDS-polyacrylamide gel. The Bio-Rad mini-trans blot cell system and mini protean pre-cast gels at 4-20% were used (Hercules, CA). Loading control was HSP60 (rabbit; 1:1000; ab45134, Abcam, Cambridge, MA). The protein was transferred onto nitrocellulose using the Bio-Rad trans blot turbo transfer system (Hercules, CA), probed with anti-SOD2 (rabbit; 1:1000; ab13533; Abcam), probed with

secondary antibody (alkaline phosphatase-conjugated AffiniPure Goat Anti-Rabbit IgG; 1:1000; cat #133466; Jackson ImmunoResearch Laboratories) and alkaline phosphatase was used for band detection. Band density was quantified by scanning the blot using an EPSON scanner and Adobe Photoshop to convert to grayscale and invert the image. Each band was selected with the same frame, and set measurements were used to obtain the grey mean value for each.

Multiplex Cytokine ELISA: Mouse multiplex cytokine/chemokine magnetic bead panel (cat #: MCYTOMAG-70K, Millipore, Burlington, MA) for IL-1α and IL-1β was performed according to manufacturer directions. Samples were tested in duplicates and results were averaged.

Histological Assessment of Optic Nerve: Optic nerve was post-fixed in glutaraldehyde followed by embedding in Resin 812 and Araldite 502 (cat # 14900 and 10900, Electron Microscopy sciences, Hatfield, PA) according to a previously published protocol [7,8,12,26]. A Leica EM-UC7 microtome was used to collect 1 µm-thick sections. Sections were then stained with 1% paraphenylenediamine and 1% toluidine blue and were imaged on a Nikon Eclipse Ni-E microscope using a 100x oil immersion objective (Nikon Instruments Inc., Melville, NY). Both total and degenerating axons were quantified using Image J. A grid was used to count 20% of the optic nerve cross-sectional area to avoid bias.

Electroretinograms (ERG) and Visual Evoked Potentials (VEPs): Mice were dark-adapted overnight, dilated with 1% tropicamide for 10 min, and anesthetized with 20/8/0.8 mg/kg ketamine/xylaxine/urethane according to previously published methodology [7,8,26]. Mice were placed on the heated surface of the ERG system to

maintain body temperature. Corneal electrodes with integrated stimulators were placed on eyes lubricated with Genteel drops using the Celeris system (Diagnosys LLC, Lowell, MA). Subdermal platinum needle electrodes were placed in the snout and back of the head at the location of the visual cortex. A ground electrode was placed in the back of the mouse. For VEPs, mice were exposed to 50 flashes of 1 Hz, 0.5 cd.s/m^2 white light. To collect ERGs, electrodes were placed on lubricated corneas. Mice were then exposed to 15 flashes of 1 Hz, 1 cd.s/m^2.

Experimental Design and Statistical Analysis: Western blot data was normalized to loading controls. Data were analyzed using GraphPad Prism (La Jolla, CA). All experimental groups were compared to each other using a one-way ANOVA and the Tukey post-hoc test. All groups are shown as mean ± SEM.

RESULTS AND DISCUSSION

Formulation of EPO-R76E-loaded microparticles

We and others have shown a dangerous rise in hematocrit with systemic administration of EPO [16,17,27], which we avoided here by using mutant EPO-R76E and intravitreal administration (data not shown; [13,14]). EPO-R76E was expressed with a His-tag in mammalian HEK cells, rather than bacterial cells, in order to properly glycosylate the protein (Figure 1A). Low levels of wild-type EPO and no detectable EPO-R76E was purified using the His tag (Figure 1B). To increase accessibility to the His tag, we added a 15 amino acid tobacco etch virus (TEV) linker between the protein and the tag (Figure 1A). We were then able to recover purified wild-type EPO and EPO-R76E at the expected size (Figure 1B). As further confirmation, we probed with

anti-EPO and compared our purified protein to commercially available EPO (Figure 1C). The purified proteins and purchased EPO migrated at the same size and were detected by the EPO antibody. The TEV-His-tagged EPO-R76E was used in all following experiments and is henceforth referred to as EPO-R76E.

To extend the residence time of EPO-R76E in the eye, EPO-R76E was loaded into PPS and PLGA microparticles using the W/O/W emulsion technique. PPS was synthesized by anionic polymerization and characterized by ^{1}H NMR and GPC (Figure 1D-F). In order to determine the amount of EPO-R76E loaded into the PPS and PLGA particles, the protein was labeled with Cy7 and quantified from a standard curve (Figure 1G). PPS and PLGA particles were loaded with 0.85 and 1.39 μg EPO-R76E per mg particles, respectively. Subsequent *in vitro* experiments were controlled for mass of EPO-R76E delivered. Blank and loaded particles were quantified for size by light microscopy. A representative image of unloaded PPS particles is shown in Figure 1H. Quantification shows that the PLGA particles (Figure 1I, K) were slightly larger than the PPS particles, and the size decreased slightly ($p<0.05$) for both systems with EPO-R76E loading; 3.83 ± 1.6 vs. 2.60 ± 0.81 μm for PLGA and 2.17 ± 0.69 vs. 1.78 ± 0.57 μm for PPS (Figure 1J, L).

In vitro efficacy of EPO-R76E microparticles

We compared release of EPO-R76E over time from the PPS and PLGA particles *in vitro* (Figure 2A, B). Because PPS is sensitive to ROS, we tested release in two different concentrations of hydrogen peroxide (H_2O_2), as well as PBS (Figure 2A). The PPS microparticles released EPO-R76E at a similar rate to PLGA in PBS, while rate of

release was also H_2O_2-dose dependent for the PPS microparticles. Both PPS and PLGA demonstrated sustained release of EPO-R76E in PBS for at least 3 weeks *in vitro*. Next, we assessed the cytocompatibility of different doses of empty or EPO-R76E-loaded microparticles (Figure 2C). Although some statistically significant differences were detected between groups, all groups exhibited greater than 90% viability when treated with 10-80 ng EPO-R76E in 10-80 μg PPS or 8-64 μg PLGA particles. For the remaining *in vitro* experiments, we treated cells with 50 ng EPO-R76E delivered in either 40 μg PLGA or 50 μg PPS particles based on preliminary dose-finding studies.

To demonstrate the benefit of an inherently antioxidant delivery system and decouple the antioxidant effects of PPS from those of EPO-R76E, *in vitro* cytoprotection and ROS production in oxidative conditions were studied. First, we exposed cells to 300 μM H_2O_2 and co-treated with either empty or EPO-R76E-loaded PPS or PLGA particles (Figure 2D). After 24 hrs, there was 38 ± 2.5% and 36 ± 6.0% cell death in the untreated and empty PLGA treated groups, respectively. In contrast, only 13 ± 2%, 12 ± 3%, and 9 ± 3% cell death was detected in the PLGA+EPO-R76E, PPS alone, and PPS+EPO-R76E treated groups, respectively ($p<0.0001$ vs. untreated). Therefore, any mode of EPO-R76E delivery rescued cells from ROS-induced cell death whereas PLGA alone failed to have any benefit. In contrast, there was a significant cell protective benefit of PPS alone in the presence of a large dose of H_2O_2, confirming the inherent antioxidant, cell-protective activity of PPS. This result is in agreement with previous data showing that unloaded PPS microparticles can prevent cell death at levels similar to PPS microparticles loaded with the antioxidant and anti-inflammatory compound curcumin [19].

We next quantified the level of intracellular ROS produced after exposure to 100 μM H_2O_2 for 6 hrs using DHE fluorescence (Figures 2E, F). All data were normalized to the level of DHE fluorescence in naïve cells (media) and are shown as increase from the control group. Empty PPS particles significantly decreased DHE fluorescence, and this effect was compounded with the addition of EPO-R76E, returning ROS levels to baseline (Figure 2E). The cellular ROS scavenging ability of PPS-based micro- and nanoparticles has been demonstrated previously in cell types including RAW264.7 macrophages, 3T3 fibroblasts, primary human mesenchymal stem cells (hMSCs), and BV2 microglial cells, agreeing with our results [19,24,25,28]. PLGA-mediated delivery of EPO-R76E also suppressed DHE fluorescence to control levels, with no effect from empty PLGA particles (Figure 2F). These data demonstrate that EPO-R76E can decrease ROS beyond that accomplished by PPS alone with moderate exposure to H_2O_2, and to our knowledge, are the first demonstration of the combined antioxidant effect of microparticle-mediated EPO-R76E delivery.

In vivo efficacy of EPO-R76E microparticles

To study the long-term benefits of EPO-R76E microparticles, we utilized our bITON model in which there is elevated ROS that contributes to secondary degeneration of the optic nerve [7]. First, we assessed the release of EPO-R76E in the eye after injection of the particles 1-day after the last blast exposure (Figure 3). Low levels of endogenous EPO were present in the empty PPS (Figure 3A) or PLGA- (Figure 3B) injected eyes at both 3- and 28-days post-injection. After injection of the loaded PLGA particles, the greatest quantity of EPO-R76E was measured at 1 day after

injection, consistent with a diffusionally-controlled release profile with a characteristic initial burst release (Figure 3B). In contrast, PPS delivery did not exhibit a burst release profile, and instead steadily released the protein over the course of the study (Figure 3A). Since PPS particles degrade in the presence of elevated H_2O_2 and hypochlorite [18,19], we anticipate that sustained release of EPO-R76E is at least partially controlled by ongoing production of ROS from the injury as indicated by our previous studies [7]. Notably, EPO-R76E was detected at all timepoints assessed, and our results suggest that both microparticle formulations released measurable protein quantities into the eye for at least one month. These combined data suggest that both microparticle formulations can significantly extend the persistence of EPO-R76E in the eye. For example, we have previously shown that the concentration of free EPO in the eye decreases 1000-fold by 36 hours after intra-ocular injection in mice [29], and a study in rabbits found a half-life of intravitreal EPO to be 2.84 days [30].

To investigate the antioxidant effect of sustained EPO-R76E *in vivo*, we quantified DHE fluorescence in the retina 4 weeks after bITON in mice treated with PLGA or PLGA+EPO-R76E. This experiment focused on the PLGA microparticles so that we could better identify any potential detrimental effects of the PLGA-based microparticles and also isolate the effect of the EPO-R76E protein without the complicating factor of using the ROS-scavenging PPS microparticles (Figure 4A-C). A higher DHE signal was present in the retina of bITON eyes injected with empty PLGA particles (Figure 4A) than in those treated with PLGA+EPO-R76E (Figure 4B). Quantification of the fluorescence showed a reduction to near sham levels in the PLGA+EPO-R76E eyes ($p<0.01$ as compared to PLGA alone; Figure 4C), suggesting

that the therapeutic must overpower some ROS-inducing effects inherent to the PLGA carrier.

We hypothesize that the major mechanistic difference between the antioxidant effects of PPS and EPO-R76E is that EPO-R76E can activate gene expression of antioxidant proteins whereas PPS directly reacts with ROS. To test the gene expression effects, we quantified levels of SOD2 (a mitochondria-associated enzyme that detoxifies superoxide free radicals) in the retina (Figure 4D, E). We have previously shown that levels of ROS-protective SOD2 decrease dramatically after blast injury [7]. We also have shown in a glaucoma model that systemic virus-mediated EPO-R76E gene delivery can increase expression of antioxidant proteins in the retina [31]. Here we also show a decrease in retina SOD2 levels in saline-injected bITON animals and in bITON mice injected with either the PPS or PLGA particles alone (Figure 4E). Notably, there was a greater decrease in retinal SOD2 levels in mice that received PLGA particles as compared to PPS particles. The data suggests that ROS scavenging by the PPS particles may have mitigated the loss of SOD2. Treatment with EPO-R76E-loaded PPS or PLGA particles was even more effective at preventing the loss of SOD2. The rescue of SOD2 levels in both groups of EPO-R76E treated retinas suggests that EPO-R76E and PPS have different antioxidant mechanisms that would be anticipated to have collaborative, beneficial effects on reducing ROS-mediated traumatic optic neuropathy.

Our trauma model causes an increase in ROS followed by an increase in levels of the pro-inflammatory cytokines IL-1α and IL-1β [7]. Further, blocking ROS prior to and after injury prevents increases in these cytokines along with secondary axon degeneration and vision loss [7]. Therefore, we also quantified changes in the levels of

IL-1α and IL-1β in both the retina and optic nerve (Figure 4F-I). Levels of inflammatory cytokines were higher in the retina and optic nerve from bITON eyes injected with PLGA particles alone compared to those receiving saline injection (Figure 4F-I). We measured endotoxin levels in the particles to ensure that the increase in cytokine levels was not due to endotoxin contamination, as expected, endotoxin levels were low (Supplemental Figure 1). Therefore, we expect this additional increase in inflammatory cytokines is due to the inflammatory effect of the PLGA particles or their acidic degradation products. In contrast, the antioxidant effects of PPS alone, PPS+EPO-R76E, and PLGA+EPO-R76E prevented increases in both cytokines. This result is consistent with our previous results using an antioxidant diet prophylactically [7], but with the major difference that in this study the particles were given at 1-day after injury. It is again notable that the antioxidant effect of EPO is strong enough to overcome the inflammatory cytokine increase created by PLGA administration, and this could explain positive results seen for previous PLGA+EPO systems despite the inherent inflammatory response to PLGA [13,14,32]. The ability of PPS to mitigate this effect on its own strongly supports its use as an ideal carrier for EPO-R76E in this application.

To investigate tissue damage, we assessed the optic nerve histologically 4-weeks after injury under all treatment conditions (Figure 5). Sham optic nerves showed a high density of axons with clear axoplasms and tight myelin sheaths, and normal morphology of astrocytes (Figure 5A). In contrast, the bITON optic nerves had axons with loose or collapsed myelin and hypertrophic astrocytes (Figure 5B). The optic nerves from eyes injected with the empty PPS particles appeared to have a high density of axons, although some degenerative profiles and glial hypertrophy were still evident

(Figure 5C). The optic nerves from eyes injected with PPS+EPO-R76E or PLGA+EPO-R76E displayed a morphology similar to sham (Figure 5D, F). In contrast, degenerative axon profiles were evident in the optic nerves of bITON mice injected with PLGA alone (Figure 5E). Quantification of total axons showed a significant loss of axons in the bITON mice injected with saline or PLGA; however, PPS, PPS+EPO-R76E, and PLGA+EPO-R76E all had axon counts similar to sham (Figure 5G). This illustrates the protective effects of either empty PPS or the EPO-R76E-loaded particles. As expected, there was an increase in degenerative axon profiles in the bITON mice as compared to shams, and PLGA microparticle treatment further worsened axon degeneration (Figure 5H). This is likely explained by the elevation in the pro-inflammatory cytokines IL-1α and IL-1β (Figure 4F-I). In contrast, there was no difference in degenerative axon profiles between shams and the EPO-R76E loaded PPS or PLGA particle-injected groups (Figure 5H). The PPS alone group showed an intermediate effect, demonstrating the protective effect of PPS, in opposition to the detrimental effect caused inherently by PLGA microparticles (Figure 5H).

We next assessed if post-injury delivery of the EPO-R76E loaded PPS particles, as our leading formulation, could preserve visual function (Figure 6). Representative ERG waveforms show the a- and b-waves 4-wks after blast injury (Figure 6A). Our injury paradigm causes a reduction in the ERG b-wave amplitude and an increase in the latency, indicative of synaptic dysfunction at the level of the retinal bipolar cells (Figure 6B,C) [26]. The bITON injured eyes treated with empty PPS particles trended towards improvement. However, the PPS+EPO-R76E particles provided statistically significant improvement in the ERG b-wave amplitude (Figure 6B). Both empty and EPO-R76E

loaded PPS particles showed statistically significant improvement in the latency of the b-wave (Figure 6C). Blast injury also causes a reduction in the VEP N1 amplitude and an increase in the N1 latency, indicative of damage to the optic nerve [7,8]. The VEP with the N1 waveform labeled is shown in Figure 6D. The N1 amplitude and latency were improved by treatment with empty PPS-injected bITON animals (Figure 6E,F). There was an even greater improvement in both N1 amplitude and latency by treatment with EPO-R76E-loaded PPS particles (Figure 6E,F). These data once again demonstrate the combined benefit of chemical ROS scavenging and activation of antioxidant proteins to suppress blast-induced optic nerve degeneration.

CONCLUSIONS

This study pursued an in-depth comparison of both PLGA- and PPS-based microparticles for sustained release of mutant EPO-R76E in a bITON model of traumatic neuropathy. EPO-R76E was previously proven to be effective as a viral gene therapy in this model, and herein we establish that sustained, non-viral release of EPO-R76E protein post-injury can provide neuroprotection in a therapeutic format that is more practical in a traumatic injury (non-genetic disease) clinical scenario. In these studies, both PLGA and PPS were shown to load EPO-R76E and provide sustained release for at least a month both *in vitro* and *in vivo*. Drug-free, blank PLGA particles exacerbated inflammation and injury associated with the bITON model. Despite this negative side effect of PLGA, EPO-R76E loaded PLGA particles showed an overall positive benefit, suggesting that at the doses used, EPO-R76E benefit was able to override any negative effects from the PLGA carrier. However, drug-free PPS particles,

which react irreversibly with some ROS, provided partial protection against the mechanical injury and consequent induction of inflammation (IL-1α and IL-1β levels in retina and optic nerve) and neural degeneration (axon loss). In fact, the empty PPS particles were as effective as the EPO-R76E loaded PPS particles in some of the assessed outcome measures. This both supports and extends our previous findings that ROS are causative of axon degeneration and vision loss in our bITON model. Based on our previous studies investigating optimal therapeutic doses of EPO and EPO-R76E in the eye [29,33], we expect that increasing the amount of EPO-R76E in the PPS particles should yield greater protection of visual function.

The potential clinical significance of this study is supported by our use of a relevant disease treatment scenario where treatment was given one day after three consecutive days of blast injury. Notably, we have shown that the interval between injury events is more important in determining the level of injury than the total number of injury events [12]. Thus, molecular injury processes were already initiated prior to the last day of blast-exposures and suggesting a wider therapeutic window for the treatment of secondary neurodegeneration due to neurotrauma than previously thought. In sum, this study suggests that PPS-based microparticles are a promising carrier that warrants further development and optimization for EPO-R76E sustained delivery in models of neurodegeneration.

ACKNOWLEDGEMENTS

The authors thank Purnima Ghose for assistance with histology and microscopy and the VAPR Core for assistance in purification of His-tagged EPO-R76E.

FUNDING

This work was supported by DoD W81XWH-15-1-0096 (TR), DoD W81XWH-17-2-0055 (TR), NEI R01 EY022349 (TR, CD), NEI U24 EY029893 (TR), NIBIB T32-EB021937 (CD), NIA R01 NS094595 (TR), Potocsnak Discovery Grant in Regenerative Medicine (TR), Ayers Foundation Regenerative Visual Neuroscience Pilot Grant (TR), Ret. Maj. General Stephen L. Jones, MD Fund (TR), Vanderbilt University Medical Center Cell Imaging Shared Resource core facility (Clinical and Translational Science Award Grant UL1 RR024975 from National Center for Research Resources), NEI P30EY008126 (VVRC), T32 EY021833 (VVRC) and Research Prevent Blindness, Inc (VEI). The funding sources had no involvement in the study design, or collection, analysis, or interpretation of the data. The authors confirm that there are no known conflicts of interest associated with this publication and there has been no significant financial support for this work that could have influenced its outcome.

DATA AVAILABILITY

FIGURE LEGENDS

Figure 1. Production of EPO-R76E containing microparticles. A) Schematic of two His-tagged human EPO-R76E (hEPO) that were produced. B) Detection of purified EPO-R76E using anti-His. Very little His-tagged wild-type EPO (Lane 1) and no His-tagged EPO-R76E (Lane 2) was detected. The addition of a TEV linker resulted in a large increase in the amount of detectable His-EPO (Lane 3) and His-EPO-R76E (Lane 4). Notably, both proteins are the same size. C) Detection of the TEV-His-tagged protein using anti-EPO and comparison to commercially available EPO. Lane 1: MW markers, Lane 2: wild-type EPO-TEV-His, Lane 3: EPO-R76E-TEV-His, Lanes 4-6: commercial EPO at 25ng (4), 50ng (5), and 100ng (6). All were detectable with the EPO antibody and were the same size. D) Schematic for synthesis of PPS by anionic ring opening polymerization. E) ^{1}H NMR spectra of PPS in $CDCl_3$. F) GPC refractive index detector trace of PPS (PS_{80}-OH) confirmed the formation of polymer. G) Quantification of Cy7 conjugated EPO-R76E loading into PLGA and PPS microparticles. H) Representative brightfield microscopy image of unloaded PPS microparticles. Scale bar represents 10μm. I-L) Quantitative histograms demonstrating size distribution of unloaded (I, K) and EPO-R76E loaded (J, L) PLGA (I, J) and PPS (K, L) microparticles. Note differences in axes between graphs.

Figure 2. *In vitro* studies. A, B) Cumulative release of EPO-R76E from the PPS (A) and PLGA (B) microparticles into solution over time showing mean ± s.d. C) Quantification

of cell viability after exposure to different amounts of empty and loaded particles showing mean ± s.d. D) Quantification of hydrogen peroxide induced ARPE-19 cell death after treatment with empty or EPO-R76E loaded PPS or PLGA particles. There was less cell death in PLGA+EPO-R76E or either PPS treated groups. E, F) Quantification of DHE fluorescence in ARPE-19 cells treated with PLGA (E) or PPS (F) particles to delivery 50ng of EPO-R76E. Cells were treated with the appropriate number of particles to result in delivery of 50ng of EPO-R76E based on the fluorescence quantification of EPO-R76E (Fig. 1B). EPO-R76E provides additional antioxidant benefit beyond that provided by PPS alone.

Figure 3. Levels of EPO-R76E in the retina at different time-points after bITON and injection of empty or loaded PPS (A) or PLGA (B) microparticles. Error bars = sd, ***p<0.001, $^{\#}$p<0.0001 empty compared to loaded particle-injected eyes.

Figure 4. Differential effect of microparticles on inflammation and oxidative stress in the retina and optic nerve. A, B) Representative fluorescence fundus images from bITON, PLGA (A) and bITON, PLGA+EPO-R76E (B) mice injected with DHE to detect superoxide and hydrogen peroxide. C) Quantification of DHE fluorescence. D) Representative western blots of SOD2 in all groups. E) Quantification of SOD2 levels after normalization to the GAPDH loading control. Statistical differences from sham are indicated without brackets. F, G) Quantification of IL-1α levels in the retina (F) and optic nerve (G) shown as change from saline sham. H, I) Quantification of IL-1β levels in the retina (H) and optic nerve (I) shown as change from saline sham. *p<0.05, **p<0.01, ***p<0.001, $^{\#}$p<0.0001

Figure 5. Preservation of optic nerve structure at 30-days post-injury by 1-day post-injury treatment with microparticles. A-F) Bright-field micrographs of optic nerve cross-sections from sham saline (A), bITON saline (B), bITON PPS (C), bITON PPS+EPO-R76E (D), bITON PLGA (E), and bITON PLGA+EPO-R76E (F) mice. G) Quantification of total axons. bITON saline and bITON PLGA were different from all other groups by p<0.0001. H) Quantification of degenerative axon profiles. Sham saline, bITON PPS, bITON PPS+EPO-R76E, and bITON PLGA+EPO-R76E were all statistically different from Sham. **p<0.01, ***p<0.001, # p<0.0001.

Figure 6. Preservation of visual function at 30-days post-injury by 1-day post-injury treatment with lead microparticles. A) Representative ERG waveforms. B) Quantification of the b-wave amplitude. C) Quantification of the b-wave latency. D) Representative VEP waveforms. E) Quantification of the VEP N1-wave amplitude. F) Quantification of the VEP N1-wave latency. All data shown as change from saline sham controls. *p<0.05, **p<0.01, ***p<0.001, $^{\#}$p<0.0001 compared to bITON saline.

REFERENCES

[1] C. A. Taylor, J. M. Bell, M. J. Breiding, L. Xu, Traumatic Brain Injury–Related Emergency Department Visits, Hospitalizations, and Deaths — United States,

2007 and 2013, Morb. Mortal. Wkly. Rep. Surveill. Summ. 66 (2017) 1-16. https://doi.org/10.15585/mmwr.ss6609a1.
[2] K. D. Steinsapir, R. A. Goldberg, Traumatic optic neuropathy, Surv. Ophthalmol. 38 (1994) 487-518. https://doi.org/10.1016/0039-6257(94)90145-7.
[3] L. A. Levin, R. W. Beck, M. P. Joseph, S. Seiff, R. Kraker, The treatment of traumatic optic neuropathy: The international optic nerve trauma study, Ophthalmol. 106 (1999) 1268-1277. https://doi.org/10.1016/S0161-6420(99)00707-1.
[4] K. D. Steinsapir, R. A. Goldberg, Traumatic Optic Neuropathy: An Evolving Understanding, Am. J. Ophthalmol. 151 (2011) 928-933. https://doi.org/10.1016/j.ajo.2011.02.007.
[5] E. L. Singman, N. Daphalapurkar, H. White, T. D. Nguyen, L. Panghat, J. Chang, T. McCulley, 2016. Indirect traumatic optic neuropathy, Mil. Med. Res. 3, 2. https://doi.org/10.1186/s40779-016-0069-2.
[6] G. Miliaras, G. Fotakopoulos, I. Asproudis, S. Voulgaris, A. Zikou, K. Polyzoidis, Indirect Traumatic Optic Neuropathy Following Head Injury: Report of Five Patients and Review of the Literature, J. Neurol. Surg. A Cent. Eur. Neurosurg. 74 (2013) 168-174. https://doi.org/10.1055/s-0032-1330115.
[7] A. Bernardo-Colón, V. Vest, A. Clark, M. L. Cooper, D. J. Calkins, F. E. Harrison, T. S. Rex, 2018. Antioxidants prevent inflammation and preserve the optic projection and visual function in experimental neurotrauma, Cell Death Dis. 9, 1097. https://doi.org/10.1038/s41419-018-1061-4.
[8] A. Bernardo-Colón, V. Vest, M. L. Cooper, S. A. Naguib, D. J. Calkins, T. S. Rex, 2019. Progression and Pathology of Traumatic Optic Neuropathy From Repeated Primary Blast Exposure, Front. Neurosci. 13, 719. https://doi.org/10.3389/fnins.2019.00719.
[9] R. Gaudana, H. K. Ananthula, A. Parenky, A. K. Mitra, Ocular Drug Delivery, AAPS J. 12 (2010) 348-360. https://doi.org/10.1208/s12248-010-9183-3.
[10] N. B. Shelke, R. Kadam, P. Tyagi, V. R. Rao, U. B. Kompella, Intravitreal poly(L-lactide) microparticles sustain retinal and choroidal delivery of TG-0054, a hydrophilic drug intended for neovascular diseases, Drug Deliv. Transl. Res. 1 (2010) 76-90. https://doi.org/10.1007/s13346-010-0009-8.
[11] K. Sahil, M. Akanksha, S. Premjeet, A. Bilandi, B. Kapoor, Microsphere: A Review, Int. J. Res. Pharm. Chem. 1 (2011) 1184-1198.
[12] V. Vest, A. Bernardo-Colón, D. Watkins, B. Kim, T. S. Rex, Rapid Repeat Exposure to Subthreshold Trauma Causes Synergistic Axonal Damage and Functional Deficits in the Visual Pathway in a Mouse Model, J. Neurotrauma. 36 (2019) 1646-1654. https://doi.org/10.1089/neu.2018.6046.
[13] X. Rong, S. Yang, H. Miao, T. Guo, Z. Wang, W. Shi, X. Mo, W. Yuana, T. Jin, Effects of Erythropoietin-Dextran Microparticle-Based PLGA/PLA Microspheres on RGCs, Investig. Ophthalmol. Vis. Sci. 53 (2012) 6025-6034. https://doi.org/10.1167/iovs.12-9898.
[14] W. Zhang, G. Zhou, Y. Gao, Y. Zhou, J. Liu, L. Zhang, A. Long, L. Zhang, P. Tang, A sequential delivery system employing the synergism of EPO and NGF promotes sciatic nerve repair, Colloids Surf. B. 159 (2017) 327-336. https://doi.org/10.1016/j.colsurfb.2017.07.088.

[15] W. Ji, F. Yang, H. Seyednejad, Z. Chen, W. E. Hennink, J. M. Anderson, J. J. van den Beucken, J. A. Jansen, Biocompatibility and degradation characteristics of PLGA-based electrospun nanofibrous scaffolds with nanoapatite incorporation, Biomaterials. 33 (2012) 6604-6614. https://doi.org/10.1016/j.biomaterials.2012.06.018.
[16] T. Sullivan, K. Kodali, T. S. Rex, Systemic Gene Delivery Protects the Photoreceptors in the Retinal Degeneration Slow Mouse,Neurochem. Res. 36 (2011) 613-618. https://doi.org/10.1007/s11064-010-0272-6.
[17] T. A. Sullivan, E. E. Geisert, J. Hines-Beard, T. S. Rex, Systemic adeno-associated virus-mediated gene therapy preserves retinal ganglion cells and visual function in DBA/2J glaucomatous mice, Hum. Gene Ther. 22 (2011) 1191-1200. https://doi.org/10.1089/hum.2011.052.
[18] K. P. O'Grady, T. E. Kavanaugh, H. Cho, H. Ye, M. K. Gupta, M. C. Madonna, J. Lee, C. M. O'Brien, M. C. Skala, K. A. Hasty, C. L. Duvall, Drug-Free ROS Sponge Polymeric Microspheres Reduce Tissue Damage from Ischemic and Mechanical Injury, ACS Biomater. Sci. Eng. 4 (2018) 1251-1264. https://doi.org/10.1021/acsbiomaterials.6b00804.
[19] K. M. Poole, C. E. Nelson, R. V. Joshi, J. R. Martin, M. K. Gupta, S. C. Haws, T. E. Kavanaugh, M. C. Skala, C. L. Duvall, ROS-responsive microspheres for on demand antioxidant therapy in a model of diabetic peripheral arterial disease, Biomaterials. 41 (2015) 166-175. https://doi.org/10.1016/j.biomaterials.2014.11.016.
[20] A. Napoli, M. Valentini, N. Tirelli, M. Muller, J. A. Hubbell, Oxidation-responsive polymeric vesicles, Nat. Mater. 3 (2004) 183-189. https://doi.org/10.1038/nmat1081.
[21] M. P. Lisanti, U. E. Martinez-Outschoorn, Z. Lin, S. Pavlides, D. Whitaker-Menezes, R. G. Pestell, A. Howell, F. Sotgia, Hydrogen peroxide fuels aging, inflammation, cancer metabolism and metastasis, Cell Cycle. 10 (2011) 2440-2449. https://doi.org/10.4161/cc.10.15.16870.
[22] B. S. Zolnik, D. J. Burgess, Effect of acidic pH on PLGA microsphere degradation and release, J. Control. Release. 122 (2007) 338-344. https://doi.org/10.1016/j.jconrel.2007.05.034.
[23] M. K. Gupta, J. R. Martin, B. R. Dollinger, M. E. Hattaway, C. L. Duvall, Thermogelling, ABC Triblock Copolymer Platform for Resorbable Hydrogels with Tunable, Degradation-Mediated Drug Release, 2017. Adv. Funct. Mater. 27, 1704107. https://doi.org/10.1002/adfm.201704107.
[24] M. K. Gupta, J. R. Martin, T. A. Werfel, T. Shen, J. M. Page, C. L. Duvall, Cell Protective, ABC Triblock Polymer-Based Thermoresponsive Hydrogels with ROS-Triggered Degradation and Drug Release, J. Am. Chem. Soc. 136 (2014) 14896-14902. https://doi.org/10.1021/ja507626y.
[25] B. R. Dollinger, M. K. Gupta, J. R. Martin, C. L. Duvall, Reactive Oxygen Species Shielding Hydrogel for the Delivery of Adherent and Nonadherent Therapeutic Cell Types, 2017. Tissue Eng. Part A. 23, 19-20. https://doi.org/10.1089/ten.tea.2016.0495.
[26] S. Naguib, A. Bernardo-Colon, C. Cencer, N. Gandra, T. S. Rex, Galantamine protects against synaptic, axonal, and vision deficits in experimental

neurotrauma, 2019. Neurobiol. Dis. 134, 104695. https://doi.org/10.1016/j.nbd.2019.104695.
[27] S. K. Tripathy, E. C. Svensson, H. B. Black, E. Goldwasser, M. Margalith, P. M. Hobart, J. M. Leiden, Long-term expression of erythropoietin in the systemic circulation of mice after intramuscular injection of a plasmid DNA vector, Proc. Natl. Acad. Sci. U.S.A. 93 (1996) 10876-10880. https://doi.org/10.1073/pnas.93.20.10876.
[28] O. Rajkovic, C. Gourmel, R. d'Arcy, R. Wong, I. Rajkovic, N. Tirelli, E. Pinteaux, Reactive Oxygen Species-Responsive Nanoparticles for the Treatment of Ischemic Stroke, 2019. Adv. Ther. 2, 7. https://doi.org/10.1002/adtp.201900038.
[29] T. S. Rex, Y. Wong, K. Kodali, S. Merry, Neuroprotection of photoreceptors by direct delivery of erythropoietin to the retina of the retinal degeneration slow mouse, Exp. Eye Res. 89 (2009) 735-740. https://doi.org/10.1016/j.exer.2009.06.017.
[30] J.-f. Zhang, Y.-l. Wu, J.-y. Xu, W. Ye, Y. Xhang, H. Weng, W.-d. Shi, G.-x. Xu, L. Lu, W. Dai, S. H. Sinclair, W.-Y. Li, G.-T. Xu, Pharmacokinetic and toxicity study of intravitreal erythropoietin in rabbits, Acta Pharmacol. Sin. 29 (2008) 1383-1390. https://doi.org/10.1111/j.1745-7254.2008.00885.x.
[31] J. Hines-Beard, W. S. Bond, J. R. Backstrom, T. S. Rex, Virus-mediated EpoR76E gene therapy preserves vision in a glaucoma model by modulating neuroinflammation and decreasing oxidative stress, 2016. J. Neuroinflammation. 13, 39. https://doi.org/10.1186/s12974-016-0499-5.
[32] W. Zhang, Y. Gao, Y. Zhou, J. Liu, L. Zhang, A. Long, L. Zhang, P. Tang, Localized and Sustained Dlivery of Erythropoietin from PLGA Microspheres Promotes Functional Recovery and Nerve Regeneration in Peripheral Nerve Injury, 2015. BioMed Res. Int. 2015, 478103. https://doi.org/10.1155/2015/478103.
[33] J. Hines-Beard, S. Desai, R. Haag, N. Esumi, L. D'Surney, S. Parker, C. Richardson , T. S. Rex, Identification of a Therapeutic Dose of Continuously Delivered Erythropoietin in the Eye Using An Inducible Promoter System, Curr. Gene Ther. 13 (2013) 275-281. https://doi.org/10.2174/15665232113139990024.

SUPPLEMENTARY INFORMATION

Supplemental Methods

Quantification of particle endotoxin levels: Endotoxin levels were quantified using the commercially-available ToxinSensor™ Chromogenic LAL Endotoxin Assay Kit (GenScript) according to the manufacturer's protocol. Briefly, 0.4mg particles in 100 µl endotoxin-free PBS were combined with 100 µl reconstituted Limulus Amebocyte Lysate (LAL) and incubated at 37°C for 10 minutes. 100 µl chromogenic substrate was added, incubated for 6 min, followed by 500 µl stop solution and 1 ml color stabilizer. Each sample was plated in triplicate (100 µl per well) in a black-walled 96-well plate and the absorbance was read at 545 nm on a plate reader. The endotoxin levels were quantified from a standard curve.

Supplemental Figure 1. Intraocular cytokine levels are not due to particle endotoxin. A) Quantification of endotoxin levels in PPS-blank, PPS-EPOR76E, PLGA-blank, and PLGA-EPOR76E. B) Particle endotoxin levels displayed with a reference line for endotoxin levels previously shown to induce uveitis upon injection in the eye [Supplemental Reference 1].

Supplemental References

[1] K. Adibkia, M. Siahi Shadbad, A. Nokhodchi, A. Javadzedeh, M. Barzegar-Jalali, J. Barar, G. Mohammadi, Y. Omidi, Piroxicam nanoparticles for ocular delivery: Physicochemical characterization and implementation in endotoxin-induced uveitis, J. Drug Target. 15 (2007) 407-416. https://doi.org/10.1080/10611860701453125.

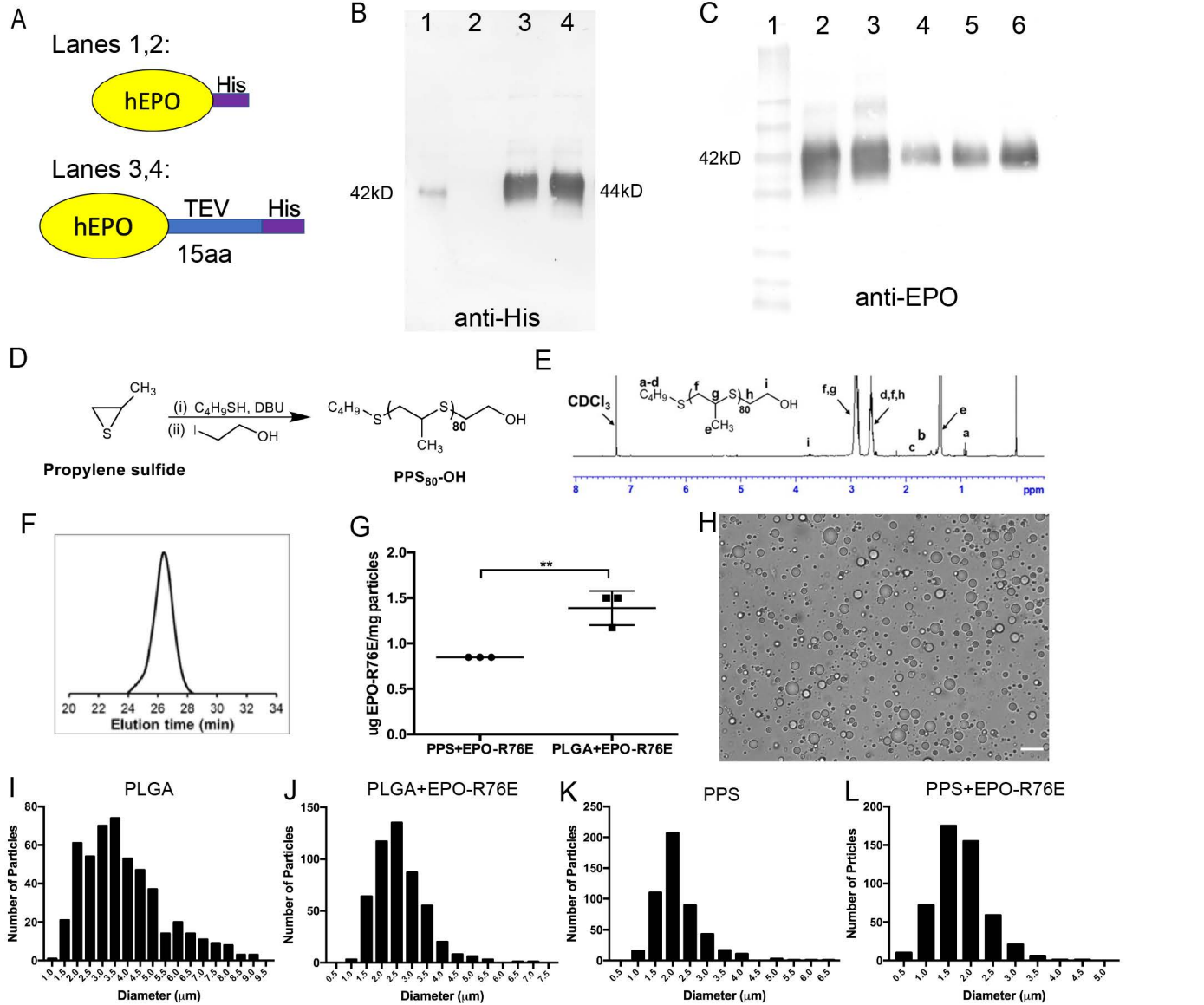
A
Lanes 1,2:
hEPO
His
Lanes 3,4:
hEPO
TEV
His
15aa
B
1 2 3 4
42kD
44kD
anti-His
C
1 2 3 4 5 6
42kD
anti-EPO
D
(i) C4H9SH, DBU
(ii)
OH
Propylene sulfide
PPS80-OH
E
CDCl3
a-d
f,g
d,f,h
e
b
c
a
i
ppm
F
Elution time (min)
G
ug EPO-R76E/mg particles
**
PPS+EPO-R76E
PLGA+EPO-R76E
H
I
PLGA
Number of Particles
Diameter (μm)
J
PLGA+EPO-R76E
Number of Particles
Diameter (μm)
K
PPS
Number of Particles
Diameter (μm)
L
PPS+EPO-R76E
Number of Prticles
Diameter (μm)

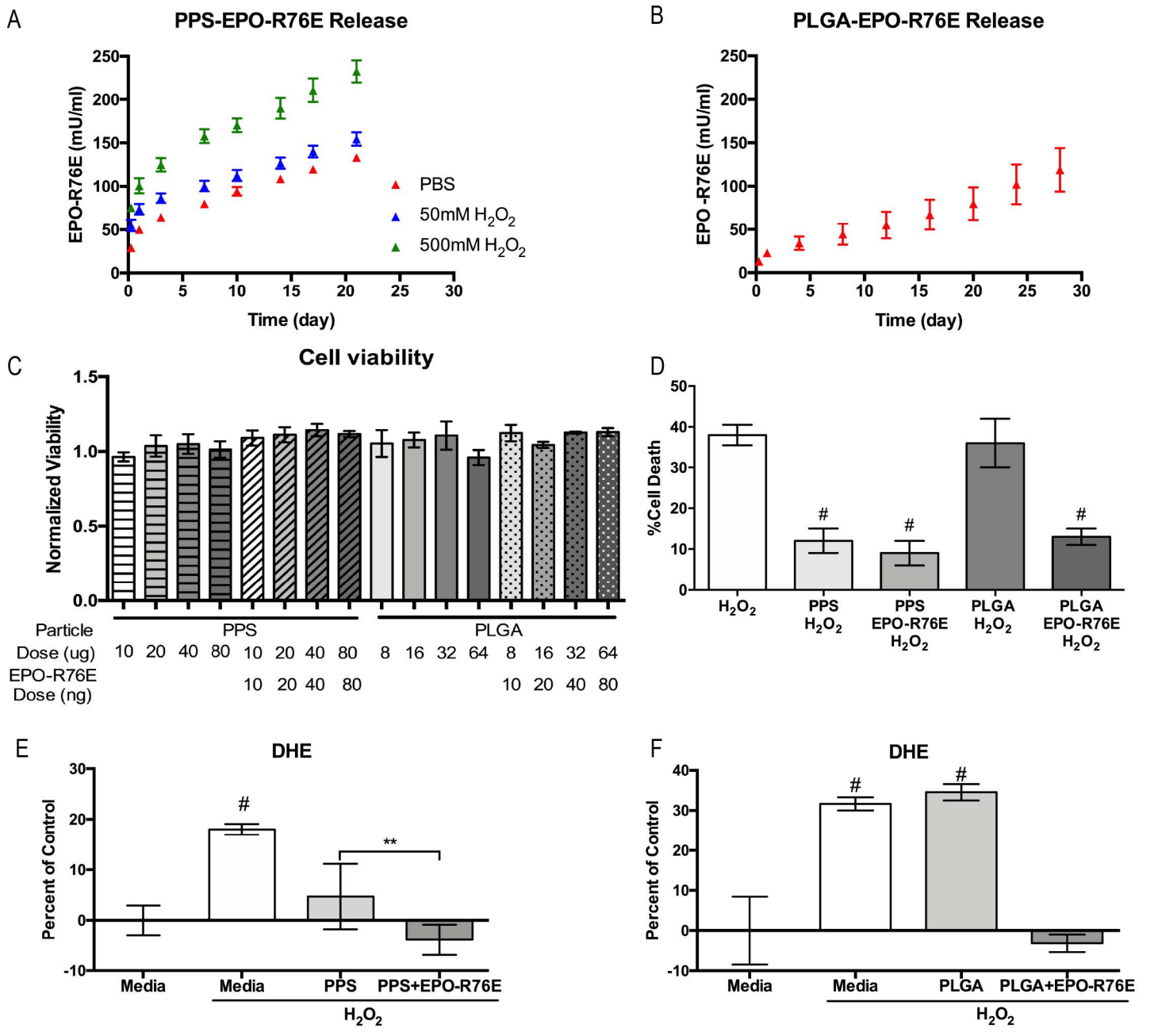
A
PPS-EPO-R76E Release
EPO-R76E (mU/ml)
Time (day)
PBS
50mM H2O2
500mM H2O2
B
PLGA-EPO-R76E Release
EPO -R76E (mU/ml)
Time (day)
C
Cell viability
Normalized Viability
Particle
PPS
PLGA
Dose (ug)
10 20 40 80 10 20 40 80 8 16 32 64 8 16 32 64
EPO-R76E Dose (ng)
10 20 40 80 10 20 40 80
D
%Cell Death
H2O2
PPS H2O2
PPS EPO-R76E H2O2
PLGA H2O2
PLGA EPO-R76E H2O2
E
DHE
Percent of Control
Media
Media
PPS
PPS+EPO-R76E
H2O2
F
DHE
Percent of Control
Media
Media
PLGA
PLGA+EPO-R76E
H2O2

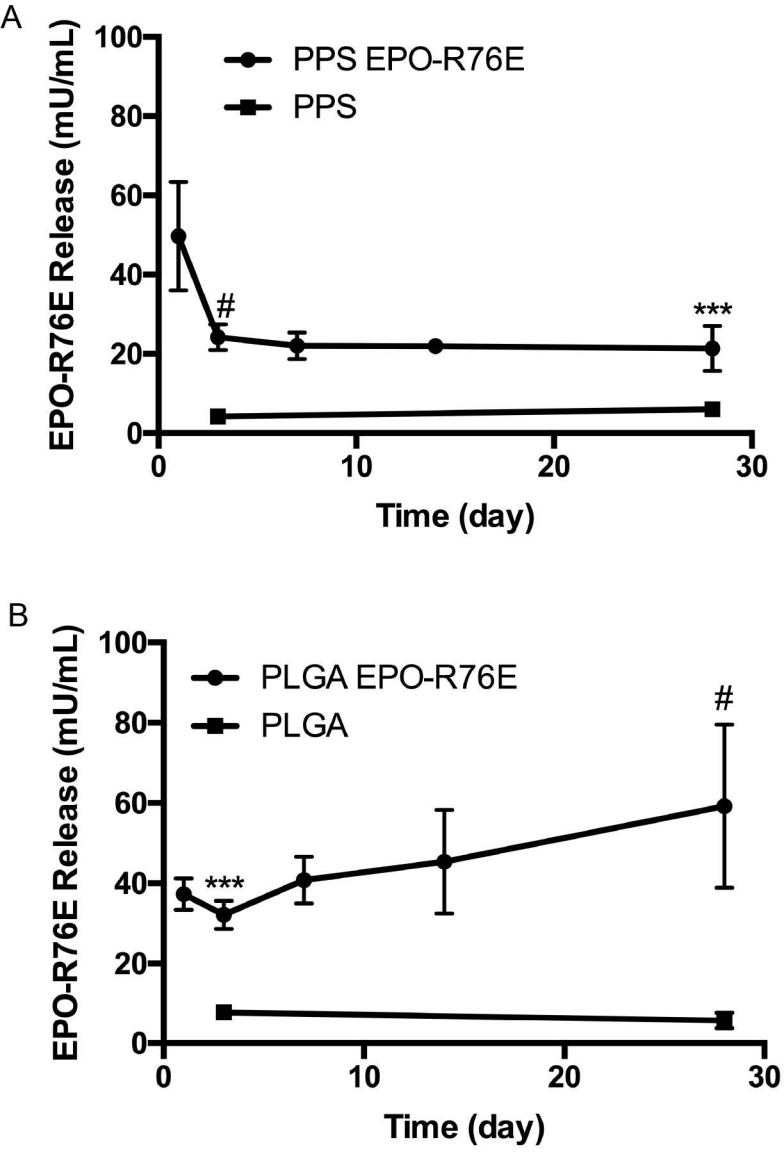
A
EPO-R76E Release (mU/mL)
100
80
60
40
20
0
PPS EPO-R76E
PPS
#
***
0
10
20
30
Time (day)
B
EPO-R76E Release (mU/mL)
100
80
60
40
20
0
PLGA EPO-R76E
PLGA
#
***
0
10
20
30
Time (day)

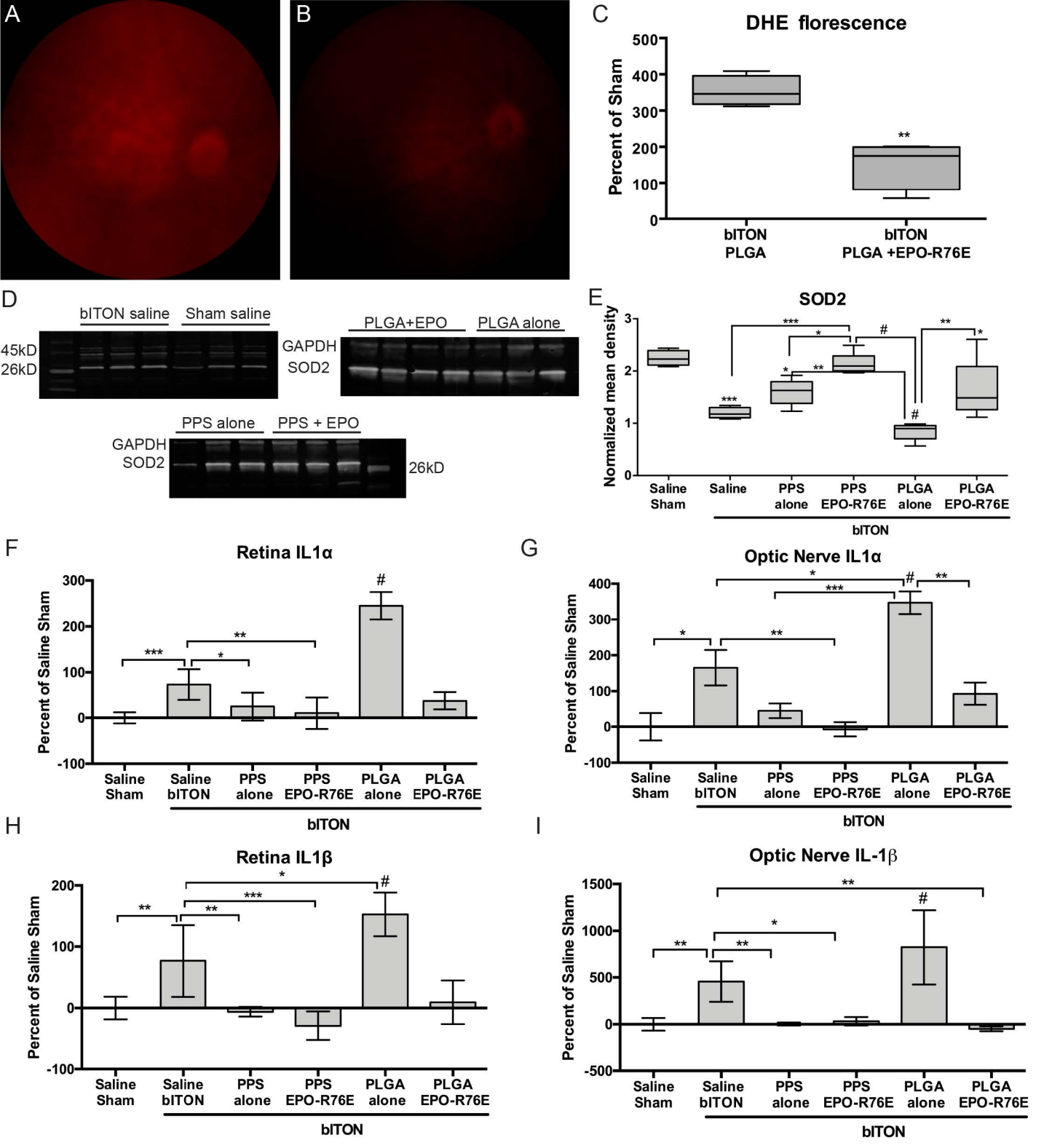
A
B
C
DHE florescence
Percent of Sham
500
400
300
200
100
0
**
bITON PLGA
bITON PLGA +EPO-R76E
D
bITON saline
Sham saline
45kD
26kD
PLGA+EPO
PLGA alone
GAPDH
SOD2
PPS alone
PPS + EPO
GAPDH
SOD2
26kD
E
SOD2
Normalized mean density
3
2
1
0
Saline Sham
Saline
PPS alone
PPS EPO-R76E
PLGA alone
PLGA EPO-R76E
bITON
F
Retina IL1α
Percent of Saline Sham
300
200
100
0
-100
Saline Sham
Saline bITON
PPS alone
PPS EPO-R76E
PLGA alone
PLGA EPO-R76E
bITON
G
Optic Nerve IL1α
Percent of Saline Sham
400
300
200
100
0
-100
Saline Sham
Saline bITON
PPS alone
PPS EPO-R76E
PLGA alone
PLGA EPO-R76E
bITON
H
Retina IL1β
Percent of Saline Sham
200
100
0
-100
Saline Sham
Saline bITON
PPS alone
PPS EPO-R76E
PLGA alone
PLGA EPO-R76E
bITON
I
Optic Nerve IL-1β
Percent of Saline Sham
1500
1000
500
0
-500
Saline Sham
Saline bITON
PPS alone
PPS EPO-R76E
PLGA alone
PLGA EPO-R76E
bITON

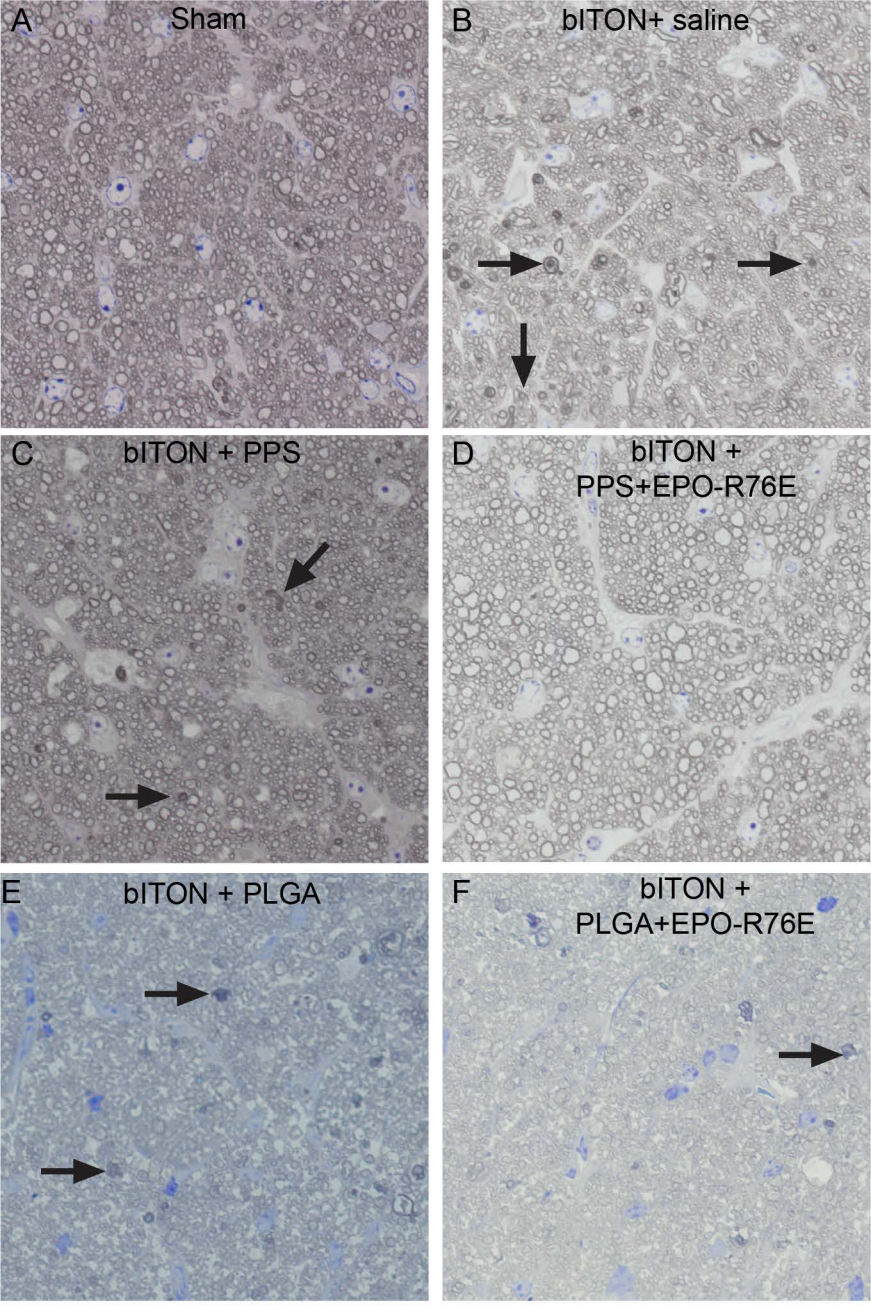
A
Sham
B
bITON+ saline
C
bITON + PPS
D
bITON +
PPS+EPO-R76E
E
bITON + PLGA
F
bITON +
PLGA+EPO-R76E

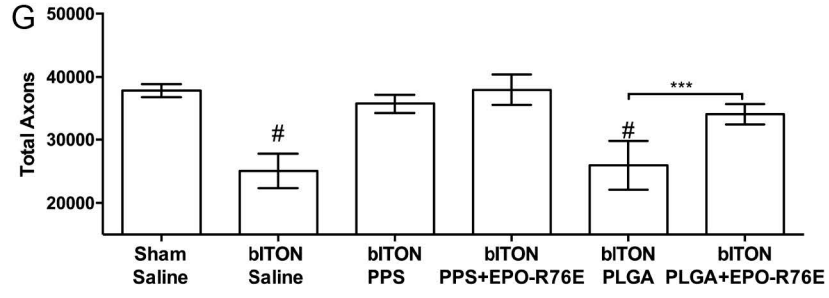
G
Total Axons
50000
40000
30000
20000
#
#
***
Sham
Saline
bITON
Saline
bITON
PPS
bITON
PPS+EPO-R76E
bITON
PLGA
bITON
PLGA+EPO-R76E

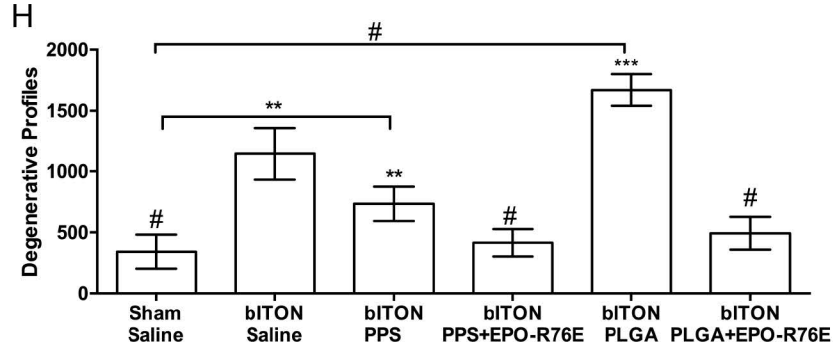
H
Degenerative Profiles
2000
1500
1000
500
0
#
#
**
**
#
***
#
Sham
Saline
bITON
Saline
bITON
PPS
bITON
PPS+EPO-R76E
bITON
PLGA
bITON
PLGA+EPO-R76E

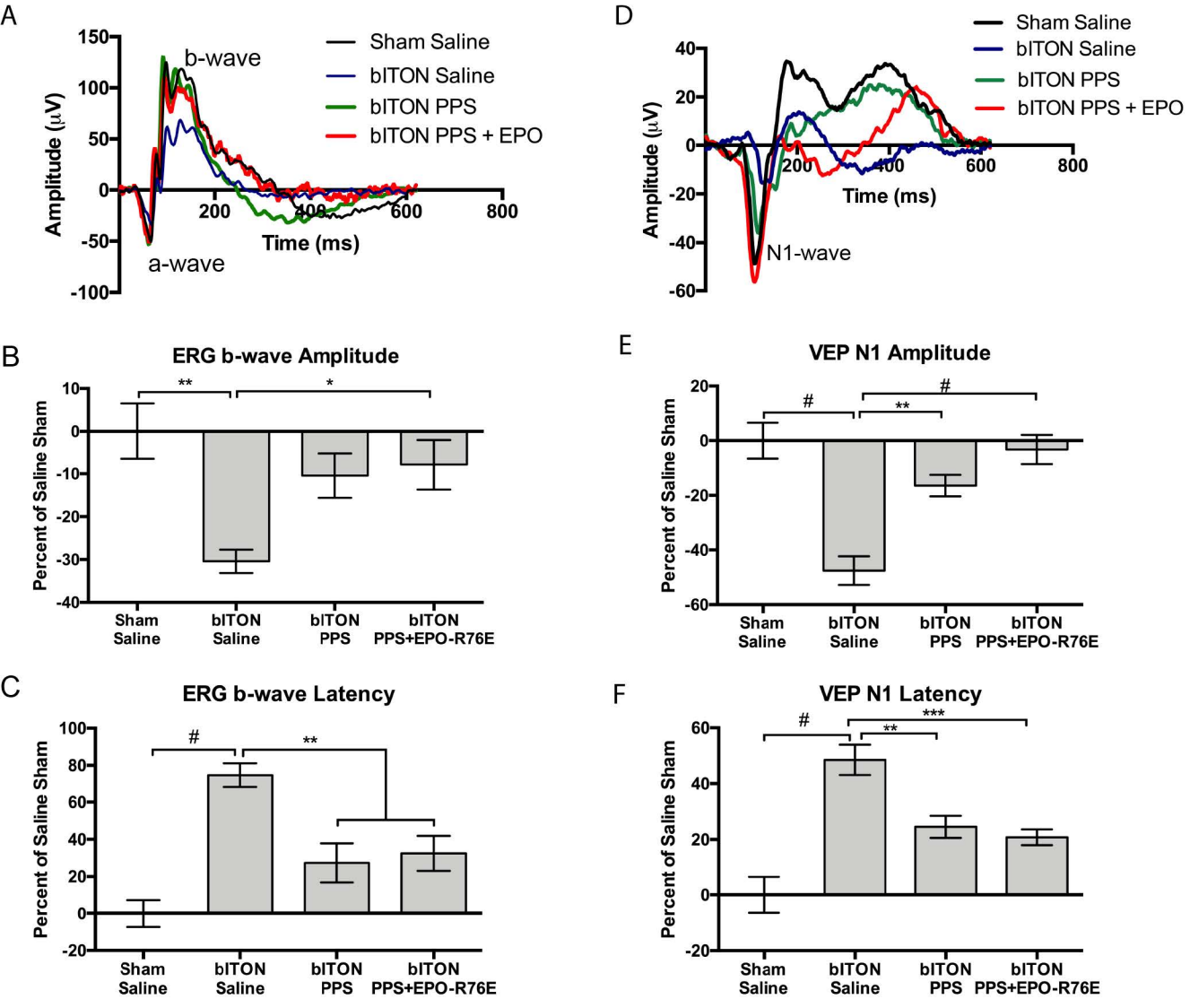
A
b-wave
a-wave
Sham Saline
bITON Saline
bITON PPS
bITON PPS + EPO
Amplitude (μV)
Time (ms)
D
N1-wave
B
ERG b-wave Amplitude
Percent of Saline Sham
Sham Saline
bITON Saline
bITON PPS
bITON PPS+EPO-R76E
E
VEP N1 Amplitude
C
ERG b-wave Latency
F
VEP N1 Latency

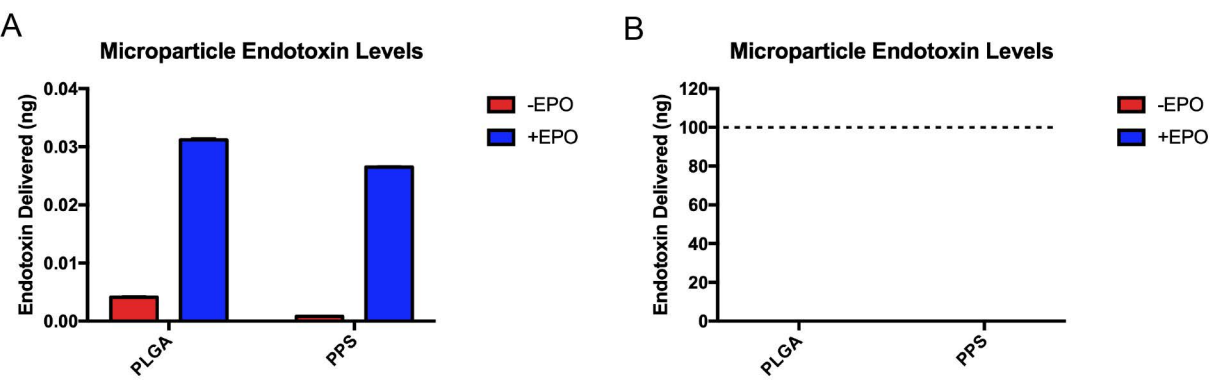
A
Microparticle Endotoxin Levels
Endotoxin Delivered (ng)
0.04
0.03
0.02
0.01
0.00
PLGA
PPS
-EPO
+EPO
B
Microparticle Endotoxin Levels
Endotoxin Delivered (ng)
120
100
80
60
40
20
0
PLGA
PPS
-EPO
+EPO